TECHNICAL SUMMARY REPORT
L/S U-819

IMPROVEMENT OF IGNITION SYSTEM FOR SIMULTANEOUS IGNITION OF RETRO AND ULLAGE MOTORS ON SATURN V

Prepared For

NASA/ MARSHALL SPACE FLIGHT CENTER
Huntsville, Alabama

CONTRACT NO. NAS 8-11472

Prepared By

LINK ORDNANCE DIVISION
GENERAL PRECISION, INC.
Sunnyvale, California

JULY 30, 1965

TECHNICAL SUMMARY REPORT
L/S U-819

IMPROVEMENT OF IGNITION SYSTEM FOR SIMULTANEOUS IGNITION OF RETRO AND ULLAGE MOTORS ON SATURN V

Prepared For

NATIONAL AERONAUTICS AND SPACE ADMINISTRATION
GEORGE C. MARSHALL SPACE FLIGHT CENTER
Huntsville, Alabama

CONTRACT NO. NAS 8-11472

Prepared By

D. E. Davenport, Ph.D.
L. D. Pitts
J. N. Gardner

LINK ORDNANCE DIVISION
GENERAL PRECISION, INC.
Sunnyvale, California

JULY 30, 1965

CONTENTS

ILLUSTRATIONS

ILLUSTRATIONS (Continued)

ILLUSTRATIONS (Continued)

ILLUSTRATIONS (Continued)

I INTRODUCTION

A. PROBLEM DEFINITION

The mechanics of the transition from deflagration to detonation in explosives have, during recent years, been given close and extensive attention by investigators in the solid propellant rocket industry and others; however, the reverse transition from detonation to deflagration has been largely neglected. The retro- and ullage-rocket initiators (known as Through Bulkhead Initiators or TBI's) used in the Saturn V Confined Detonating Fuze (CDF) ordnance system require detonation-to-deflagration transitions since they must accept a detonation reaction and emit a flame. In addition, the motor igniter will not accept a highly brisant initiator output.

At the onset of this study, the program to develop such a CDF initiator was experiencing difficulties. These difficulties were caused by a lack of knowledge of exactly what factors were involved in the detonation-to-deflagration transition and how to control them in such a way as to produce the desired initiator output.

Therefore, this program was set up to investigate the following three areas:

(1) Mechanical techniques for causing transition from detonation to deflagration within less than 1 inch with minimum residual shock.

(2) Chemical techniques for causing transition from detonation to deflagration within less than 1 inch with minimum residual shock.

(3) Methods of evaluating the effectiveness of the above techniques, e.g., microscopic examination of initiator body, metal hardness surveys, optical stress coating analyses, electronic detonation velocity measurements, etc.

B. STUDY LIMITATIONS

Although it would have been desirable to do a broad and fundamental study of the detonation-to-deflagration transition (referred to as inverted DDT or, alternatively, as TDD), the applied nature of the results desired dictated several limitations on the geometry and materials to be used in the study. Because the initiator design concerns itself with CDF type initiation, the explosive input to

the transition zone was chosen as a 1/10 inch diameter PETN train similar to that in the CDF output. This geometry and material selection made it possible to translate the results obtained in the study to the hardware being developed with a minimum of extrapolation. From a theoretical point of view it would have been desirable to use a somewhat larger diameter explosive train to simplify some of the measurements and to eliminate some of the edge effects. However, from an experimental point of view, the small size had the advantage of enabling one to perform a great number of experiments quite simply and quite rapidly.

The deflagrating materials chosen for the study were selected from a list of desirable igniter materials and included only granular pyrotechnic mixes and pressed explosives. This decision was based on a general observation (unsupported by significant data) that it is very difficult to make the transition from detonation to a steady state deflagration in a cast type mixture. The general basis for this conclusion was the observation that in the case of propellants and TNT, and other cast materials, if the impulse was not large enough to initiate detonation the reaction induced by a strong shock was always a decaying reaction which quenched. Many general comments could be made as to why this seems to be true, and it meets the normal logic concerned with initiation and propagation of reactions. However, in view of the ill-defined nature of these arguments, they will not be presented here.

The studies were carried out with heavy-walled confinement since this represented the practical initiator geometry. The heavy walls increase the effective diameter of the charge and also transmit a stronger shock from the PETN into the deflagrating region. Since a strong shock is believed to have a deleterious effect on the deflagration propagation, it was felt important to maintain this similarity to the initiator. In many cases the assembly was surrounded by an additional momentum trap of low-melting alloy to minimize the expansion of the tube. It is believed that this additional layer had little or no effect on the deflagration data.

The three types of pyrotechnics selected for the deflagration zone vary in their velocity from near-detonation (the RDX-aluminum mix) to a very slow

deflagration (copper oxide-magnesium mix). The intermediate velocity $KClO_4$-Al mix is also intermediate in the quantity of gas and pressures generated in the deflagration process. It was felt that these three frequently used ignition mixes embody a representative cross sectional pattern of the types which are normally encountered. A study of the three mixes should determine if detonation-to-deflagration transition is more easily made in one type than the other. Hopefully, if one has chosen the important parameters, one may then extrapolate the conclusions to the more generalized base as to whether the transition can be made more successfully in one type of igniter mix than the other.

C. PREVIOUS INVESTIGATIONS

Through a comprehensive literature search, conducted during the early part of this study, and discussions with several prominent persons in the field, it was determined that very little data was available on the specific phenomenon of detonation-to-deflagration transition (inverted DDT). However, some applicable information was found. Dr. Eyring, in some of his work (Ref. 58), discusses the phenomenon of overdriving a detonation, and somewhat intuitively extends his considerations to the case of detonation-to-deflagration transitions.

His original derivation (based on the assumption of slightly overdriven detonation) shows that the detonation velocity, D, should decay to the steady state value, D_o, according to the equation:

$$a \frac{dD}{dx} = 0.333(D_o - D) \qquad (1)$$

where "a" is the reaction zone thickness and the constant, 0.333, is from an empirical fit to a more complicated equation. (It should be noted that the constant was tested over a range of $\frac{D}{D_o}$ of only 0.4 to 1.4.) This equation was applied to the transition for several explosives using the integrated form:

$$\ln(D_o - D) = \frac{-.333\,x}{a} + B, \qquad (2)$$

with the results shown in Table I. In this table, $D_{initial} - D_o$ represents the overdriving and "a" is the reaction zone length calculated from the plot (on a

semilog scale) of $D_o - D$ versus x. The fact that the values of "a" were reasonable for those explosives was taken as confirmation of the reasonableness of the theory.

Table I

	$D_{in} - D_o$ mm/μs	a(cm)
Nitroguanidine (ρ = 0.53)	1.5	0.88
TNT (ρ = 1.0)	-3.0	0.075
80/20 Amatol (ρ = 1.64)	0.7	3.9

In his usual intuitive form, Dr. Eyring tests the theory when applied to the more severe condition of a shock decaying in an inert gas, using some calculations of von Neumann. To do this Eyring replaces "a" by "x" on the basis that the total energy of the shock is being distributed over the length of the inert path, and arrives at the equation:

$$\frac{dD}{dx} \cong -k \frac{D}{x} \tag{3}$$

In the case of a detonating medium the constant was 0.33 but for a material such as an unreacted explosive it would be about 0.12. For other organic or more slowly reacting solids, the constant may be assumed to lie between the two values, since it depends on the equation of state of the products. In its integrated form this equation will lead to:

$$\ln \frac{D}{D_1} = -k \ln x, \tag{4}$$

where D_1 is the velocity at unit distance from the interface. Erying shows that this result agrees quite closely with the corresponding equation that von Neumann derived for a shock in gas from quite different considerations. On this basis he concluded that the form should be applicable for the general case of shock transitions, whether large or small, increasing or decreasing in intensity.

The only other data applicable to these experiments have been derived from some studies of attempts to initiate detonation in subcritical to critical diameters of propellants. Unfortunately, in most of these studies the data obtained for the subcritical systems are usually discarded. There is, however, one program underway at the present time (Air Force Contract AF04(611)-9945 with Aerojet and Shock Hydrodynamics) which is examining the subcritical cases. The study is directed toward charges 2 inches to 48 inches inclusive in diameter and is, therefore, dealing with much larger diameter charges than those involved in this study. Nevertheless, generalized formulas such as those of Eyring should fit equally as well to the large diameter or the small diameter results. Unfortunately, the results from these experiments are not available at present and so cannot be used to compare with the results presented here.

D. APPROACH AND TECHNIQUES

The measurement techniques which proved to be the most useful in monitoring the reaction through the transition zone were: (1) an electrical probe technique, which gave a continuous record of the velocity from the detonation through the transition zone into the deflagration zone; and (2) a metallurgical technique which gave a measure of the shock pressure generated in the reaction zone.

The electrical probe technique has been used by several others (Refs. 2, 31). In the course of this work we had the opportunity to refine and extend it to the point that reliable and reproducible results could be obtained down into the deflagrating region, even in this small geometry. It is reported that others (Van Dolah, private communication) have been able to extend the measurements down into the deflagrating zone, but most data which have been available in the literature indicate significant problems with the probe in this region.

The metallurgical techniques have not been used before as a detailed monitor technique, but showed very interesting results in giving information such as is needed in the study of the transition zone. This technique is based upon the fact that the detonation velocity within a given compound is associated with a

specific peak pressure which induces a characteristic shock pressure into the surrounding steel. As the reaction velocity decreases, the peak pressure in the detonation zone will also decrease, until the detonation becomes a deflagration. Thus, by monitoring the shock pressure induced by the peak pressure, the velocity of the detonation at given points can be determined. A convenient method for monitoring the shock pressure within the steel adjacent to the explosive is to measure the increase in hardness in the steel. Measurements of this type have been made over a wide range of pressures for several metals and are reported in Refs. 23, 24, 25, 53. In the normal case there is little desire for very precise measurements so that variations of 10 to 20 percent in hardness readings are of no particular concern. However, if the hardness measurement is to be used for indirect measurement of the reaction velocity by determination of peak pressures, the measurements must be as accurate as possible. In this case, we had hoped to be able to measure the pressures to a matter of a few percent.

With the particular geometry involved in these experiments (cylindrically symmetric with the explosive loaded in a core at the center of the metal piece, as later shown in Figure 10), a complicating metallurgical effect is introduced. The shock wave can result in a significant expansion of the steel cylinder and accompanying mechanical working of the steel as the hole in the internal portion of the cylinder expands. This effect was minimized by casting the metal pieces in an alloy known as Cerralow, which served as a momentum trap on the external surface of the cylinder. Even with this precaution, however, the holes in the cylinder were found to expand about 33 percent. Thus, corrections must be made empirically for the effects of the mechanical work hardening, which accompanied the shock hardening.

II MEASUREMENT TECHNIQUES

A. ELECTRICAL PROBE

1. Possible Measurement Techniques

Detonation and deflagration front velocities may be determined by measuring the velocity of some electrical phenomena (such as light output or conductivity) associated with the reaction front, or by measuring the time rate of change of the electrical parameters (inductance, induced emf, capacitance, or resistance) of some electrical element directly affected by the reaction front.

Velocity of the luminous front may be measured by means of a framing camera, a streaking camera, or a photovoltaic device. Framing camera and streaking camera records (Ref. 19) can be extremely revealing about front contours but have the disadvantages of requiring expensive equipment and complex setups, and of being unusable on opaquely confined explosives and pyrotechnics. Also, in the case of the framing camera, only incremental velocities are obtained. The use of a photocell and light probes at intervals on the test body has the disadvantages of giving only incremental velocities, and disturbing the explosive confinement.

However, the photocell method was attempted for these studies as a confirmatory test for detonation velocities obtained with resistance wire probes. The light probes consisted of three 0.032-inch diameter holes drilled in the brass test bodies of 1.25-inch length, 0.75-inch O.D., 0.100-inch I.D. Lexan, a clear plastic, was extruded into the three holes. The test bodies were loaded with PETN and fired. An International Rectifier B2M selenium photocell attached to a lucite rod was positioned to sense the light output for a Tektronix 555 oscilloscope. However, due to the poor response time of the selenium photocell, no conclusive results were derived from these tests. A silicon photocell, such as the Texas Instruments H38 or 1N2175, has sufficiently fast rise time (under 2 μsec) to give a fairly accurate indication of time of light appearance at a point

in the pyrotechnic. Experiments would have been performed with such a photocell, had time permitted.

Ionization front velocity measurements using the Doppler effect at microwave frequencies (Ref. 20) appear to produce good results in detonation, but there is no evidence in the literature that equivalent results could be expected in deflagration where ionization front conductivity is presumably much lower than in detonation. Also to be considered are the expensive equipment and complicated setup required.

While the measurement of time rate of change of inductance, capacitance, or induced emf may offer interesting methods for reaction front velocity measurement with a minimum of interference with a given explosive geometry and confinement, no such technique has been fully developed thus far. Such techniques would probably prove to be fairly complex and particularly geometry-dependent.

The resistance wire probe (a type of which was selected for experiments in this study) produces some small disturbance of the explosive, but requires no complex instrumentation, is easy to assemble, and delivers a continuous record of instantaneous velocities in detonation and deflagration, and the transition between the two.

Resistance probes commonly function by continuous shorting (caused by the reaction front) of a resistance wire carrying a constant current. Front velocity may then be computed from Equation (1):

$$D = \frac{1}{ir} \frac{dV}{dt} \tag{5}$$

where: D = instantaneous velocity (mm/μsec)

i = constant current (amperes)

r = resistivity of resistance wire (ohms/mm)

$\frac{dV}{dt}$ = slope of voltage vs. time curve on oscilloscope trace (volts/μsec).

The resistance probe described by Amster in his very helpful article (Ref. 2) utilizes the ionization front and the metallic confinement for the return path

for current through a bare resistance wire buried in cast explosive. Our experiments with a bare #30 copper wire down the center of a standard brass test body loaded with pressed PETN showed significant fluctuations in ionization front resistance and excessive spuriously generated emf's. Thus, when resistance wire was used down the center of a PETN column pressed in a standard test body, the result was the unreadable trace of Figure 1, rather than the straight slope which should have been observed had not the above problems been present.*

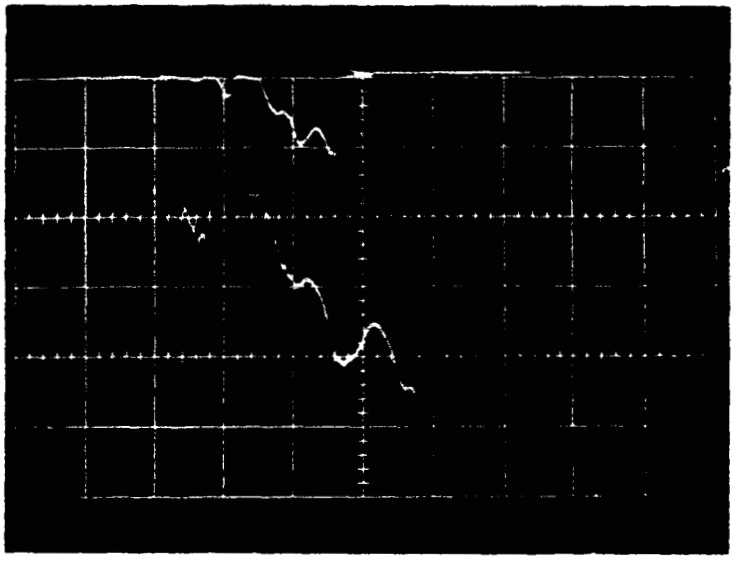

Figure 1

Horiz: Upper 2 μsec/cm
Lower 1 μsec/cm
(3 μsec delay)

Vert: Upper 5 V/cm
Lower 2 V/cm

Load: PETN (constant density)

Probe: 1-mil Nichrome wire down center of explosive

The resistance probe described by Bowser (Ref. 31) utilizes resistance wire coiled around an insulated copper conductor. The resistance wire is progressively shorted to the copper conductor as the reaction front destroys the thin insulation. This probe has the advantages of being useful in different geometries and having the proven pressure sensitivity necessary for measurements at the relatively low pressures experienced in deflagration. This probe configuration was rejected principally because of the difficulty inherent in its manufacture and because of the problems associated in loading explosives around such a probe.

*A spacial ram with a 0.010-inch diameter hole down the center was manufactured for these experiments. The center hole was produced by the spark erosion technique.

The probes adopted for our experiments were modifications of the resistance probes described by Bowser and Amster. They consisted of resistance wire laid down the confinement wall parallel to the long axis of the test body, and thus normal to the reaction front. The wire was insulated from the wall by a thin strip of mylar tape or transformer paper or by enamel insulation deposited on the wire. In most cases another thin strip of mylar tape was placed over the wire, separating the wire from the explosive. Pressure from the reaction front forced a continuous shorting of the wire through the outer insulation to the wall.

Figure 2 shows the trace produced by the shock wave in the acceptor of a Thru-Bulkhead geometry test body where failure to initiate reaction in the acceptor occurred. Since hot gases cannot pass the bulkhead, and temperature gradients cannot pass through in a few microseconds, this shot offers proof that the mechanism of probe closure need not include ionization or heat, but only pressure.

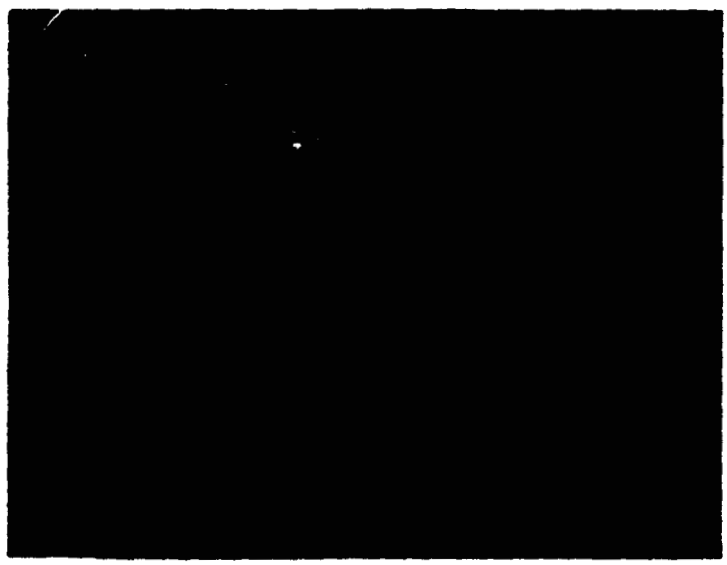

Figure 2
Horiz: 2 μsec/cm
Vert: 5 V/cm
Thru-Bulkhead Geometry (detonation failed to transfer)
Donor: PETN (1.7 gm/cm)
Receptor: PETN (1.0 gm/cm)
Probe: 0.5-mil Moleculoy probe

This technique provides simple probe assembly, simple explosive loading techniques, high reliability, good pressure sensitivity even in deflagration, and accurate results. The effect of the wire on burning rate, as mentioned by Amster (Ref. 1), is minimized by use of such a probe since the wire is initially insulated from the pyrotechnic mix and is coupled to the cold wall at the reaction

front. It should also be noted that our experiments utilized pyrotechnic mixes with velocities in the range from 0.5 to 3.0 mm/μsec, much too rapid for heat transfer down the probe wire to have any significant effect on burning rate.

2. Selected Probes

Three configurations of the wall probe were found useful for detonation-to-deflagration velocity experiments. They are: (1) a sandwich probe consisting of 1-mil diameter bare Nichrome wire, sandwiched between an upper layer of 0.25-mil thick mylar tape and a lower layer of 0.25-mil thick mylar tape or 0.2-mil thick NDC coil paper; (2) a 1.2-mil, enamel-insulated Nichrome wire covered by a layer of 0.25-mil thick mylar tape; and (3) a 0.5-mil, enamel-insulated Moleculoy wire without tape covering.

Most experiments were performed using the sandwich probe, since its sensitivity in deflagration was more reproducible than the covered 1.2-mil insulated Nichrome wire probe. However, when particularly low deflagration pressures were encountered the 0.5-mil Moleculoy probe was developed, and showed the greatest pressure sensitivity of all the probes tested. Nevertheless, for most purposes the sandwich probe is preferable for its relatively good assembly and loading characteristics. The constant slope of Figure 3 illustrates the typical operation of the sandwich resistance probe in a test body loaded with PETN at a constant density.

In general, it was found that wire diameter should be 1.5 mil or less. Larger wire tended to give slower response, be less pressure sensitive, and take longer to break its final contact. The smaller wires appeared to have a desirable knife-edge effect, slicing through the insulation. Figures 3 and 4 show the contrast of trace linearity between a probe using 1-mil Nichrome wire and a probe using 3-mil Nichrome wire, respectively. The probes are otherwise identical and the PETN loads are identical. However, smaller wire does have the disadvantage of being difficult to handle due to its weakness in tension and its lack of stiffness. It was found nevertheless that even the 0.5-mil wire could be handled successfully under proper conditions.

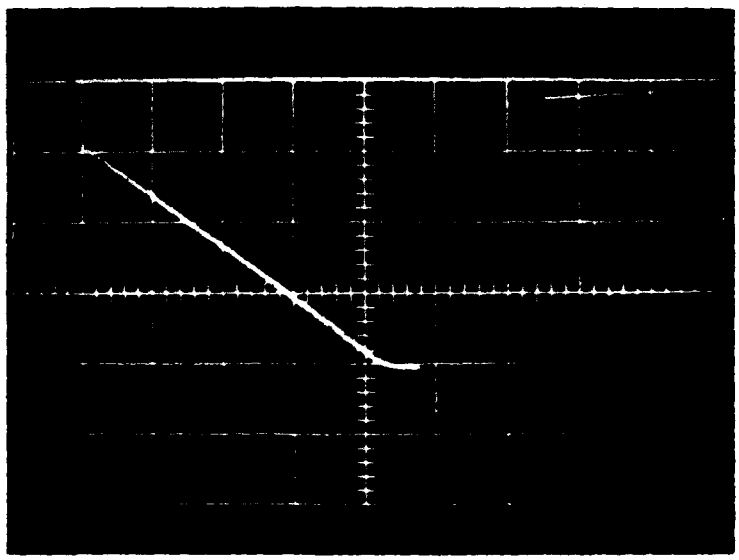

Figure 3

Horiz: 1 μsec/cm

Vert: 2 V/cm (3 μsec delay)

Load: PETN

Probe: 1-mil Nichrome sandwich probe

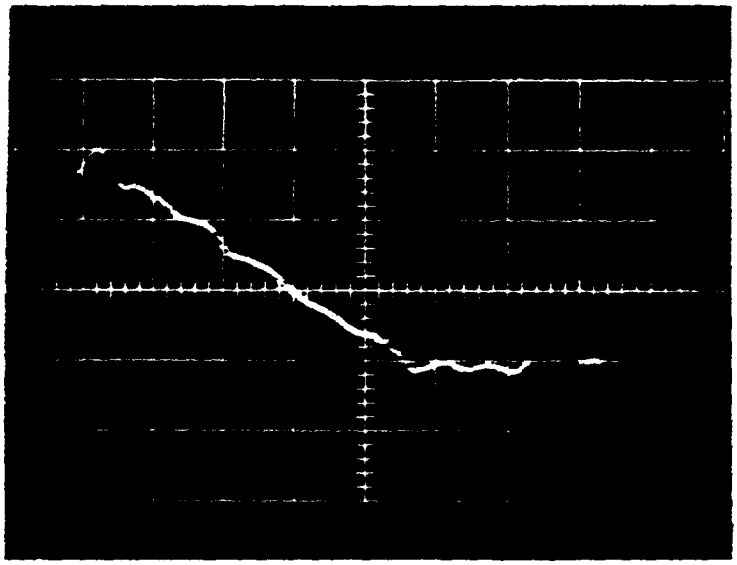

Figure 4

Horiz: 1 μsec/cm (3 μsec delay)

Vert: 0.2 V/cm

Load: PETN (constant density)

Probe: 3-mil Nichrome sandwich probe

The other consideration in choosing wire size is that the wire should have a resistivity which will give a drop of 1 to 10 volts over the desired wire length when a current of 1 to 200 milliamperes is applied to the probe. Currents over this range are easily generated from a 30-volt power supply and a solid state current generator such as used in these experiments. If the total voltage change is under 1 volt, line interference, firing pulses, and trigger circuit pulses may cause considerable distortion of the oscilloscope trace.

Mylar tape, UCC and NDC coil paper,* and regular enamel wire coating all proved satisfactory as insulation between the resistance wire and the confining

*Obtained from Peter Schweitzer Div. of Kimberly-Clark Corporation.

metal wall. The most important factor in choosing the insulation is that it should be as thin as possible so that it can be broken more easily by deflagration pressures. The insulation must, however, be able to withstand loading pressures. Figures 3 and 5 show the comparison of traces obtained with 0.25-mil insulation and 3-mil insulation on shots identically loaded with PETN. Mylar tape, which has greater tensile strength and less tendency to tear in cutting than coil paper, is easier to load and cut. However, the transformer paper gave better results at the low deflagration pressures. Other insulating materials which might be tried include teflon tape and metal-coated capacitor paper.

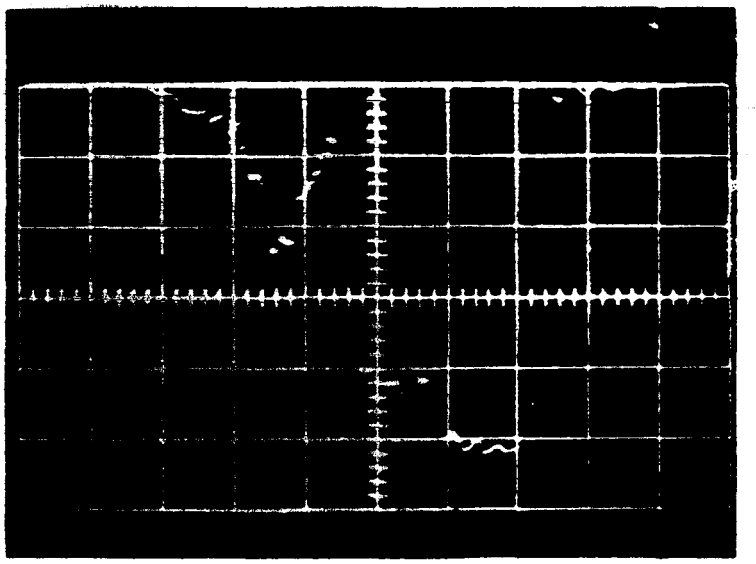

Figure 5

Horiz: 1 μsec/cm (2 μsec delay)

Vert: 1 V/cm

Load: PETN (constant density)

Probe: 1-mil Nichrome sandwich probe with 3-mil Mylar tape between wire and wall

For all probes except the 0.5-mil insulated Moleculoy wire it was found to be very important to include a layer of mylar tape over the resistance wire. This appeared to serve the function of holding the resistance wire and lower layer of insulation in place during probe insertion and loading so that no kinking occurred. Figures 3 and 6 show a comparison of shots with and without the upper layer of tape. Note the linear slope in Figure 3 and the irregularities in the slope of Figure 6. The thickness of covering tape did not appear to influence results greatly but thinner tape was preferred since it altered the geometry of the explosive less. It should be noted, however, that the most sensitive probe developed, the 0.5-mil insulated Moleculoy wire, functioned best without any covering layer of insulation.

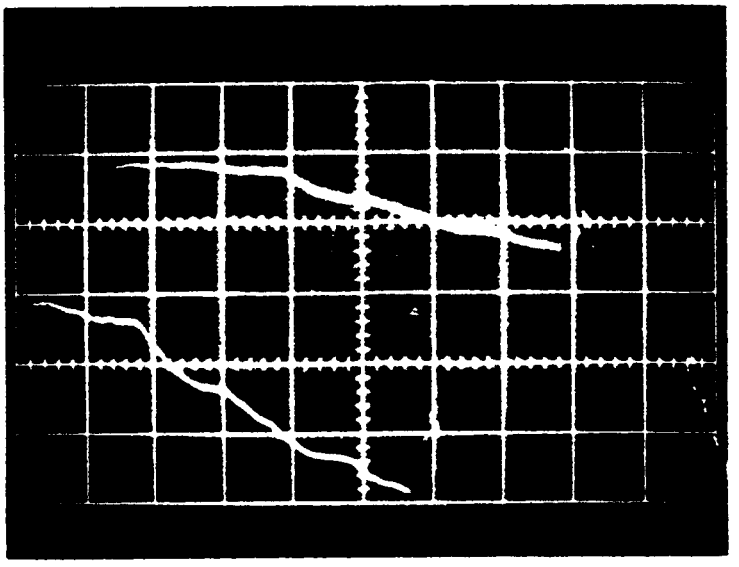

Figure 6

Horiz: 1 μsec/cm
1 μsec/cm (2 μsec delay)

Vert: 5 V/cm
2 V/cm

Load: PETN (constant density)

Probe: 1-mil Nichrome probe with no covering layer of Mylar tape

Pressure sensitivity is very important at the low deflagration pressures, especially in the transition region between detonation and deflagration where pressures are particularly low. Principal methods of achieving this sensitivity are: (1) use of 1.2-mil wire or smaller; (2) use of a thin (0.5-mil or less) insulator between wire and wall; and (3) proper probe tension, apparently just enough to assure that the probe lies straight.

It was noted early in the program that the probes often showed an open, or no resistance change, for a period of a few microseconds right at the interface between the PETN and the pyrotechnic mix. This problem has apparently been encountered by others (Ref. 32). After this phenomenon was observed repeatedly, it was interpreted as being due to the reaction near the interface initiating only in the core of the pyrotechnic mix and some finite time (on the order of a few microseconds) being required for the complete reaction to reach the wall. Once the complete cross sectional area was reacting, the core reaction zone could drag the wall reaction along.

Though the mix might not be completely reacting at the wall, some sort of pressure gradient, non-zero at the wall, appeared to be present since some shots (Figure 7, for example) showed continuous velocity measurements through the transition region. If the assumption about transition region pressures being greater near the center of the pyrotechnic mix is correct, further experiments

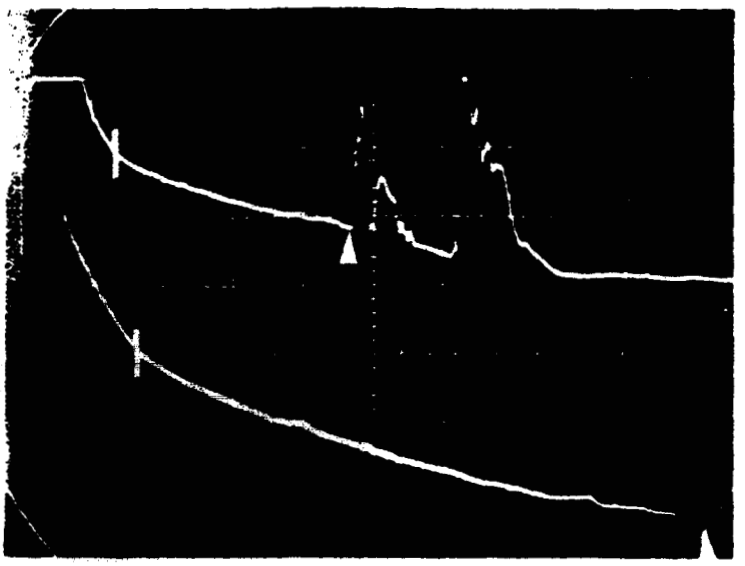

Figure 7

Horiz: Upper 5 μsec/cm
Lower 2 μsec/cm
(3 μsec delay)

Vert: Upper 5 V/cm
Lower 2 V/cm

Load: 0.500" PETN
(1.0 gm/cm^3)
0.750" 60% $KClO_4$-
40% Al (1.2 gm/cm^3)

Probe: 0.5-mil insulated
Moleculoy probe

should show that good probe traces are more easily attained at diameters smaller than the 0.100 inch used for the present study, and less easily attained at diameters greater than 0.100 inch.

It was also observed that the opens of the probe during transition were more likely to occur when the PETN density was 1.2 gm/cm^3 than when it was 1.0, for the same pyrotechnic mix at the same density. For instance, in the series of 12 stainless steel shots using pyrotechnic mixes, all six shots containing PETN at 1.2 gm/cm^3 showed discontinuities at the PETN-pyrotechnic interface lasting at least 1 microsecond such as that shown in Figure 8, while the six shots containing PETN at 1.0 gm/cm^3 showed interface discontinuities in only three shots

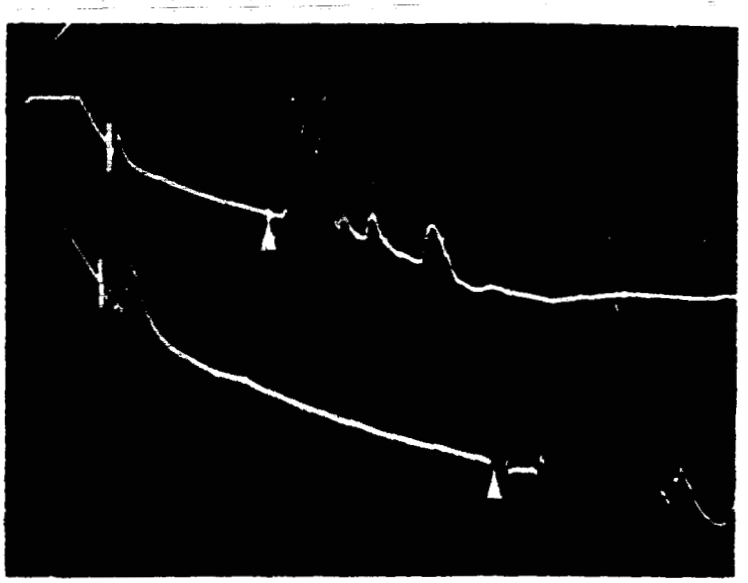

Figure 8

Horiz: Upper 5 μsec/cm
Lower 2 μsec/cm
(3 μsec delay)

Vert: Upper 5 V/cm
Lower 2 V/cm

Load: 0.500" PETN
(1.2 gm/cm^3)
0.750" 60% $KClO_4$-
40% Al (1.2 gm/cm^3)

Probe: 0.5-mil insulated
Moleculoy probe

and no discontinuity lasted as long as 1 microsecond. If shock pressure were the sole cause of closure, the reverse would have been expected to be true. Again, this suggests that the reaction zone ionization is contributing and that the stronger shock leads to delayed ignition in the pyrotechnic. Further investigation of this phenomena could be done by initiating similar mixes with PETN at densities of 0.8 and 1.5 gm/cm^3.

3. Shot Preparation

Shot preparation procedure included the following basic steps:

(1) probe installation in the test body

(2) pressing of weighed increments of PETN and pyrotechnic mix into the test body

(3) potting of test body in Cerralow*

(4) installation of ion probe trigger wire on PETN MDF detonating cord

(5) attachment of detonating cord to input of test body

(6) attachment of test body assembly to a 3 by 8-inch board

(7) soldering of ground wires and probe wires to terminals attached to board

(8) connection of #6 electric blasting cap to input end of detonating cord just prior to firing.

Figure 9 shows the test assembly setup. In assembly of sandwich probes, the 1/16-inch wide strip of mylar tape or coil paper was inserted first in the test body. Then the resistance wire was added, and finally the covering strip of 1/16-inch wide mylar tape. The whole assembly was secured by scotch tape covering each end of the test body. The 0.5-mil Moleculoy probe was simply inserted and taped down on each end.

The PETN and pyrotechnic charges were loaded in increments, commonly of 0.100-inch length. The higher density end, requiring greater pressing pressures, was pressed first. Pressing was done to a stop on a hydraulic press. The ram

*Step (3) was eliminated for all shots for which metallurgical study of the test body was not contemplated.

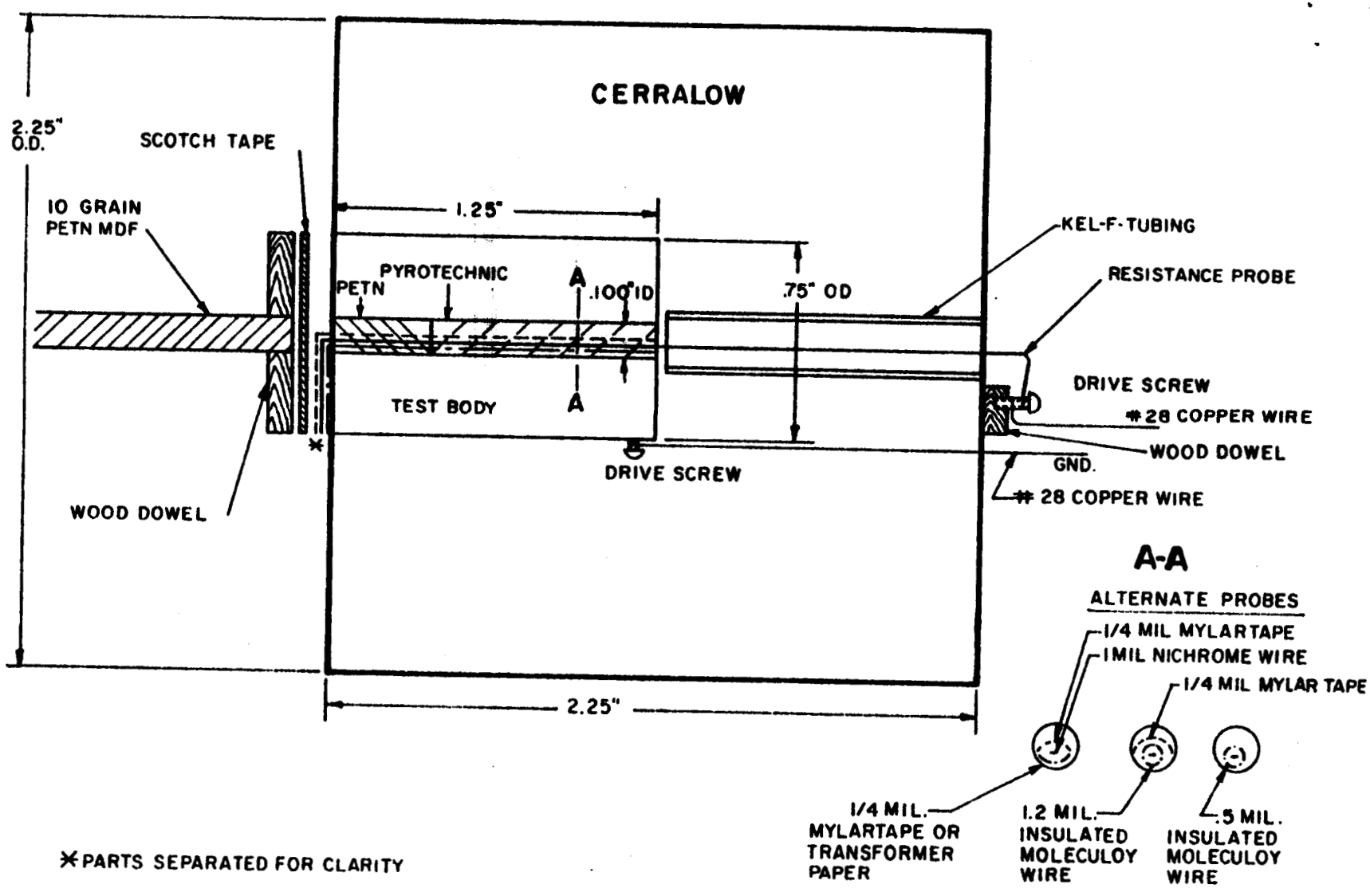

Figure 9. Loaded Test Body

[illegible] on one side to prevent damage by the probe. Care in [illegible] and frequent resistance checks were required to assure that the probe [illegible] to the test body, particularly at the lip of the hole.

The ionization trigger probe consists of a #37 insulated copper wire taped into a notch 1 inch from the output end of a 3-inch length of 10-grain PETN MDF detonating cord. The detonating cord was inserted into a slide of 0.75-inch O.D. [illegible] taped to the input end of the test body. (See Figure 10.)

Figure 10. Standard Brass Test Body Ready for Firing

For unpotted shots the output end of the test body was covered by another slide of 0.75-inch diameter doweling. The wall probe wire was brought along the side of the doweling and soldered to a drive screw on the flat outer surface of the doweling. A copper wire soldered to the same drive screw was connected to a terminal on the terminal board tacked to the 3- by 8-inch board, on which the whole assembly rested. Grounds were provided through copper wires connected to an alligator clip fastened to the lead case of the detonating cord and connected to a drive screw inserted in a hole near the output end of the test body. The ionization trigger probe was connected to the third terminal of the terminal board.

Though some experiments were made in the TBI (Through Bulkhead Initiator) geometry with single section units, the final series of shots was made with two section TBI's consisting of a B1113 mild steel donor, including bulkhead, and a brass acceptor. (See Figure 11.) Bulkhead thicknesses of 75, 90, and 105 mils were used. The two-section construction considerably simplified probe installation since the wall probe was not inserted in a blind hole but could be pulled completely through the acceptor hole and cut off on the bulkhead side when the shot was assembled. TBI preparation procedure was similar to that for the standard straight-through test bodies except that the two sections were held in place by a special steel fixture.

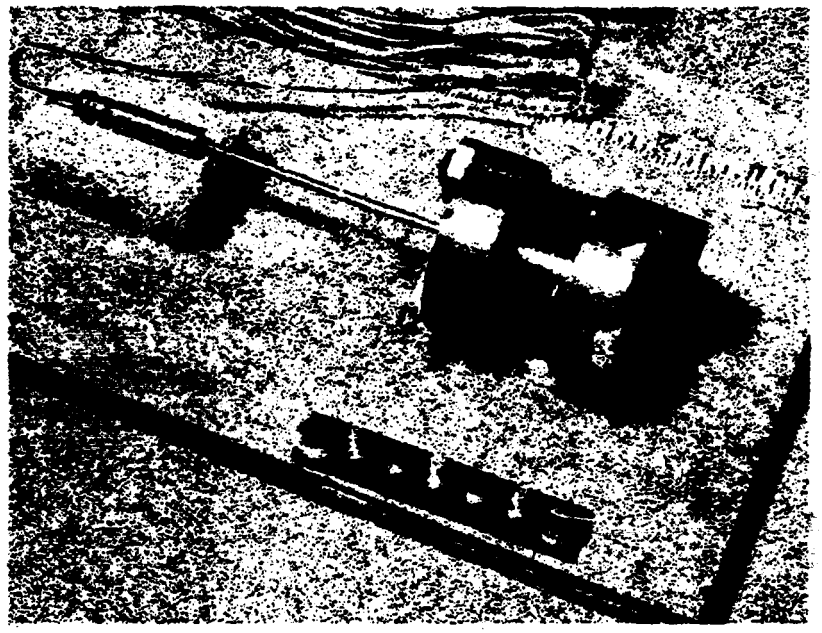

Figure 11. Two-Section TBI Ready for Firing

4. Instrumentation

Instrumentation used in the probe experiments consisted of a 200 ma solid state current generator and an RC pulse network. Additionally, a Hewlett-Packard 30-volt, Model 721A power supply, a Tektronix C19 oscilloscope camera, and a Tektronix 555 oscilloscope with two L plug-in amplifiers were used. Figure 12 illustrates a typical instrumentation setup for a firing. The constant current generator, whose schematic is presented in Figure 13, uses an NPN

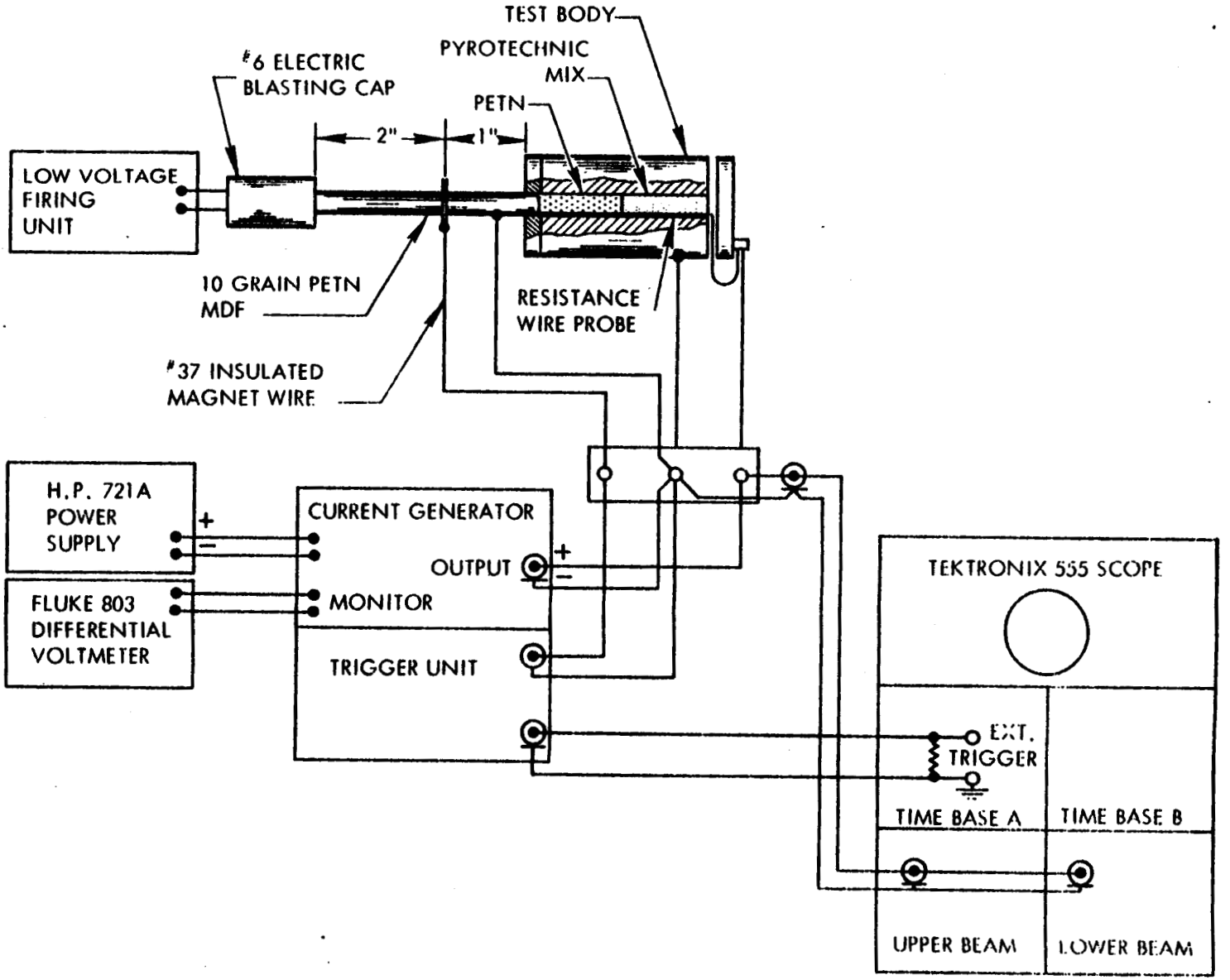

Figure 12. Instrumentation Setup

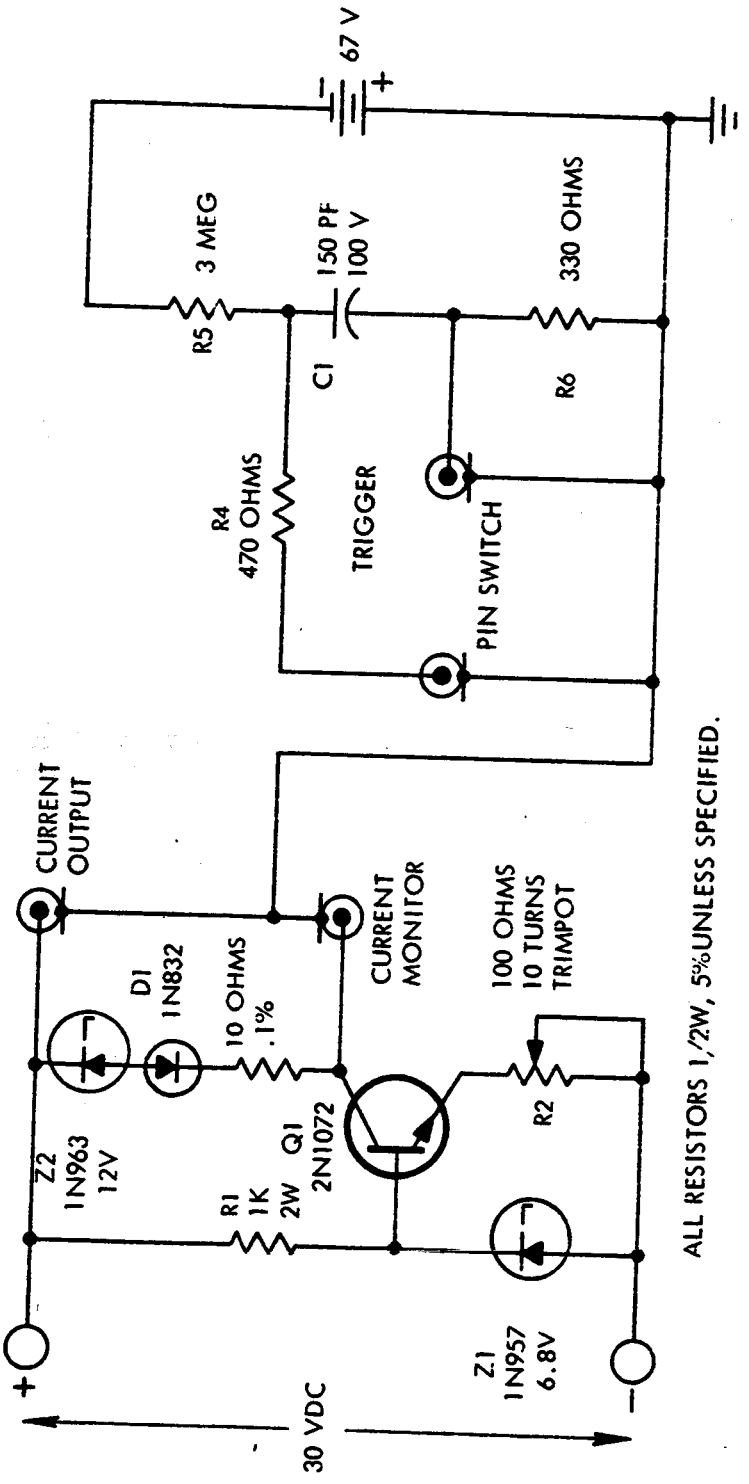

Figure 13. Constant Current Generator and Trigger Circuit, Schematic Diagram

silicon power transistor, rather than large vacuum tubes such as in the current generators described in Refs. 24 and 28. Advantages of the solid state generator include:

(1) higher reliability

(2) a small package which is easier to move and set up and can be placed in the firing chamber if properly protected

(3) no deterioration of electrical characteristics with time

(4) simpler construction

(5) no high voltages present in explosive environment.

Generally transistors, as can be seen from their characteristic curves, maintain a constant collector current when base bias is held constant. In the current generator of Figure 12, the 6.8-volt zener diode Z1 maintains the constant base drive. R1 serves to keep Z1 conducting. R2 presents a negative feedback path which helps hold collector current constant and is used to adjust the output current to an exact value. R2 should be larger than 100 ohms if currents under 50 milliamperes are desired. Most experiments in this study were performed with 100-milliampere currents except for the 0.5-mil Moleculoy probe shots for which 20 milliamperes were used. These currents were chosen to produce sufficient voltage drop across the resistance probe to override any low level noise. Otherwise, different current levels seemed to have no effect on probe performance. The transistor used, a 2N1072, is a special power transistor, no longer manufactured, but such transistors as the 2N2781 and 2N3327 have adequate power handling capability and frequency response for this application.

A 10-ohm, 0.1 percent precision resistor was employed in series with the output as a current monitor. Output current was then determined from the voltage across this resistor as read out on a John Fluke differential voltmeter, Model 803. Regulation into loads from 0 to 100 ohms was 0.1 percent and short term drift was less than 0.3 percent after stabilization. Most error was thus due to the Tektronix 555 oscilloscope, explosive loading error, and test body machining tolerance. However, calibration shots showed total system accuracy to be consistently within 4 percent.

Zener diode Z2 across the output serves to keep the transistor Q1 turned on prior to a firing, and to limit the voltage drop when initial probe shorting occurs. Diode D1 in series with Z2 is a microwave diode, forward biased to decrease the effect of the 1000 pf zener region capacitance of Z2 during initial probe shorting (Ref. 37). In some cases Z2 was replaced by two zener diodes, to further decrease the capacitance effect.

Cables and leads were chosen so as to approach a critically damped system, so that the velocity slopes had no ringing and initial fall time was as fast as possible. Flat lead, #28 stranded wire, and lossy line from a Tektronix 10:1 attenuator probe were eventually used to provide a satisfactory system. It is also important to use a fast response power supply such as the Hewlett-Packard Model 721A. The oscilloscope capacitance of 20 pf per channel has a negligible effect. The natural response of the current generator was in excess of 10 Mc, which was quite satisfactory.

It was found desirable to get reliable external scope triggering from an ionization probe closure on the detonating cord approximately 4 microseconds before the cord detonation reached the input of the test body. This permitted use of the lower beam of the Tektronix 555 delay oscilloscope in the delayed mode at a faster sweep speed than for the upper beam. The RC trigger circuit was designed to work from probe closure, provide a fast rising and fast decaying (0.1 microsecond fall time) pulse, radiate minimum electromagnetic energy to the signal channel, suppress spurious trigger pulses for 500 microseconds after the initial pulse, and allow insensitive oscilloscope trigger level setting, thus preventing spurious noise from accidentally triggering the oscilloscope.

During this study, various methods of obtaining trigger wire closure to the grounded lead sheath of the detonating cord were tried, including #37 insulated magnet wire laid across a notch in the detonating cord, the same type magnet wire wrapped around unnotched detonating cord, and 3-mil thick copper strip laid over a notch in the cord. All these methods performed satisfactorily. The ionization jet and the shock wave at the surface of the lead sheath are both strong enough to assure low resistance contact between the lead sheath and the wire or

strip. The most important part of such a triggering system appears to be an appropriately designed pulse forming trigger network to provide the trigger pulse for the oscilloscope.

5. Calibration

A calibration curve for PETN density vs. velocity was obtained from a series of shots fired in standard test bodies and employing ionization probes, a capacitor discharge circuit, and a Tektronix 555 oscilloscope. Figure 14 shows the experimental points from these data plotted on the same graph with a curve (solid line) plotted from the accepted equation relating ideal PETN velocity and density (Ref. 9):

$$D = 1.650 + 3.950\,\rho \qquad (6)$$

where: D = detonation velocity (mm/μsec)

ρ = PETN density (gm/cm^3)

Velocities obtained from 1-mil sandwich probe measurements in constant density PETN were compared with the experimental data from the ionization probe experiments. Densities were calculated from test body weight before and after loading and from known test body diameters and lengths. Velocities were then taken from Figure 14. A correlation appears in Tables I and II.

Table I

CALIBRATION VELOCITY DATA

Shot No.	Velocity (Probe) mm/μsec	Velocity (Density) mm/μsec
5	6.4	6.2
6	6.1	6.2
7	6.4	6.5
8	6.4	6.7
9	6.4	6.3
10	6.6	6.6
11	6.6	6.7
12	6.6	6.8
13	6.6	6.6

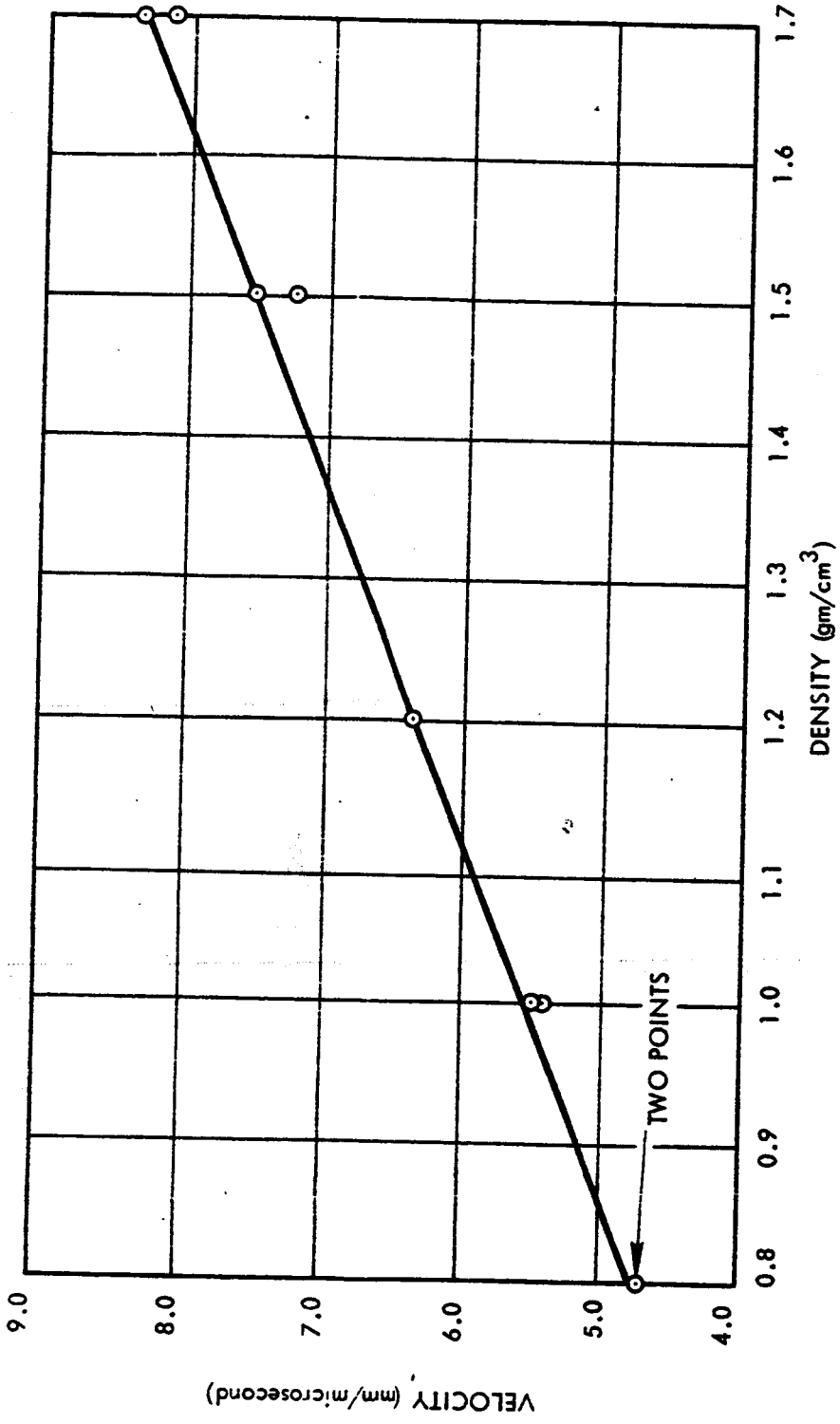

Figure 14. Plot of Density vs. Detonation Velocity for 325 Mesh PETN

Table II

CALIBRATION CORRELATION

Deviation mm/μsec	Number
0	2
0.10	4
0.20	2
0.30	1

A further series of calibration shots for the sandwich probe was fired, employing test bodies loaded for 0.625-inch with one density of PETN and for the remaining 0.625-inch with another density of PETN. Approximate densities of 0.8, 1.0, and 1.2 gm/cm^3 were used. A typical trace appears in Figure 15. Tables III and IV present the results.

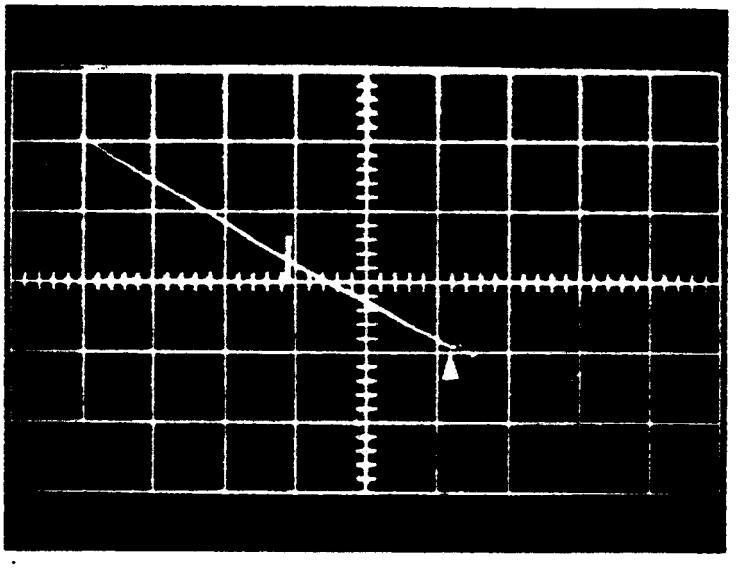

Figure 15

Horiz: 1 μsec/cm (3 μsec delay)

Vert: 2 V/cm

Load: 0.625" PETN 1.2 gm/cm^3 0.625" PETN 0.8 gm/cm^3

Probe: 1-mil Nichrome sandwich probe

Table III

CALIBRATION VELOCITY DATA

Shot No.	Velocity 1 (Density)	Velocity 1 (Probe)	Velocity 2 (Density)	Velocity 2 (Probe)
1	5.8	6.0	5.5	5.6
2	6.3	6.3	5.6	5.9
3	6.3	6.3	5.6	5.7
5	5.6	5.7	4.7	4.9
6	6.2	6.3	4.7	4.8
7	6.3	6.4	—	—
9	6.3	6.1	4.7	4.9

(All velocities are in mm/μsec)

Table IV

CALIBRATION CORRELATION

Deviation mm/μsec	Number
0	2
0.10	6
0.20	4
0.30	1

Tables I through IV indicate that correlation was better than 4 percent in some 90 percent of the cases. Later experiments showed even better correlation for both the sandwich probe and the 0.5-mil Moleculoy probe.

Figures 16 through 18 show typical traces obtained from test bodies loaded for the first 0.625-inch with PETN and for the 0.625-inch with the individual pyrotechnic mixes. These shots were obtained with the 1-mil Nichrome sandwich probe. Transition regions are clearly visible in all three pictures, except for a brief hesitation in the $KClO_4$-Al in Figure 17. In Figure 18, the voltage drop in the CuO-Fe_2O_3-Mg was not as large as calculated for complete propagation, indicating that the burning was effectively extinguished after about 0.4-inch down the pyrotechnic column.

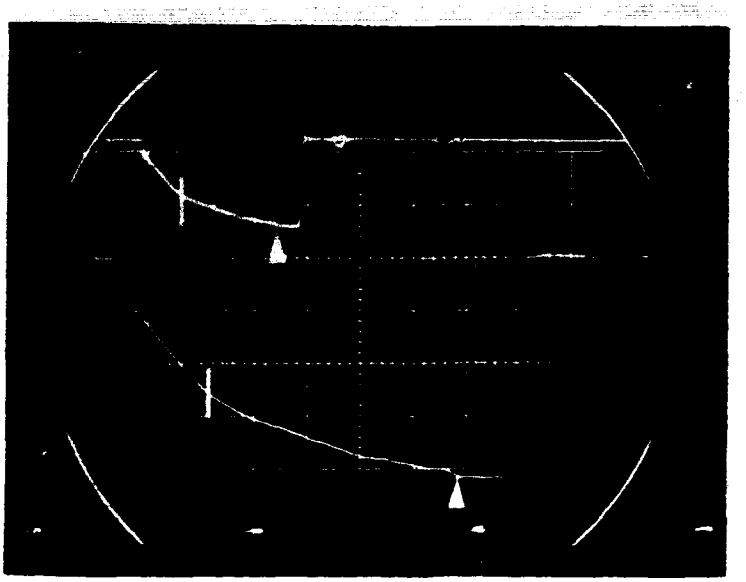

Figure 16

Horiz: Upper 5 μsec/cm
Lower 2 μsec/cm
(3 μsec delay)

Vert: Upper 5 V/cm
Lower 2 V/cm

Load: 0.625" PETN
(1.0 gm/cm^3)
0.625" 25% RDX-
75% Al (1.0 gm/cm^3)

Probe: 1-mil Nichrome
sandwich probe

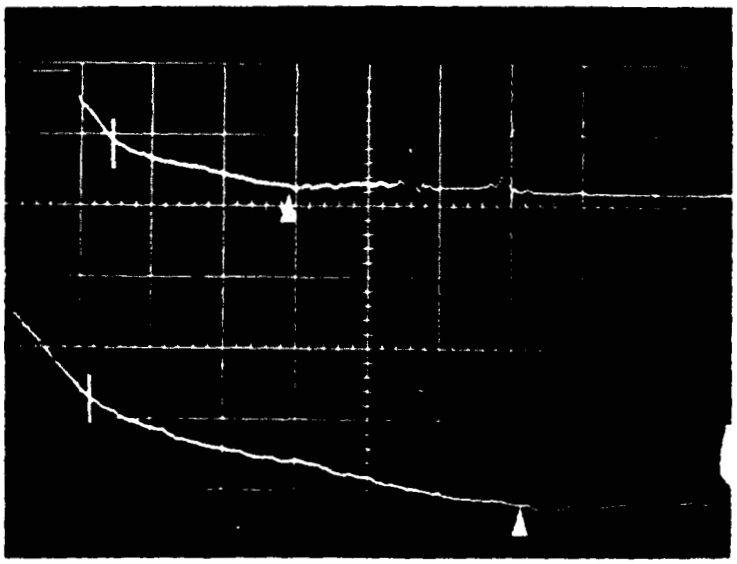

Figure 17

Horiz: Upper 5 μsec/cm
Lower 2 μsec/cm
(5 μsec delay)

Vert: Upper 5 V/cm
Lower 2 V/cm

Load: 0.625" PETN
(1.0 gm/cm^3)
0.625" 60% $KClO_4$ -
40% Al (1.5 gm/cm^3)

Probe: 1-mil Nichrome
sandwich probe

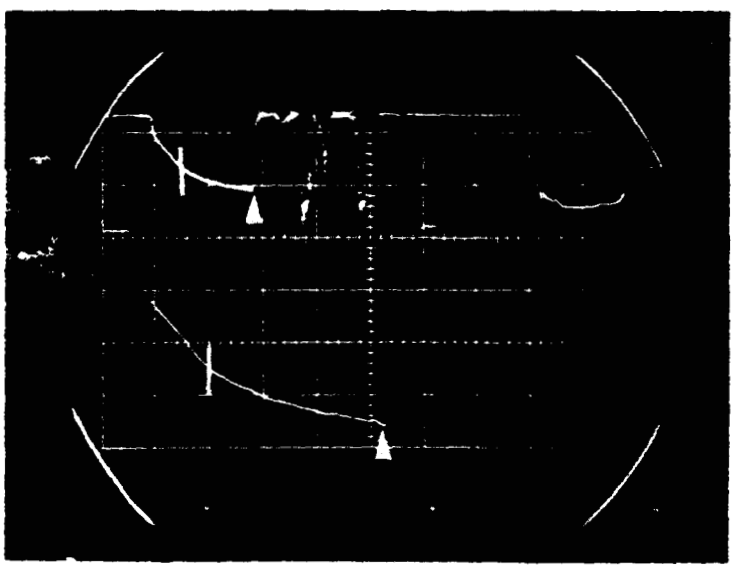

Figure 18

Horiz: Upper 5 μsec/cm
Lower 2 μsec/cm
(3 μsec delay)

Vert: Upper 5 V/cm
Lower 2 V/cm

Load: 0.625" PETN
(1.0 gm/cm^3)
0.625" CuO-Mg
(1.5 gm/cm^3)

Probe: 1-mil Nichrome
sandwich probe

Figures 19 through 21 are oscilloscope traces obtained from shots of test bodies loaded for 0.500-inch with PETN and for the remaining 0.750-inch with the three individual pyrotechnic mixes. The 0.5-mil insulated Moleculoy wire probe was employed in these shots. Because of the short PETN column and slow turn-on response with this type of probe, the PETN section of the curve is not as linear as in Figures 16 through 18. However, the deflagration traces definitely are more readable for the 0.5-mil Moleculoy probe.

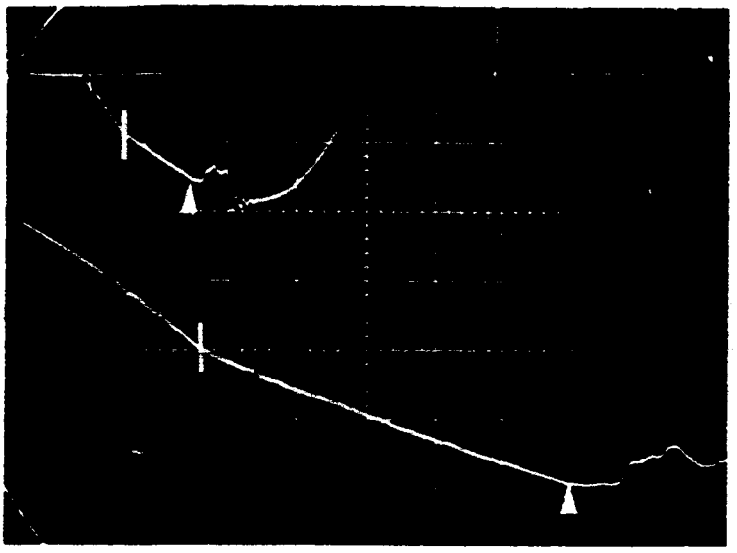

Figure 19

Horiz: Upper 5 μsec/cm
Lower 1 μsec/cm
(4 μsec delay)

Vert: Upper 5 V/cm
Lower 2 V/cm

Load: 0.500" PETN
(1.0 gm/cm^3)
0.750" 50% RDX -
50% Al (1.0 gm/cm^3)

Probe: 0.5-mil insulated
Moleculoy wire

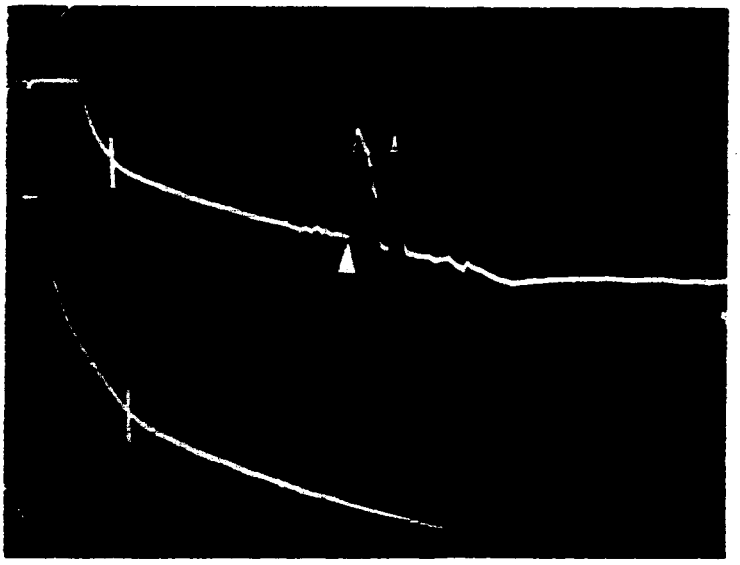

Figure 20

Horiz: Upper 5 μsec/cm
Lower 2 μsec/cm
(3 μsec delay)

Vert: Upper 5 V/cm
Lower 2 V/cm

Load: 0.500" PETN
(1.0 gm/cm^3)
0.750" 60% $KClO_4$ -
40% Al (1.2 gm/cm^3)

Probe: 0.5-mil insulated
Moleculoy wire

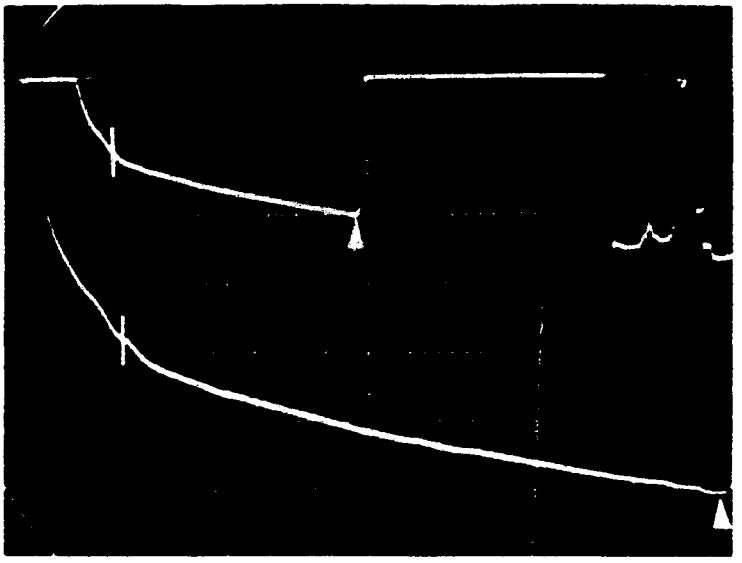

Figure 21

Horiz: Upper 5 μsec/cm
Lower 2 μsec/cm
(3 μsec delay)

Vert: Upper 5 V/cm
Lower 2 V/cm

Load: 0.500" PETN
(1.0 gm/cm^3)
0.750" CuO-Mg
(1.7 gm/cm^3)

Probe: 0.5-mil insulated
Moleculoy wire

A trace (Figure 22) obtained from a 1-mil Nichrome sandwich probe in the acceptor of a two-section TBI configuration clearly discloses an almost constant voltage for 0.4 μsec after the initial fall time. This represents the period prior to high order detonation when the reaction was slowly building up.

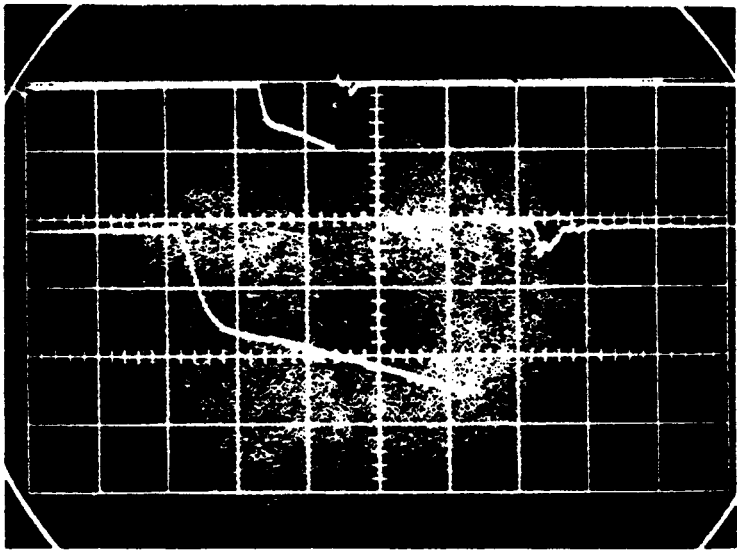

Figure 22

Horiz: Upper 2 μsec/cm
Lower: 0.5 μsec/cm
(5 μsec delay)

Vert: Upper 5 V/cm
Lower 2 V/cm

Simulated TBI geometry
(90-mil bulkhead)

Load: Donor: PETN
(1.65 gm/cm^3)
Acceptor: PETN
(1.25 gm/cm^3)

Probe: 1-mil Nichrome
sandwich probe

B. METALLURGICAL

To monitor the transition of detonation to deflagration in the Through Bulkhead Initiator development, metallurgical microhardness measurement techniques were employed. The use of the microhardness method of monitoring the shock hardening of metals permits investigation of changes of hardness over the submillimeter range.

Experiments were conducted in metal samples to determine the transition pressure in systems where electrical probes were used as backup and in systems where other monitoring methods could not be used. The tests were made in Armco magnetic ingot iron and Austenitic stainless steel which covered the Chapmann-Jouguet pressure region generated by a 0.100-inch diameter column of PETN at densities of 0.8 to 1.7 gm/cm^3.

The usefulness of metallurgical measurements depends upon the fact that as an explosive detonates, the peak pressures generated within the explosive (Chapman-Jouguet pressure) depend upon the detonation velocity. The general relationship between the detonation velocity, D, the explosive density, ρ, and the Chapman-Jouguet pressure, P, is given by:

$$P = K\rho D^2, \tag{7}$$

where K is a constant that depends upon the energy release of the explosive and the equation of state of the products. From this equation it can be seen that the pressure is a sensitive function of the reaction wave velocity and would be an interesting quantity to monitor to determine velocity.

Although it is rather difficult to monitor the Chapman-Jouguet pressure directly, the induced shock pressure in the metal walls containing the explosive can be monitored, and by appropriate calculations this shock pressure can be related to the detonation velocity. In this case, the relationship between metal hardness and detonation velocity will be empirically determined and the shock calculations used merely to correlate our measurements with other measurements of the change in hardness with shock pressure.

Through the transition zone it will be assumed that the relationship between shock strength and reaction wave velocity is the same in the pyrotechnic as it was in PETN. This, of course, is not strictly true, but will not seriously affect the measurements of the lengths of the transition zones.

1. Metallurgical Measurements

a. General Theory. When a rapid reaction takes place in a confined vessel, any pressure generated by the reaction will cause deformation of the material comprising the confinement vessel. If, as in the case of an explosive charge, the pressure generated is in the form of a shock wave of sufficient magnitude, the metal in immediate contact with the reaction will be rigorously condensed. As the pressure-induced compressive waves move into the material they are attenuated and the magnitude of the wave drops rapidly to a value which will not have sufficient strength to affect the metal.

A metal is said to have been cold worked if its grains are in a distorted condition when plastic deformation is completed.* Plastic deformation of metal is defined as mechanical deformation at a temperature below the transformation temperature. Not only the external appearance of the metal is changed during plastic deformation, but pronounced changes are manifested in the physical properties of the metal.

*Elements of Physical Metallurgy, Albert G. Grey, 1951.

The hardness of the metal, a term metallurgically defining the metal's ability to resist indentation, undergoes the most important change during impulse loading. With progressive amounts of distortion, the resistance of the metal to further deformation constantly increases as a result of strain or work hardening. In conjunction with an increase in hardness during the explosive working of metal, the tensile strength of the material is also increased. The resistance to indentation is directly related to compressive strength. Many of the metals and metal alloys show a close relation among hardness tests and between hardness and tensile strength.

Under microscopic examination the results of the compressive stress waves can be observed in the grains of the material. The microstructural appearance will vary to some extent depending on the magnitude of the stress wave generated by the explosive charge. Figure 23 is a micrographic comparison of the Armco control sample, used to determine the hardness in an annealed condition and in a functioned test body which had a PETN density of 1.0. Figure 23b shows the permanent plastic deformation in the form of crystallographic twinning. Crystal twinning represents shear movements of atoms where the crystals shear across certain crystallographic planes in certain directions. Twining of iron and many steels can occur by impact loading at room temperature and by slow deformation at low temperatures.

b. Hardness Testing. Several methods have been developed for the determination of the hardness value for metal systems. The most popular hardness test used in metallurgical analysis is the "Indentation Hardness Test." This title identifies the tests utilizing indenters of fixed geometry under static loads. To intelligently interpret the hardness value a knowledge of the composition and condition of the metal during the test is required.

Due to the extreme range of hardness exhibited by the ferrous and nonferrous metals, at least eight methods for determination of hardness have been devised. The principal of all tests is, however, the same. It usually consists of impressing an indenter of fixed geometry into a specimen which has been prepared and is resting on a rigid platform. The indenter is under a known static

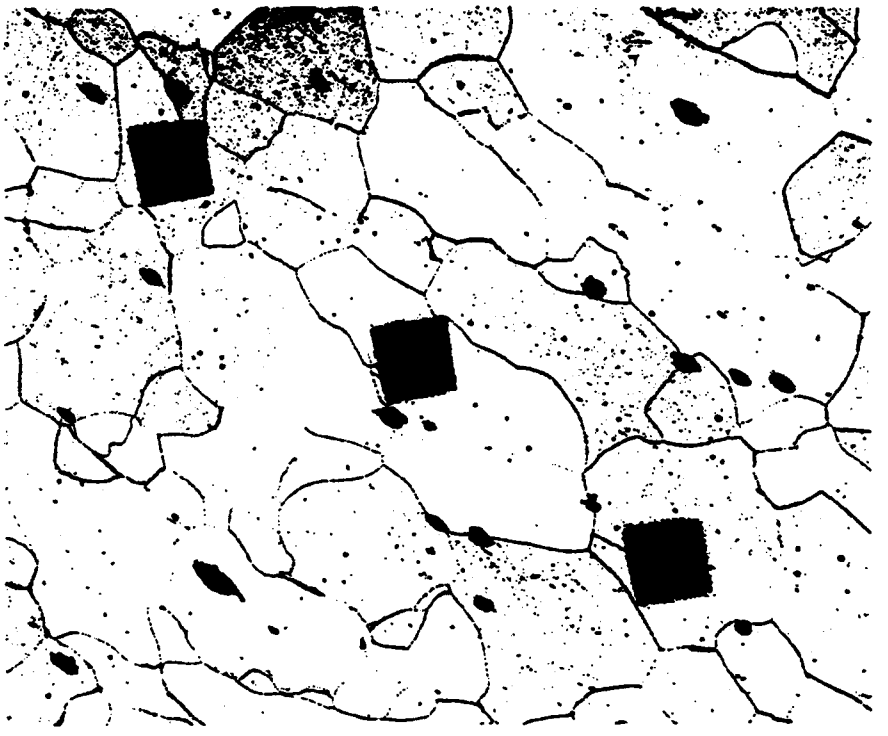

Figure 23a. Control Sample of Armco Iron in Annealed Condition

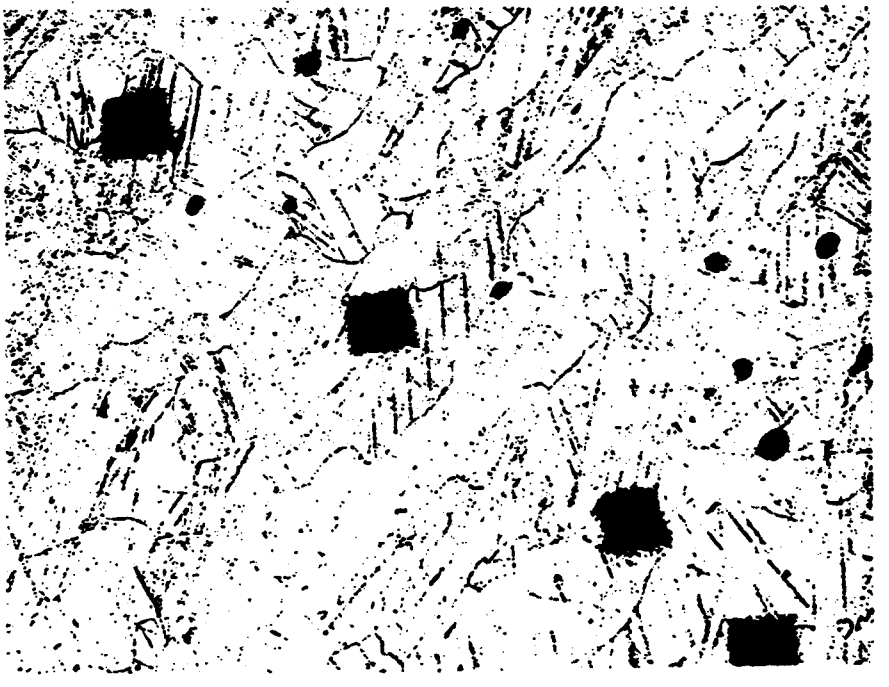

Figure 23b. Test sample that was explosively loaded with a 1/10-inch column of PETN at a density of 1.0. Figure indicates plastic deformation in the form of crystallographic twinning.

load applied either directly or by means of a lever system. There are copious amounts of metallurgical literature which discuss the various types of hardness tests. The Knoop and Vickers tests were selected for this study. The diamond indenters were preferred since they deform less than those made of steel.

c. Knoop Hardness Test. The Knoop hardness test employs a long, narrow, rhombic diamond point, shown in Figure 24. This indenter is a pyramidal form; the longitudinal angle is 172 degrees, 30 minutes; the transverse angle is 130 degrees. The longitudinal length is 7.11 times the transverse length. The range of load weights for this test is 25 grams to 50 kilograms. This test is recommended for hardness determination of extremely thin materials, plated surfaces, and exceptionally hard and brittle materials. The long diagonal is slightly affected by elastic recovery when the load is removed. With the long narrow indenter, more readings can be taken over a given length of surface if the indentations are placed so that the long axes are parallel to each other.

d. Vickers Diamond Pyramid Hardness (DPH) Test. The Vickers test employs a square based diamond pyramid indenter with an included angle of 136 degrees between opposite faces as shown in Figure 25. The indenter is forced into the test material with loads ranging from 5 grams to 100 kilograms. Three-hundred gram loads were used for this study. The impression dimensions made by the indenter are measured through a microscope which has a knife-edge micrometer. The depth of indentation varies with load and is approximately 1/7 the length of the measured diagonal. The DPH technique with a 300-gram load was used since it offered simpler measurement procedures and gave a deeper penetration for a given area of indentation.

e. Surface Preparation. To reduce the error in the hardness measurements the material surfaces must be lapped and free from scratches and pits which might influence the hardness value. The smaller the indentation, due either to light loads or hard material, the better the surface must be. It is almost impossible to prepare metal surfaces without influencing the surface hardness of the first few microns. Small impressions will be influenced a great deal by any transient hardness increase. It is stated that if the length of

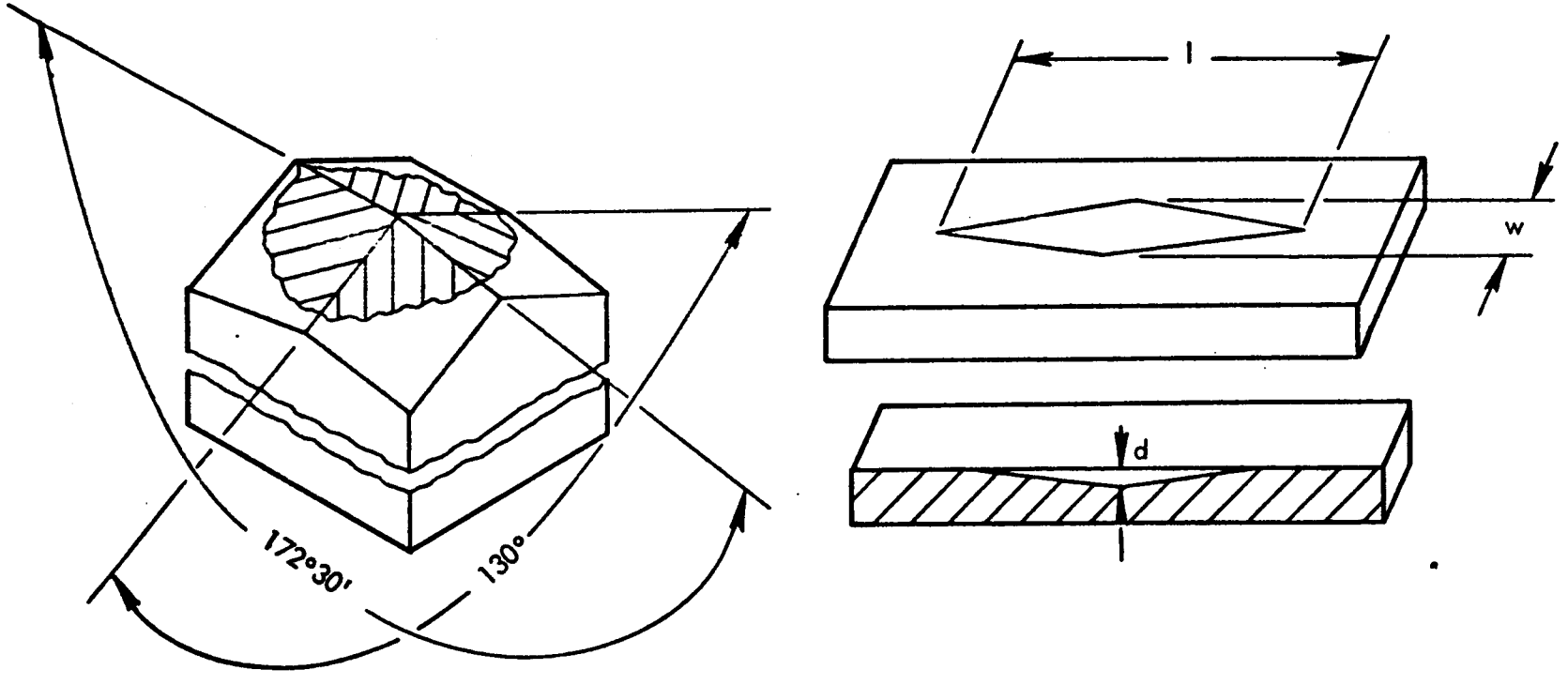

Figure 24. Illustrates schematically the shape of the Knoop indenter and associated shape of the surface impression. (From The Principles of Metallographic Laboratory Practice, Kehl, McGraw-Hill, 1959.)

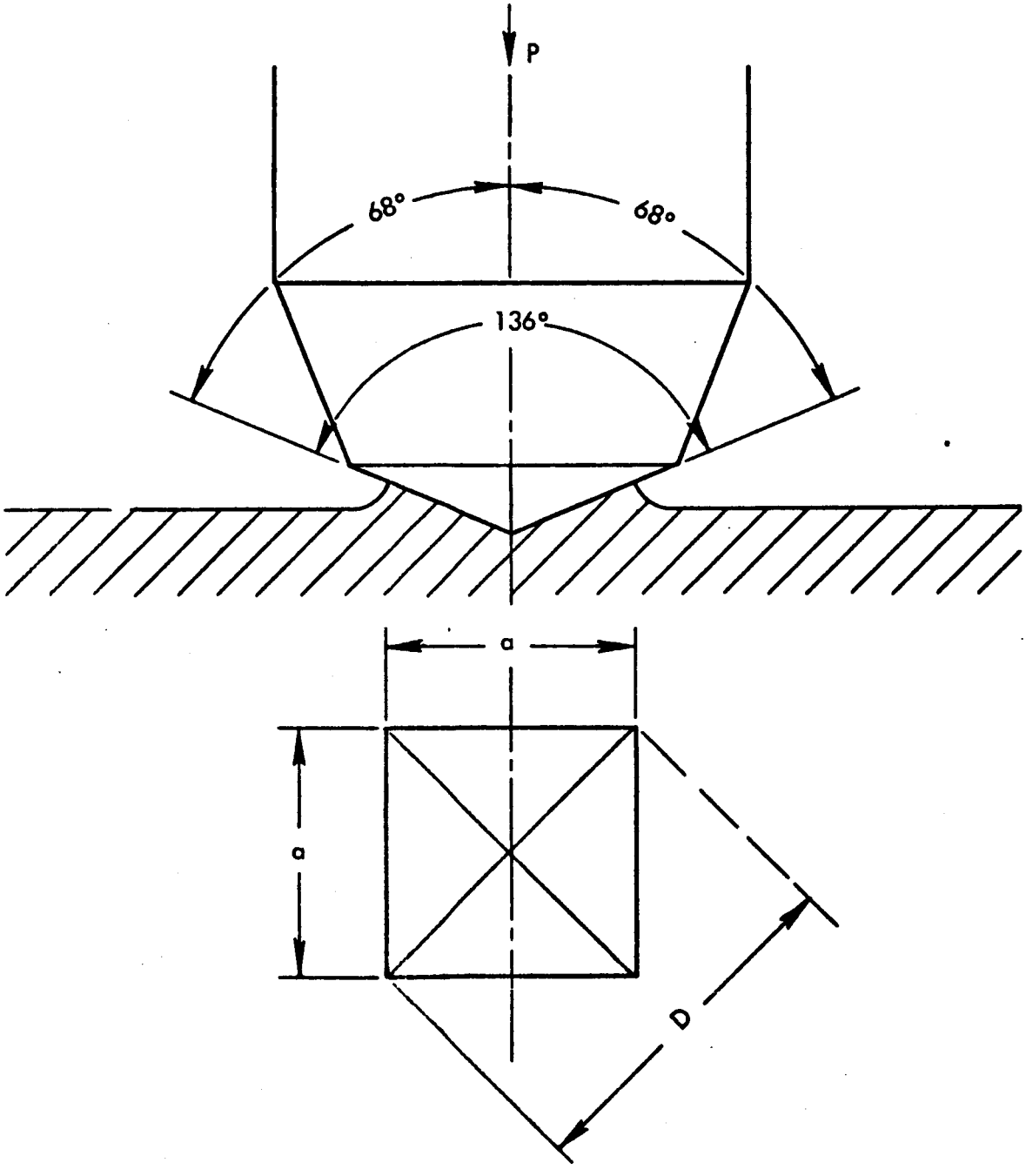

Figure 25. Illustrates schematically the Vickers indenter and the impression formed on the test surface. (From The Principles of Metallographic Laboratory Practice, Kehl, McGraw-Hill, 1949.)

the impression of the Knoop indenter is about 90 percent of the long diagonal of the indenter the error will be negligible. Thus, testing with light loads is not recommended except where required.

2. Preliminary Metal Selection

Three metals were investigated for possible use for this study. Since the hardness reading is affected by impurities in a system, the three metals were selected because of their homogeneous nature. Where mechanical and chemical properties remain quite uniform in a specimen or group of specimens, differences in behavior should not be great.

a. Armco Ingot Iron. Shock hardening response of various metals available from the literature (see Figure 26), indicated that Armco iron has a good response over the shock pressure range from 0 to 130 kilobars. At about 130 kilobars the iron undergoes a phase change or transition. The transition point of 130 kilobars for this metal will serve as a calibration point for the study. Armco Ingot Iron is a high purity commercially available material.

b. Stainless Steel. The Link Ordnance CDF Pyrogen Initiator is manufactured from 303 stainless steel. The initial study of this steel revealed a considerable amount of scatter which is attributed to the sulphur stringers, characteristic of 303 stainless steel. Stainless steel 301, which is a more homogeneous stainless, but not available commercially, was produced at the Stanford Research Institute Metallurgical Laboratory. This was done after testing revealed that stainless steel 304 and 321 had too much scatter in hardness readings. Stainless steel, according to SRI data, has good sensitivity in the intermediate or 100 to 350 kilobar shock pressure range, and fair sensitivity over the low pressure range.

Stainless steel 301, 304, and 321 are considered austenitic stainless steel. This steel classification is nonmagnetic and cannot be hardened by heat treatment. These metals can, however, be hardened considerably by cold working. Because of its low chromium and nickel content (17 Cr - 7 Ni), 301 stainless produces the maximum work hardening.

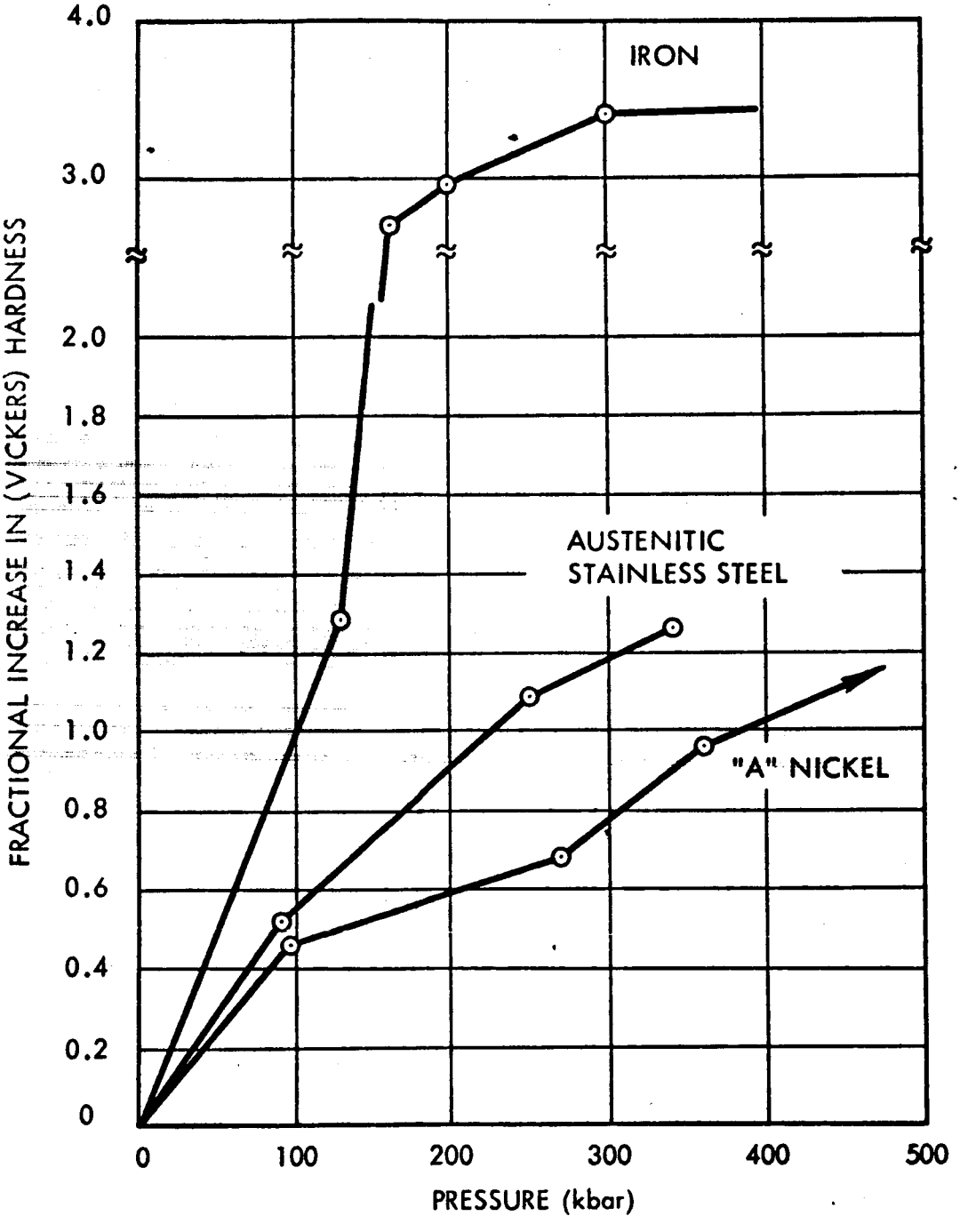

Figure 26. Shock Hardening of Various Metals from International Science and Technology, George E. Duvall, April 1963

c. Nickel. Nickel 200 was selected for this program because it is a face-centered cubic metal. Face-centered cubic metals such as nickel, unlike the body-centered cubic iron and mild steels, change uniformly with intensification of stress. Nickel and many of the other face-centered cubic metals deform in about the same way under impulsive loading as under static loading.* It was hoped that if transformation twinning and dislocation responded erratically, it would permit clear interpretation of the simple hardening mechanisms. The shock hardening curve for nickel indicates fair sensitivity above a shock pressure of 350 kilobars, although quite low sensitivity in the range of interest.

3. Final Metal Selection

a. Armco Iron. Figure 27 is a composite graph of the results of the plotting of hardness vs. distance from the explosive-inert interface. The range of the average value of hardness vs. explosive density is from a hardness of 90 for the control sample to a high of 260 ±10 for the sample with an explosive density of 1.7. The hardness deviation was worse than expected, and measurements in general showed a deviation of plus or minus 10 points.

b. Nickel 200. Figure 28 shows a composite graph of all nickel 200 shots at explosive densities ranging from $\rho = 0.85$ to $\rho = 1.72$. The average hardness values over this density range are from 120 ±10 for the control sample and 245 ±5 to 260 ±10 for those loaded with PETN. Since the nickel exhibited such a small hardness range over the selected density range and some extreme variations within a sample, it was eliminated from the test program.

c. Stainless Steel. Preliminary tests on stainless steel 321 revealed a scatter which was considered excessive. An attempt to purchase stainless steel 301 in experimental lot sizes proved futile. Due to schedule slippage, Stanford Research Institute was authorized to manufacture 20 pounds of vacuum cast stainless steel 301. No preliminary data were taken for this material, due to tight schedule; it was used for calibration without submission to the PETN-inert series.

*Rinehart and Pearson, Explosive Working of Metals, MacMillan, 1963.

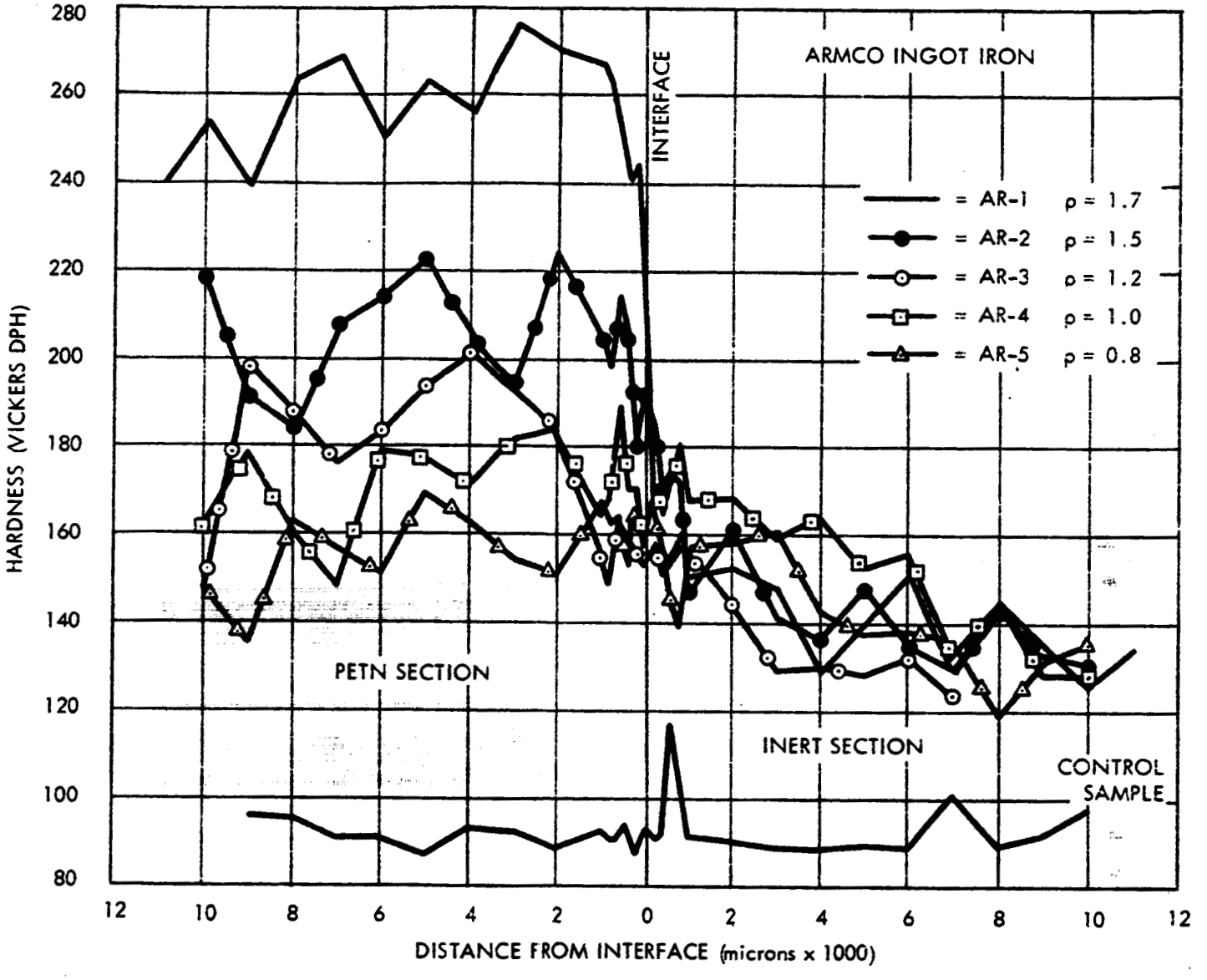

Figure 27. Plot of Hardness vs. Distance from PETN-Inert Interface for Armco Ingot Iron

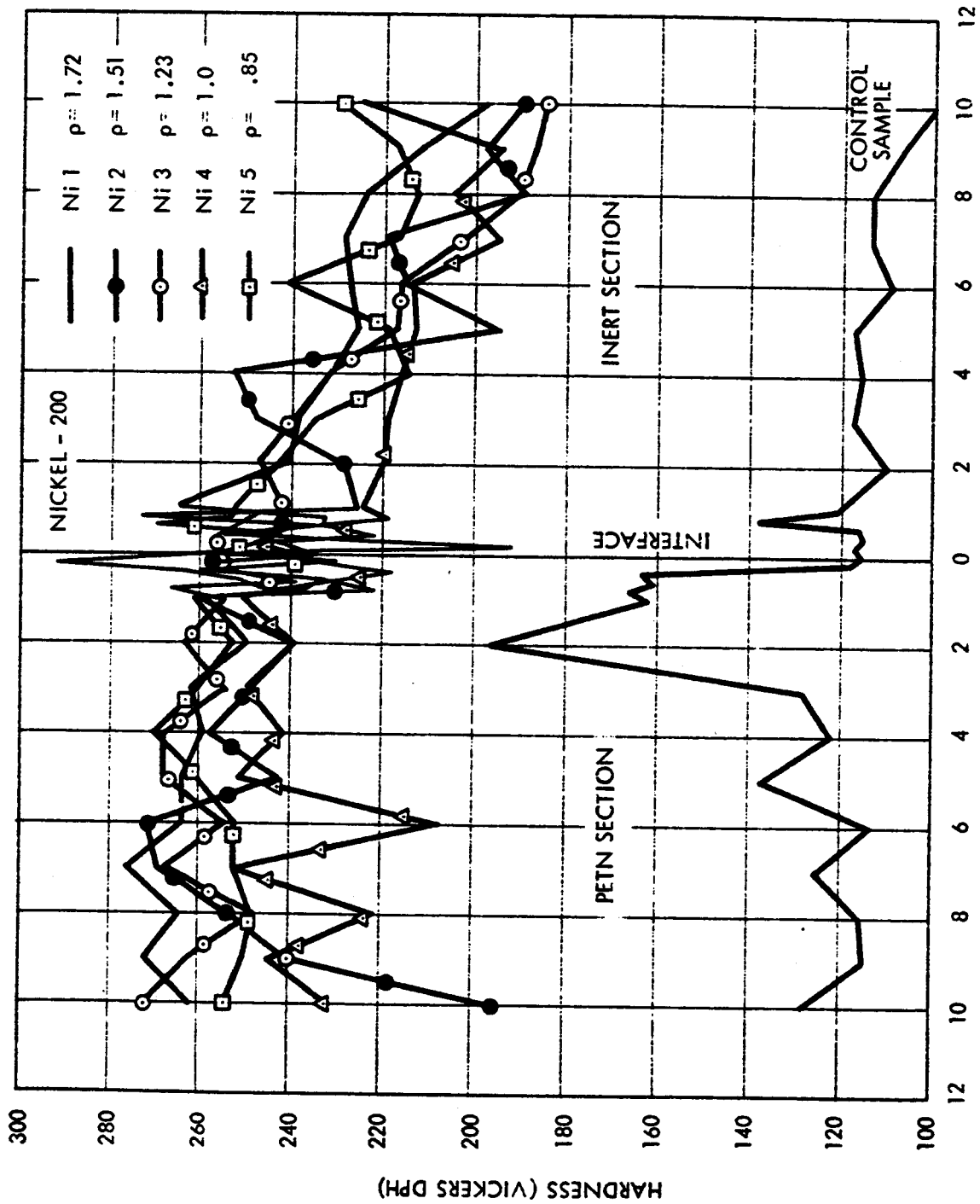

Figure 28. Plot of Hardness vs. Distance from PETN-Inert Interface for Nickel 200

4. Calibration

To observe the detonation pressure decay in an explosive-inert system, the standard test samples of Armco iron and nickel 200 were loaded with a 0.500-inch long, 0.100-inch diameter column of PETN. The remaining 0.750-inch of the 1.250-inch test sample was loaded with $CaCO_3$. The PETN and the $CaCO_3$ were pressed into the 0.100-inch diameter column in increments of 0.100-inch. The PETN was initiated with a 3-inch section of 10-grain MDF. After the PETN had been detonated the sample was sectioned and polished, and hardness indications were taken parallel to the explosive-metal interface. The readings were taken about the explosive-inert interface. The following table gives the complete explosive density range in Armco iron.

Table V

PETN-INERT SHOT FIRED IN ARMCO IRON

Sample No.	Load Density (gm/cm^3)	Average Vickers Hardness in PETN Section (approx std deviation)		Distance from Interface to Hardness of 130 (microns)
AR-1	1.7	260	(10)	11,000
AR-2	1.5	205	(10)	10,000
AR-3	1.2	185	(10)	3,000
AR-4	1.0	170	(10)	8,500
AR-5	0.8	157	(10)	7,500
Unloaded Sample	—	90	(5)	—

Table VI shows the same density range in nickel 200. The stainless steel was not ready at the time of the PETN-Inert Study and, due to schedule slippage, it was never fired.

a. PETN Density vs. Hardness Curves. To obtain the curves of PETN density vs. hardness, the standard samples of Armco iron and stainless steel 301 were loaded over the complete sample length with PETN. Shots were made to

Table VI

PETN-INERT SHOT FIRED IN NICKEL 200

Sample No.	Load Density (gm/cm^3)	Average Vickers Hardness in PETN Section (approx std deviation)		Distance from Interface to Hardness of 200 in the Inert Section (microns)
Ni-1	1.7	200	(10)	9,800
Ni-2	1.5	250	(15)	4,900
Ni-3	1.2	260	(10)	7,200
Ni-4	1.0	245	(5)	6,700
Ni-5	0.8	255	(5)	(10,000 plus)
Unloaded Sample	—	120	(10)	—

represent the density range of 0.8 to 1.7 grams per cubic centimeter. These units were functioned in the manner described above and then subjected to hardness examination. Figure 29 is the plot of PETN density vs. hardness for Armco iron. Figure 30 is the plot of PETN density vs. hardness for stainless steel 301.

b. Dual Density of PETN. This test was conducted for observation of the detonation pressure decay as the detonation travels from a high density explosive into a low density of the same explosive. The standard sample was used for this series of tests; the first half of the 0.100-inch diameter column was loaded with PETN at a density greater than 1.2, the second half of the column was loaded to a density of less than 1.2. The Armco iron and the stainless steel were used as the material for the test samples. The steady state values observed in this test are shown in Table VII.

c. Results of PETN Pyromixes. Three types of pyromixes were selected for the ignition study, RDX-Al, $KClO_4$-Al and the TBI mix of CuO-Mg. The loading configuration of this series is the same as that used in the PETN-inert series. A 0.500-inch length of PETN, at densities of 1.0 and 1.2 serves as the donor charge. The receptor charge consists of 0.750-inch of either RDX-Al,

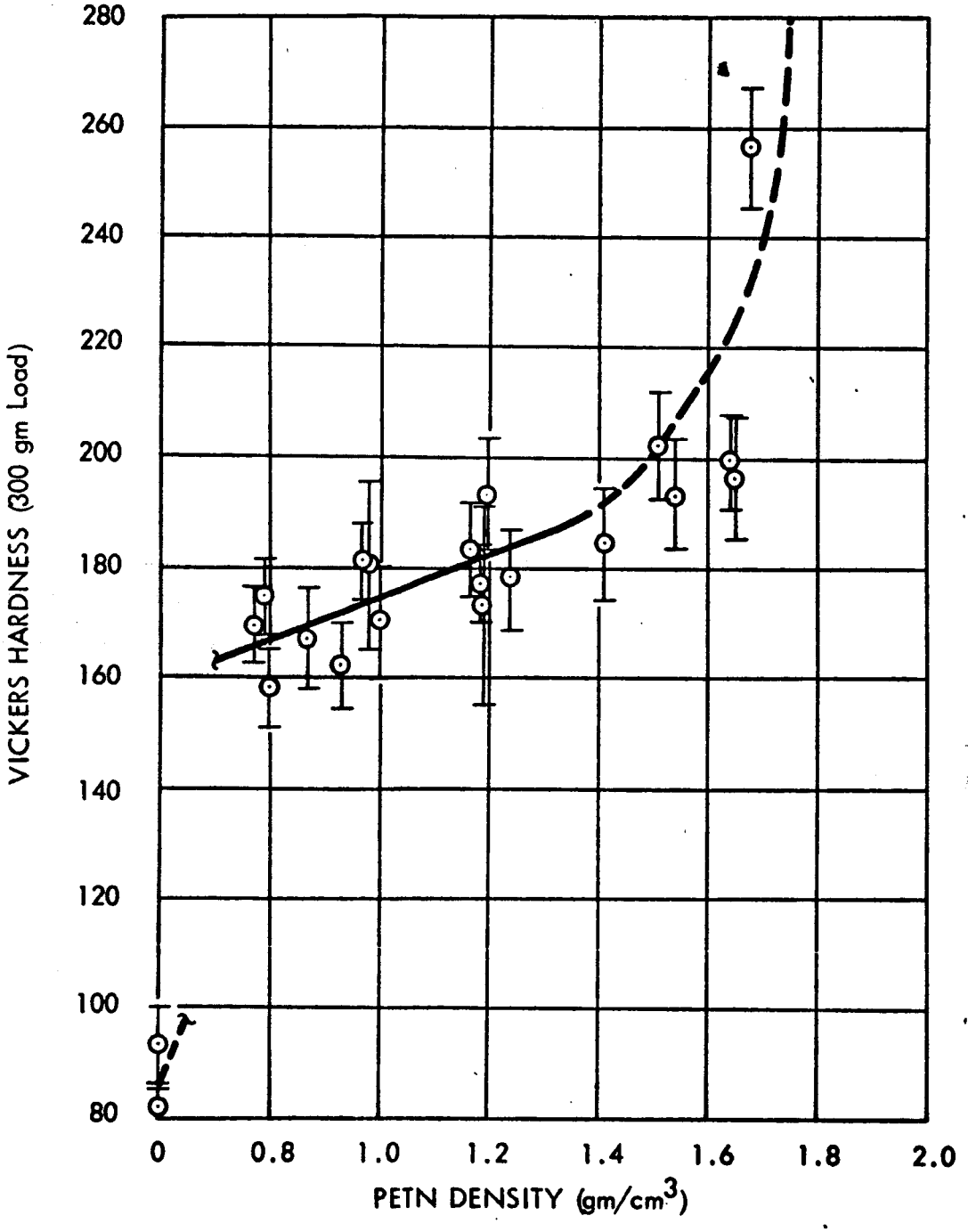

Figure 29. PETN Density vs. Hardness for Armco Iron

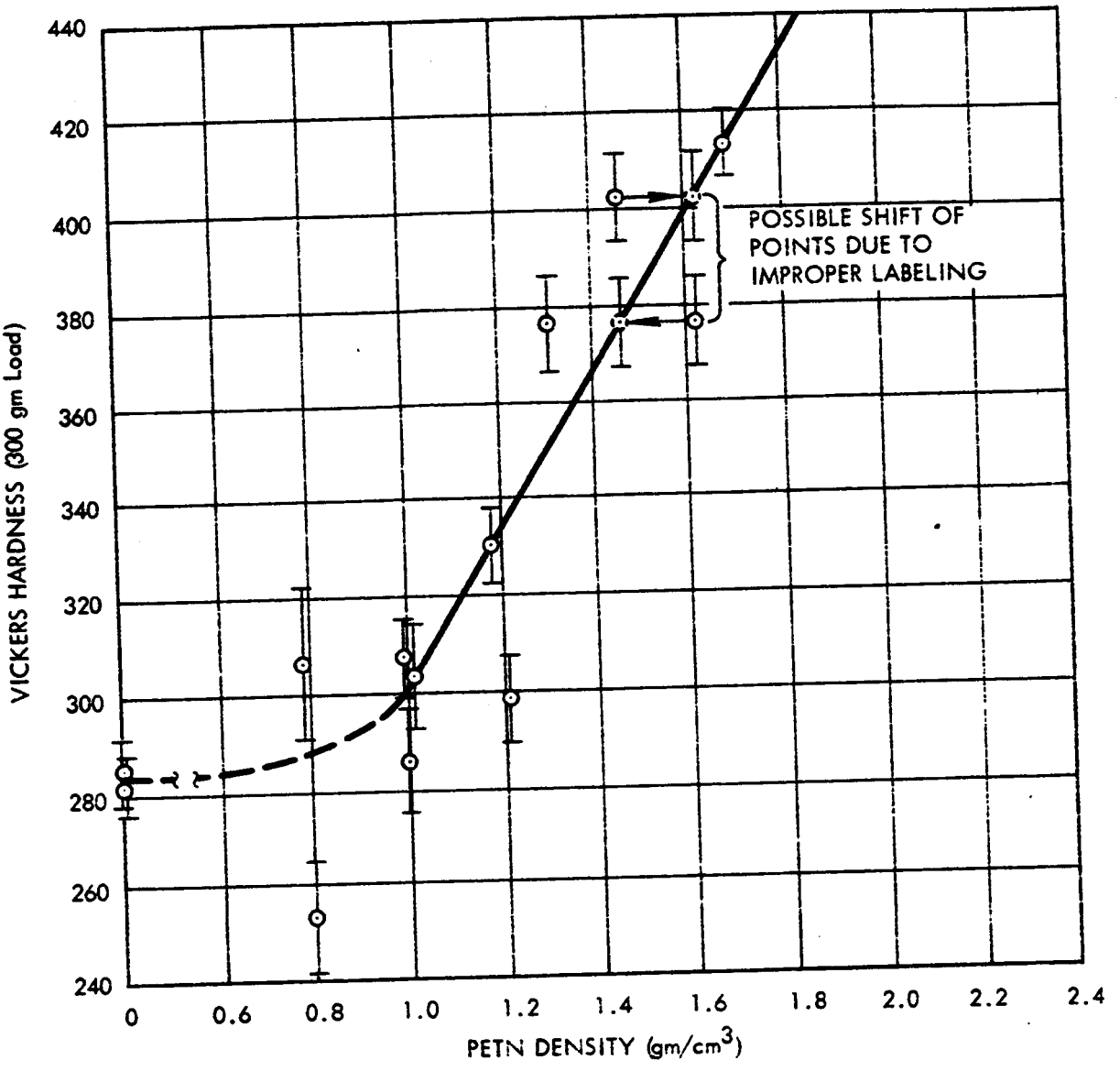

Figure 30. PETN Density vs. Hardness for Stainless Steel 301

Table VII

Sample No.	High Density Requested/Actual		Hardness	Low Density Requested/Actual		Hardness
Sl-8[a]	1.20	1.210	298 ±9	0.80	0.796	253 ±12[b]
Sl-11	1.50	1.510	376 ±10	1.00	0.995	285 ±10[b]
Sl-27	1.70	1.686	413 ±7	1.00	1.010	303 ±11
AR-25	1.70	1.640	199 ±8	1.00	0.97	181 ±6
AR-28	1.70	1.650	196 ±11	1.00	0.98	180 ±15
AR-18	1.20	1.170	183 ±9	0.80	0.77	169 ±7
AR-19	1.20	1.240	178 ±9	0.80	0.79	174 ±7

[a] Sl samples are SS 301 and AR samples are Armco iron.
[b] SS 301 sample hardnesses are equal to or less than in the annealed condition.

$KClO_4$-Al, or CuO-Mg at densities of 1.0, 1.2 and 1.7. Figure 31 is a graph of the PETN/RDX-Al shots in Armco iron. Figure 32 is the graph of the PETN/$KClO_4$-Al shots in Armco iron. Figure 33 is the graph of the PETN/CuO-Mg shots in Armco iron. The results of the pyromix shots in stainless steel 301 were too unreliable to interpret. Due to the unreliability of the stainless steel 301 in the lower ranges, the stainless steel data was eliminated from the metallurgical section of the test program.

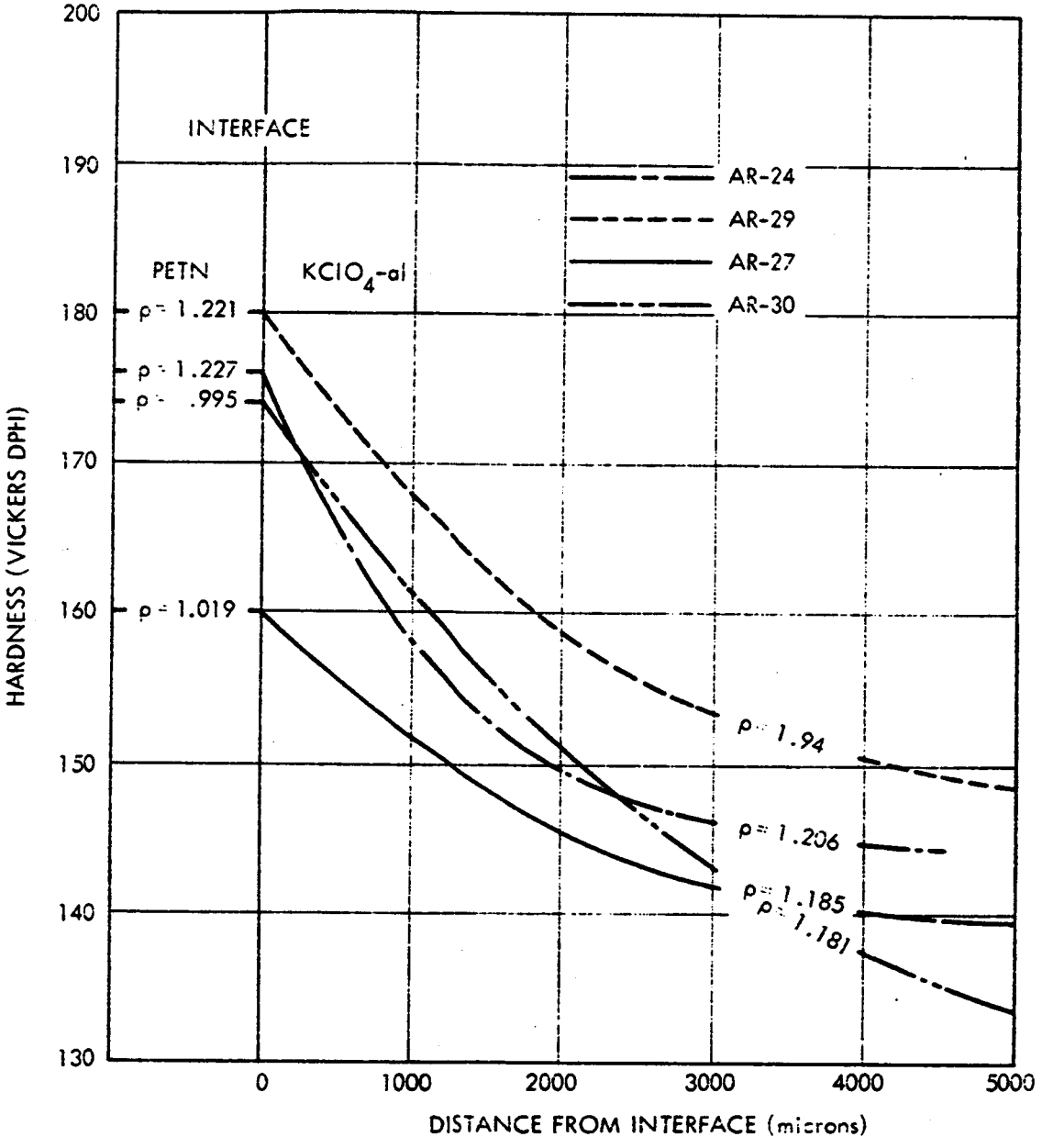

Figure 32. Armco Iron Hardness vs. Distance from PETN/$KClO_4$-Al Interface

Preceding page blank

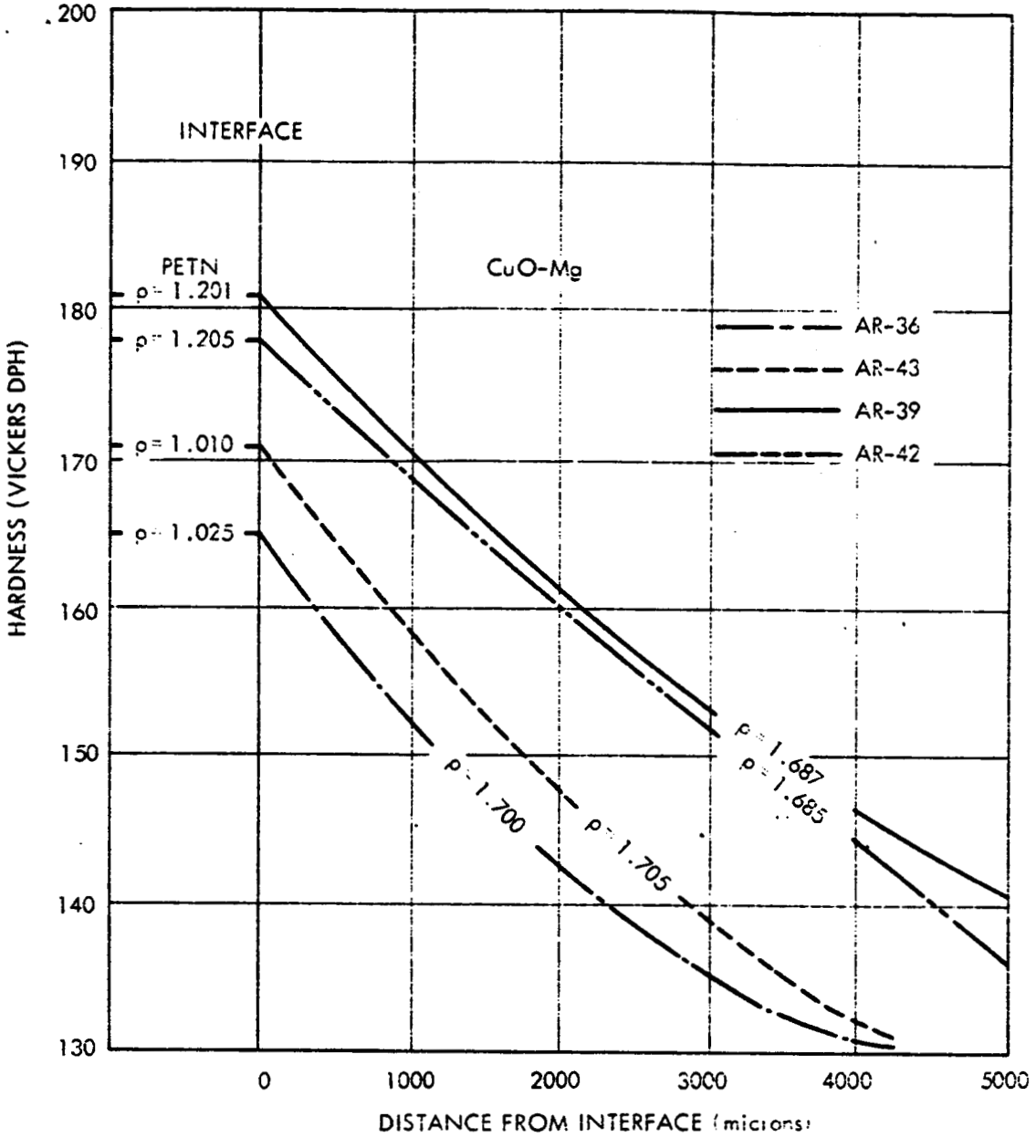

Figure 33. Armco Iron Hardness vs. Distance from PETN/CuO-Mg Interface

III RESULTS

A. PETN/INERT SYSTEM

Metallurgical analyses were made for a series of shots of test bodies loaded for 0.625 inch with constant density PETN and for the remaining 0.625 inch with inert $CaCO_3$.

The plot of detonation velocity vs. distance from the interface (shown in Figure 34) indicates that all shock velocities become constant at about 7 millimeters after the PETN/inert interface. (The method by which these graphs were obtained from hardness data is explained in following paragraphs discussing the PETN/pyrotechnic systems.)

The curve for AR-1 in Figure 34 appears to be rounded at the top as compared to the sharp initial drop of the other curves. This is due to the lack of shock attenuation in a metal system as compared to attenuation in the explosive system. The interpretation is based on detonation velocity of explosives, but the hardness traverse in the metal sample indicates pressures produced by shock attenuation in the metal at high shock strengths. This effect is not evident at lower shock strengths.

No electrical probes were used in the PETN/inert series fired in Armco iron bodies. A series was fired in brass using the "sandwich" electrical probe, but the data obtained in the inert region was inadequate to justify any velocity data. However, no measurements were attempted with the more sensitive 0.5-mil Moleculoy probe, which might have provided sufficient electrical data to substantiate the metallurgical results.

Table VIII is a tabulation of values of k for Equation (4). These values were obtained by plotting D/D_1 vs. x on two-cycle log-log paper as shown in Figure 35. D_1 is the velocity at one millimeter past the interface. All values of k for the PETN/inert series were above the 0.12 predicted by Eyring for

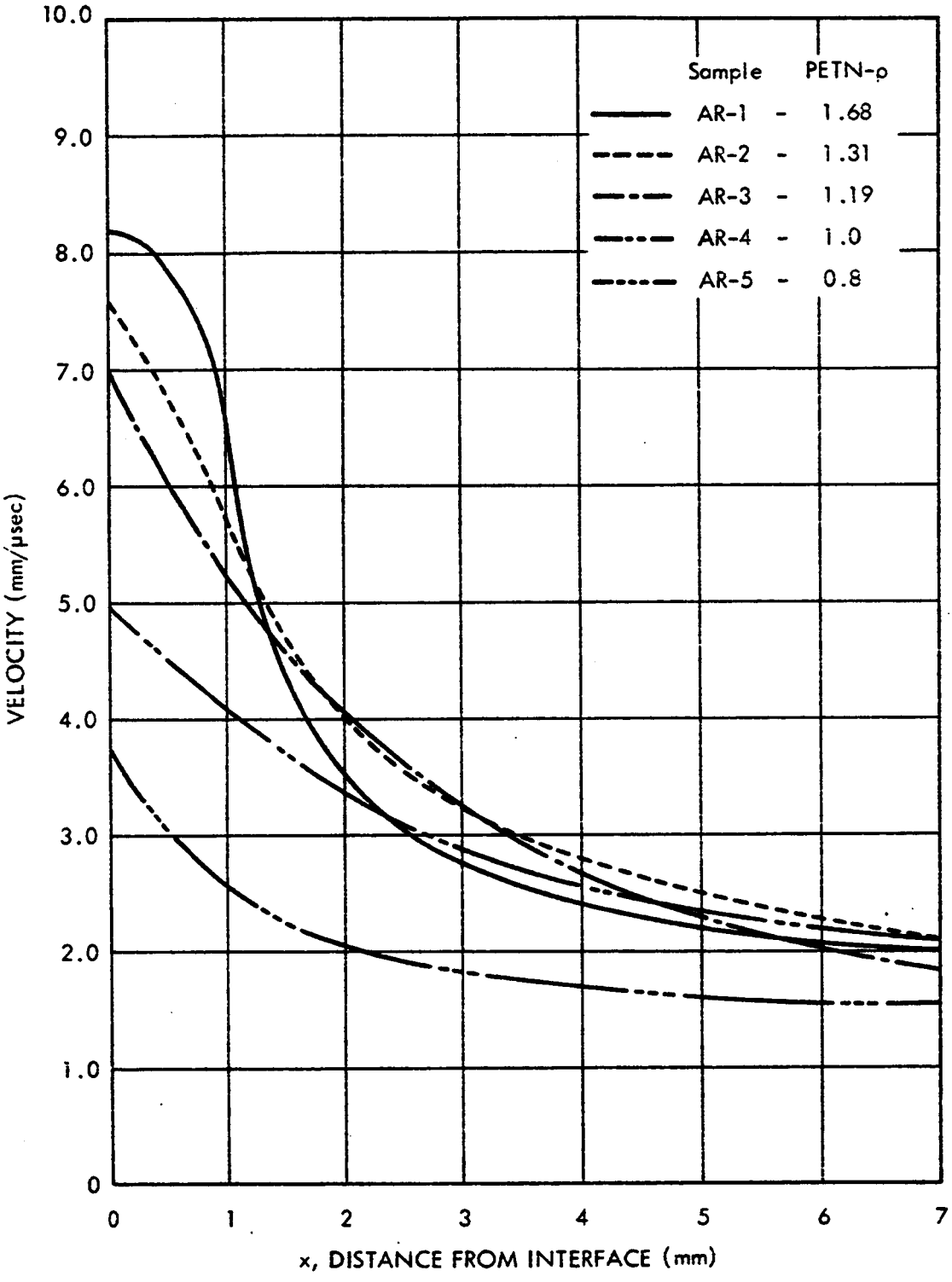

Figure 34. Plot of Velocity vs. Distance from Interface for PETN/Inert Series

Table VIII

VALUES OF k FOR PETN/INERT SERIES

Test Serial No.	PETN Donor ρ (cm/cm^3)	Inert Acceptor ρ (gm/cm^3)	k (metallurgical)
AR-1	1.68	1.68	0.48
AR-2	1.51	1.51	0.494
AR-3	1.19	1.19	0.479
AR-4	1.0	1.0	0.372
AR-5	0.8	0.8	0.301

typical explosives at crystal density. It should be noted that k is not the same for each example of this series, but decreases with decreasing explosive density and input shock.

B. PETN/PETN SYSTEM

The detonation velocity transition in the high density to low density PETN series is shown in Figure 36. Because of the short distances involved, there were not enough hardness measurements in the transition region to indicate the shape of the transition curve. Therefore, for the metallurgical measurements, a straight line is used to represent the velocity transition between the high density and low density steady state velocities.

Figure 37 shows some of the better velocity curves obtained with the electrical probe from PETN/PETN shots. This technique allowed a continuous velocity record through the transition region, but trace magnification was not adequate to permit certainty as to the velocity curve characteristics. In particular, a few curves suggested that the velocity might decrease below the steady state velocity for some portion of a millimeter, and a few curves appeared to indicate an S-shaped transition with sharp velocity decrease at each end of the transition. However, most slopes were of the exponential shape shown in Figure 37.

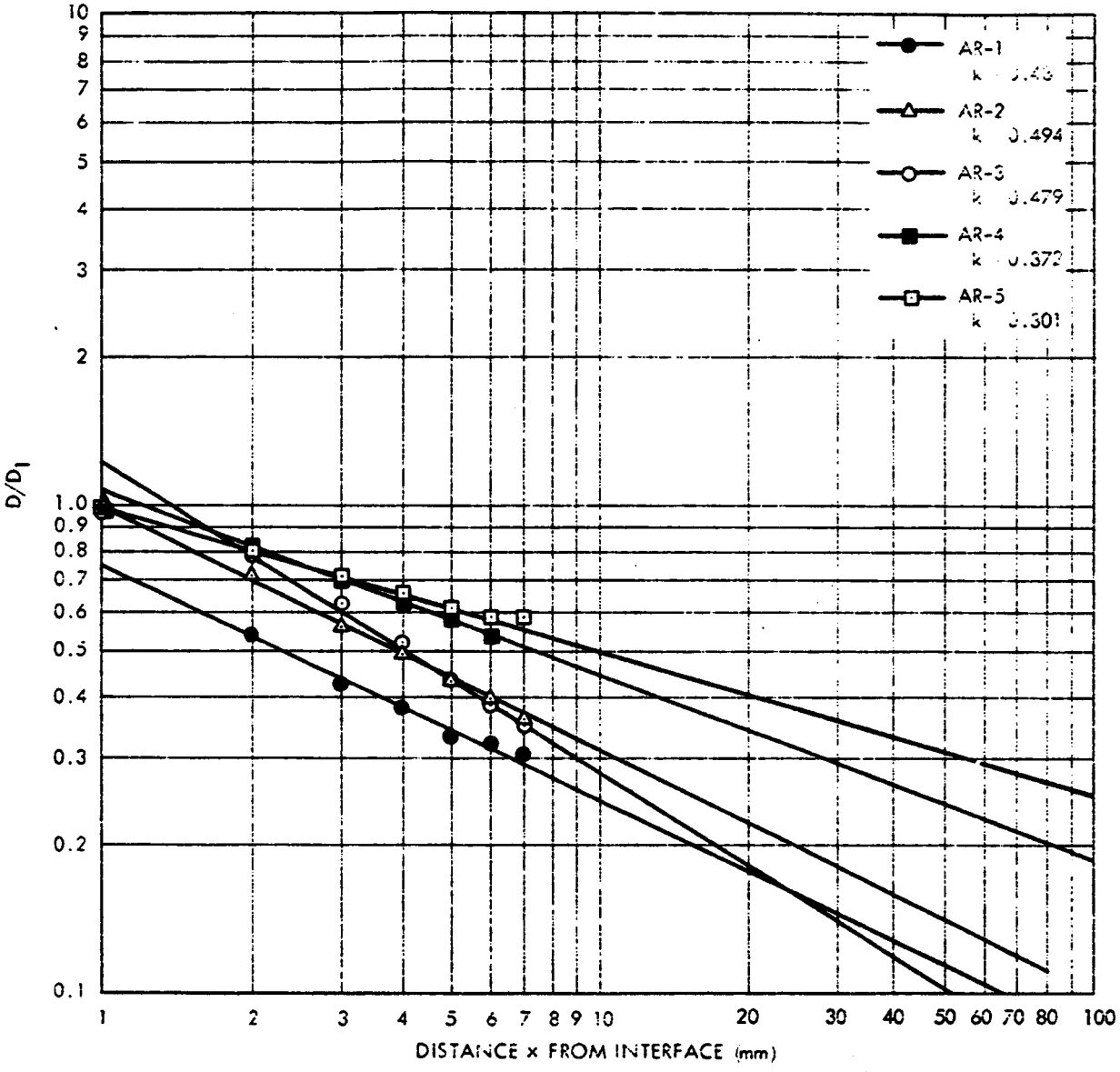

Figure 35. Plot of D/D_1 vs. Distance from Interface for PETN/Inert Series

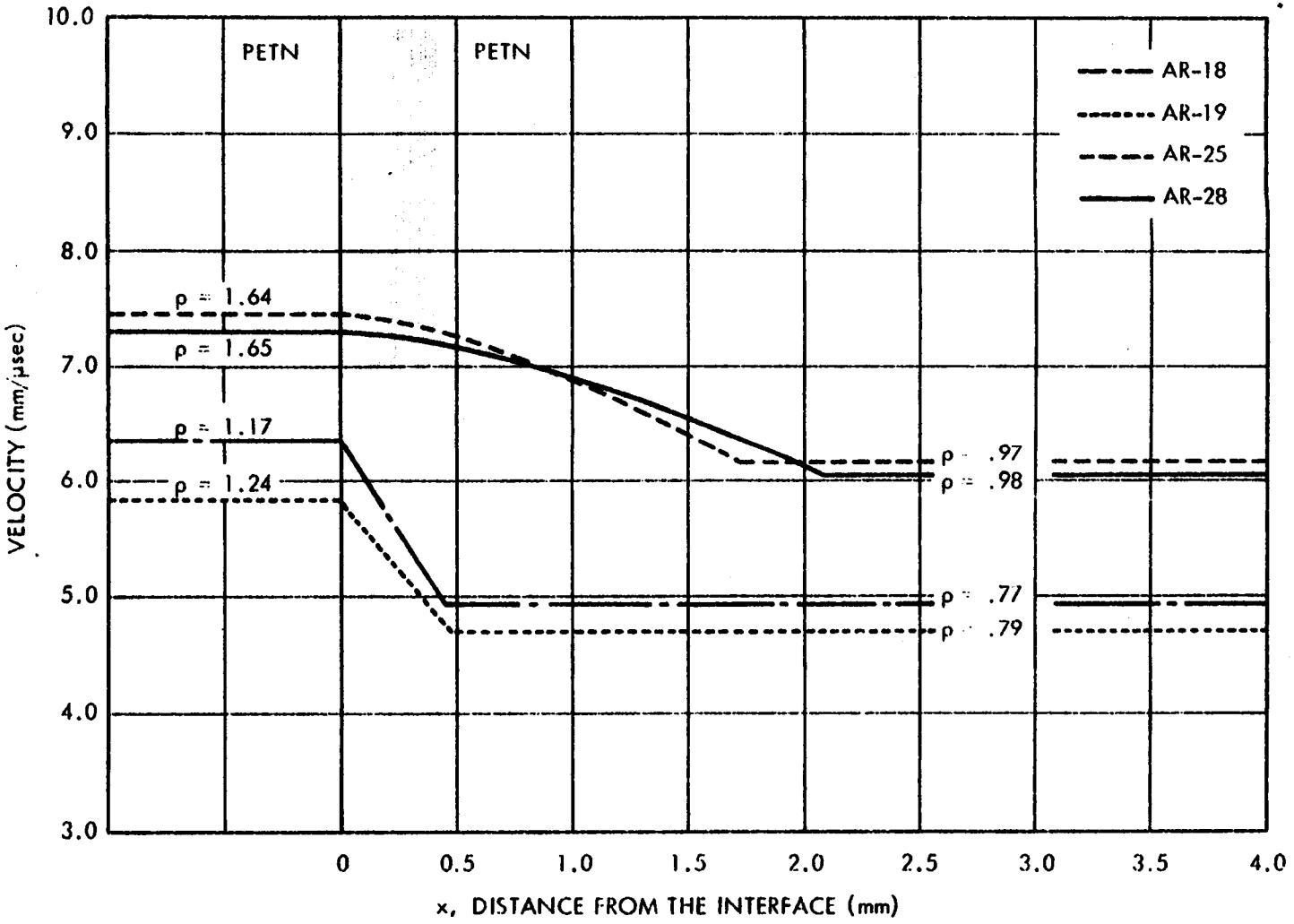

Figure 36. Plot of Velocity vs. Distance from Interface for PETN/PETN Series (Metallurgical Data)

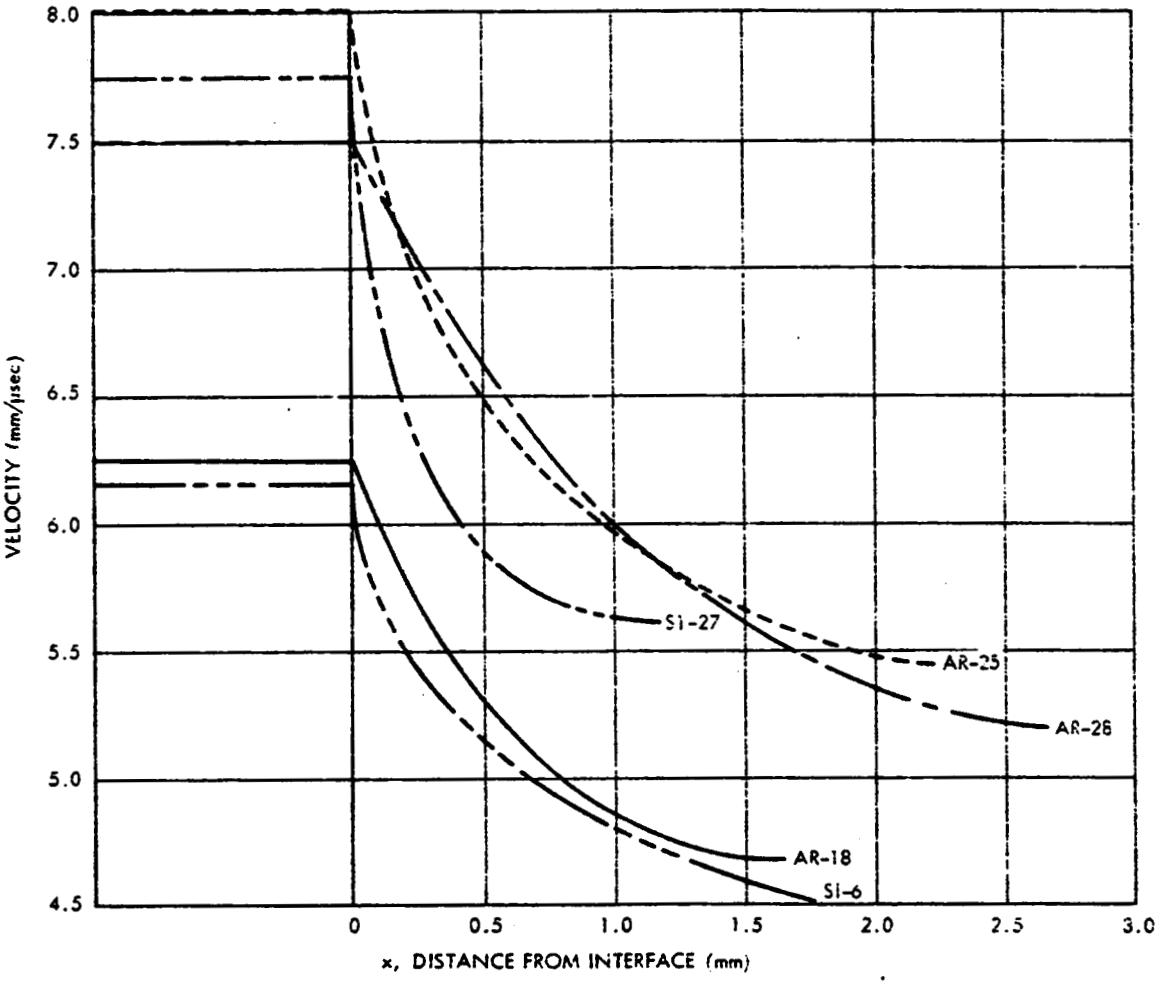

Figure 37. Plot of Velocity vs. Distance from Interface for PETN/PETN Series (Electrical Data)

Plots of $D - D_o$ (where D_o is the final steady state velocity) versus distance from the PETN/PETN interface were made from metallurgical data (Figure 38, Sheets 1 and 2) and electrical probe measurements (Figure 39, Sheets 1 2) on semilog paper. Since the velocity decay from metallurgical measurements was chosen as linear with distance, Figure 38 shows curved plots instead of the straight lines that might have been expected if the velocity transition were exponential. Therefore, straight lines were drawn to approximate the semilog plot for exponential velocity decay. Values of "a" to fit Equation (2) were calculated and tabulated in Table IX from both electrical and hardness data; this table also includes values of transition distance. Hardness data indicates that "a", which represents reaction zone thickness, is several times greater for the transition into PETN at a density of 1.0 gm/cm^3 than into PETN at 0.8 gm/cm^3. Electrical data, however, seems to indicate that variation in reaction zone thickness, if any, for varying acceptor densities, is fairly small.

Table IX

VALUES OF "a" (REACTION ZONE THICKNESS) FOR PETN/PETN SERIES

Test Serial No.	PETN Donor ρ (gm/cm^3)	PETN Acceptor ρ (gm/cm^3)	"a" (mm) Met.	"a" (mm) Elect.	Transition Distance (mm) Met.	Transition Distance (mm) Elect.
AR-18	1.17	0.77	0.06	0.17	0.45	1.75
AR-19	1.24	0.79	0.07	—	0.50	1.35
AR-25	1.64	0.97	0.22	0.23	1.7	2.05
AR-28	1.65	0.98	0.25	0.24	2.1	2.51
Sl-6	1.2	0.8	—	0.21	—	1.9
Sl-27	1.7	1.0	—	0.10	—	1.207

The transition curve could be better defined by metallurgical techniques if five times as many hardness readings were taken in the transition zone. Expanding the time scale on the oscilloscope to 0.2 μsec/cm should improve curve definition obtained by electrical probe techniques; nevertheless, the values of

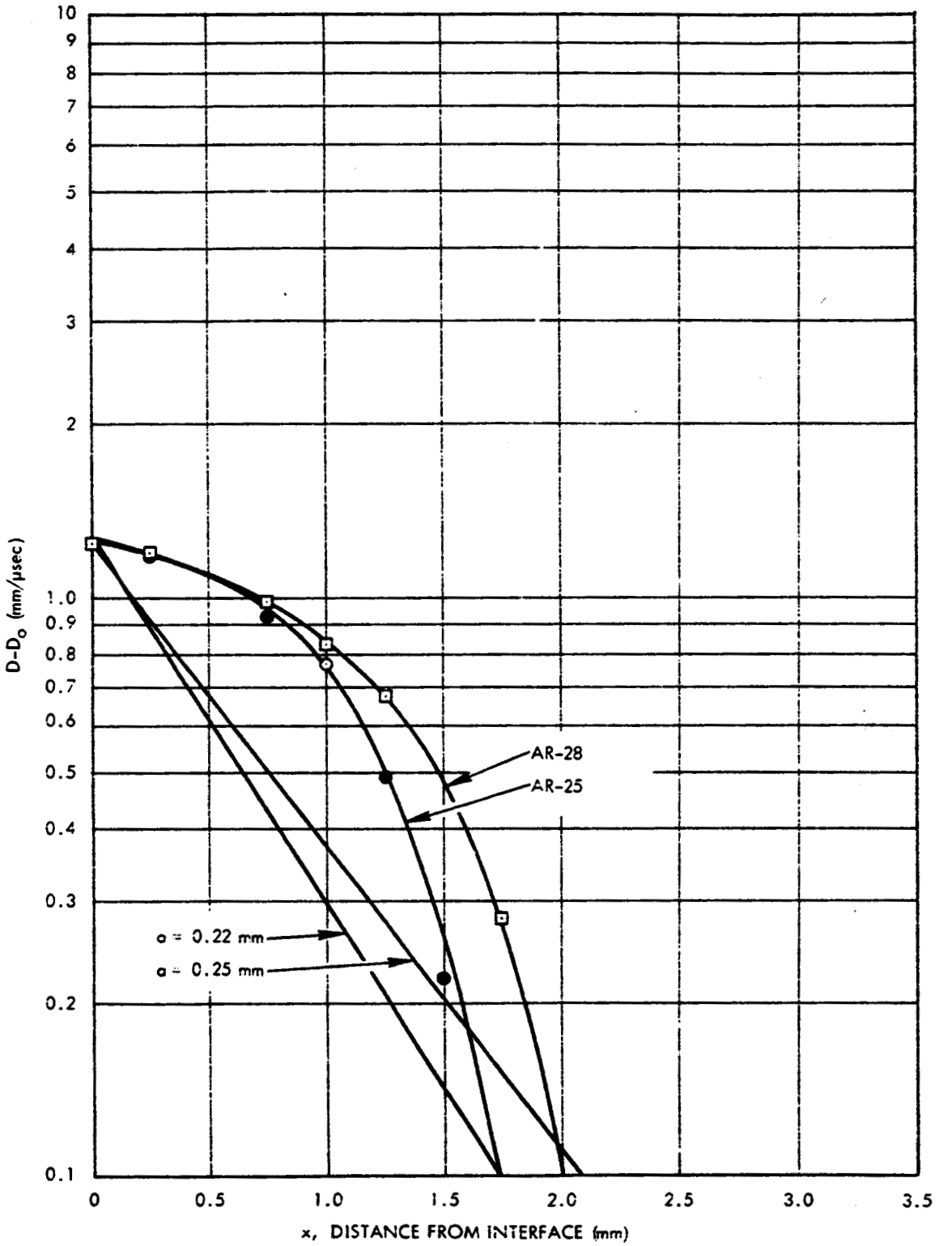

Figure 38. Plot of D - D_o vs. Distance from Interface for PETN/PETN Transition (Metallurgical Data) (Sheet 1 of 2)

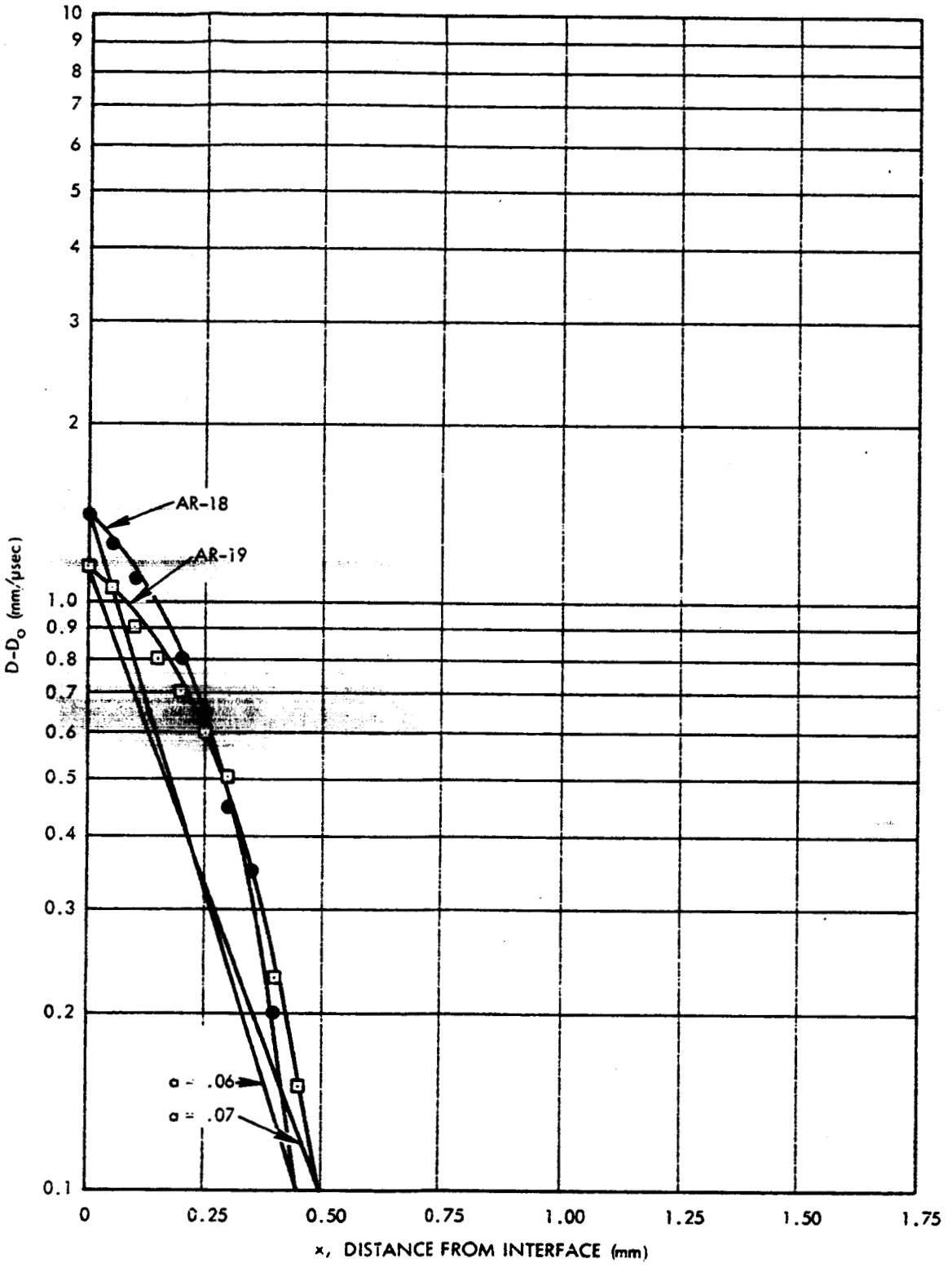

Figure 38. Plot of D - D_o vs. Distance from Interface for PETN/PETN Transition (Metallurgical Data) (Sheet 2 of 2)

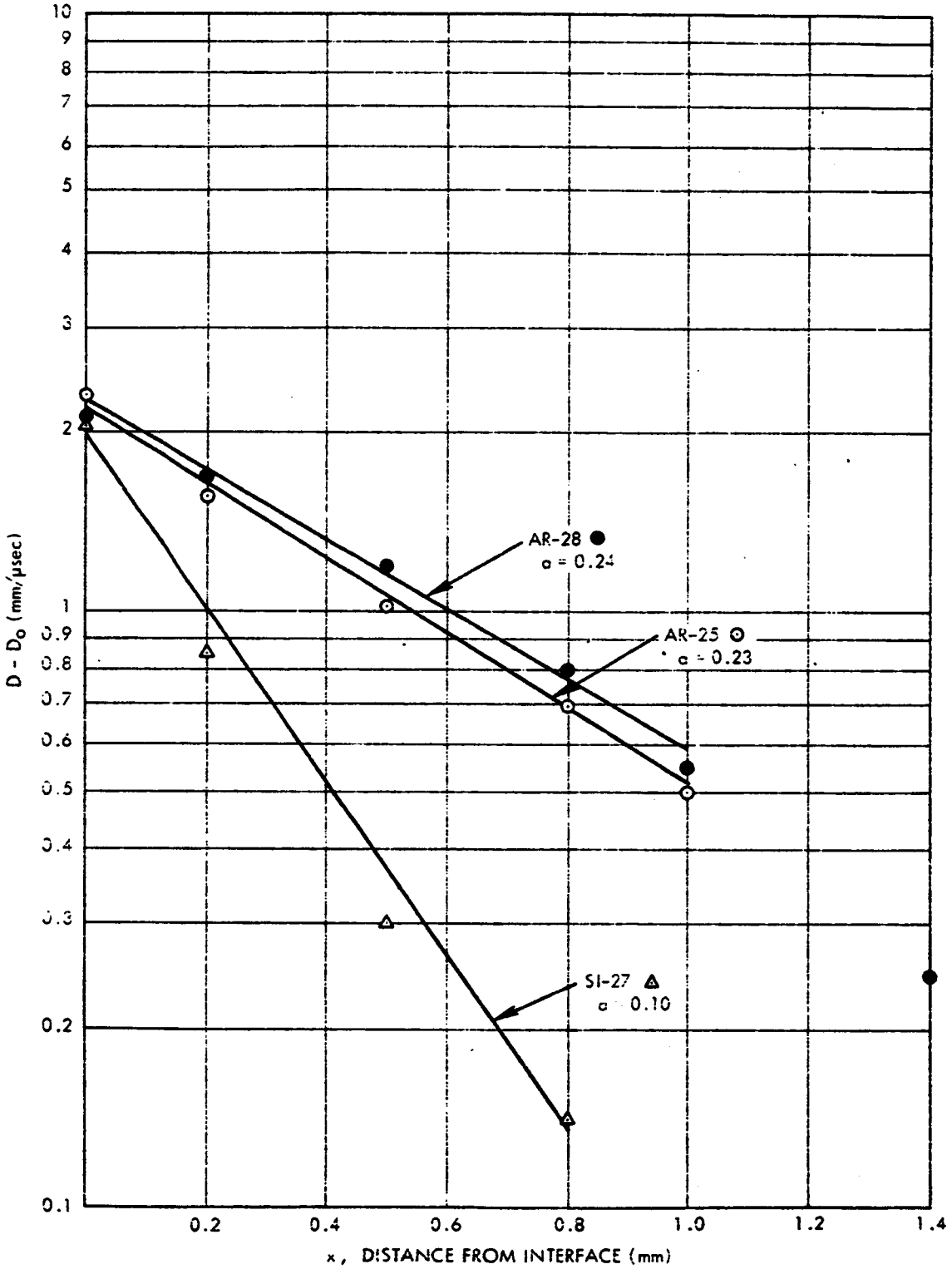

Figure 39. Plot of D - D_o vs. Distance from Interface for PETN (ρ = 1.7 gm/cm^3) to PETN (ρ = 1.0 gm/cm^3) Transition (Electrical Data) (Sheet 1 of 2)

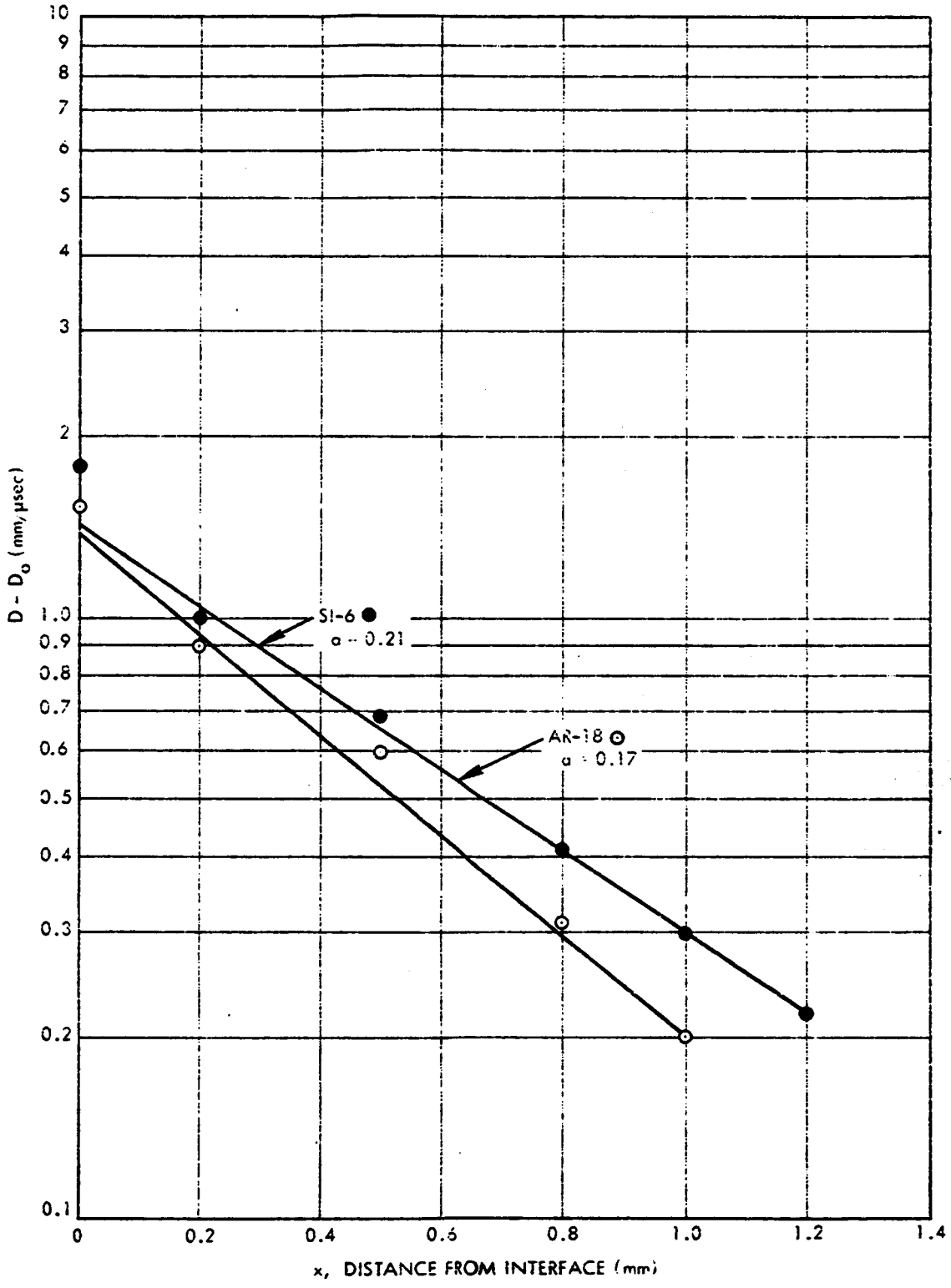

Figure 39. Plot of D - D_0 vs. Distance from Interface for PETN (ρ = 1.2 gm/cm^3) to PETN (ρ = 0.8 gm/cm^3) Transition (Electrical Data) (Sheet 2 of 2)

Table IX provide good indications of the order of magnitude of the transition distance and the reaction zone thickness.

C. PETN/PYROTECHNIC SYSTEM

The reduction of the metallurgical hardness data to detonation velocity requires an averaging of the hardness values in the donor section. From this value at the interface a "best-fit" curve is made through the hardness points for the acceptor section of the test body. A typical graph of hardness measurements made on such a test body adjacent to the explosive channel is shown in Figure 40; a line has been drawn on this graph to represent the average hardness. The curve to the right of the interface represents the hardness decay at increasing distances from the interface as shock pressure dies out.

Figure 41 is an extrapolated hardness vs. detonation velocity curve compiled from the PETN density vs. hardness calibration data. The dashed portions of the curve represent the probable hardness points for PETN detonation velocities below 4.0 mm/μsec and above 7.0 mm/μsec. This curve was used to convert the hardness vs. distance-from-interface plots to velocity vs. distance-from-interface plots.

The metallurgically determined velocity vs. distance curves for pyrotechnic mixes appear in Figures 42 through 44. The CuO-Mg (76%/24%) curves indicate the expected rapid velocity decay associated with a slightly reactive system, this decay was not as rapid as for the PETN/inert system. The 60-40 $KClO_4$-Al velocity decay was slower than the CuO-Mg, but it appeared to approach a steady state velocity at a distance beyond 5 millimeters. The 50-50 RDX-Al had the slowest decay rate. A steady state deflagration is indicated at a transition distance of 5 to 6 millimeters. Metallurgical data beyond this point is limited.

Electrical probe data was reduced in the following manner. Oscilloscope photographs were enlarged and viewed under an illuminated magnifier and voltage vs. time slopes were obtained for small time intervals. Using these slopes and known circuit constants, Equation (5) was used to calculate velocities over

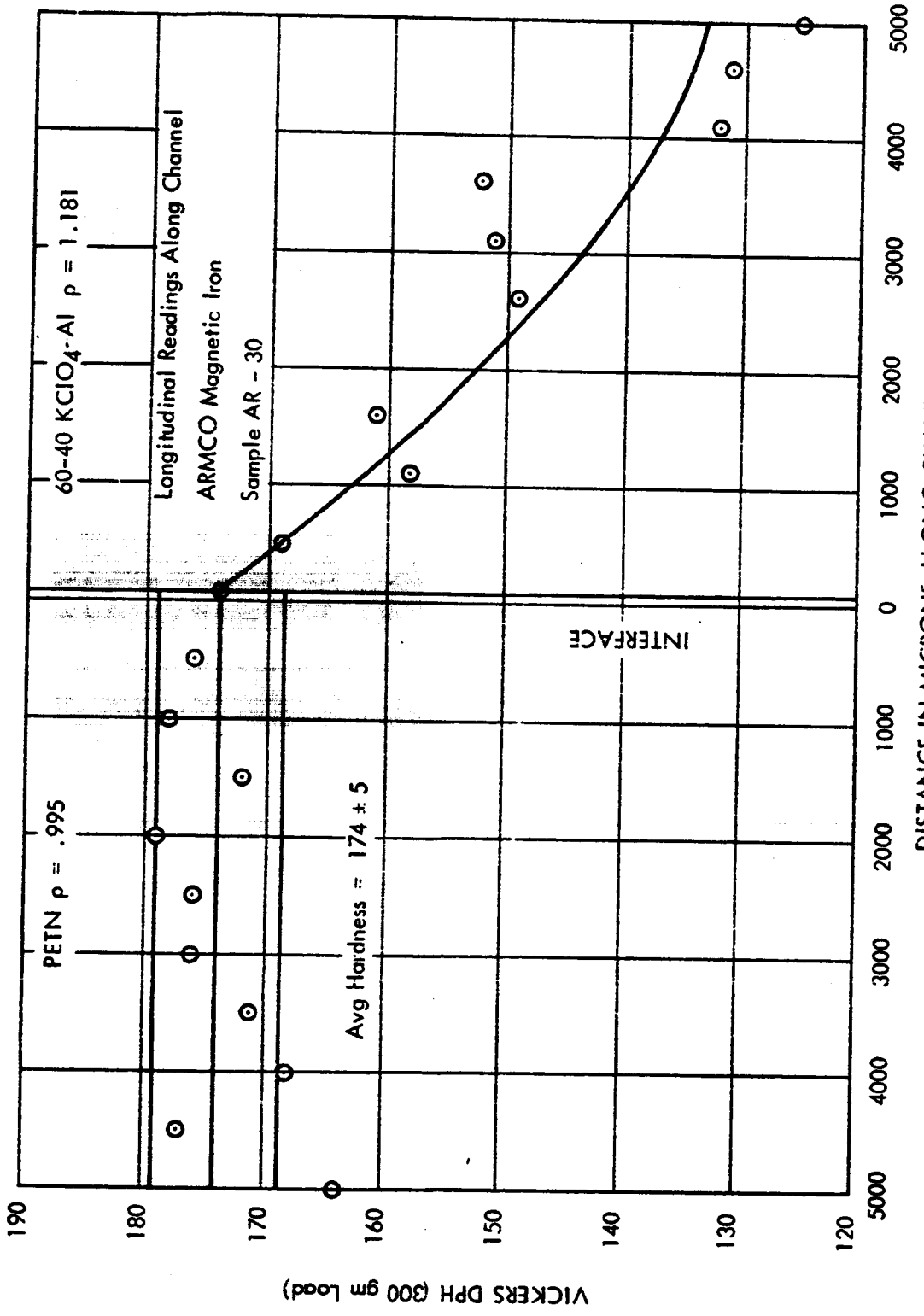

Figure 40. Plot of Typical Hardness Measurement and "Best-Fit" Curve

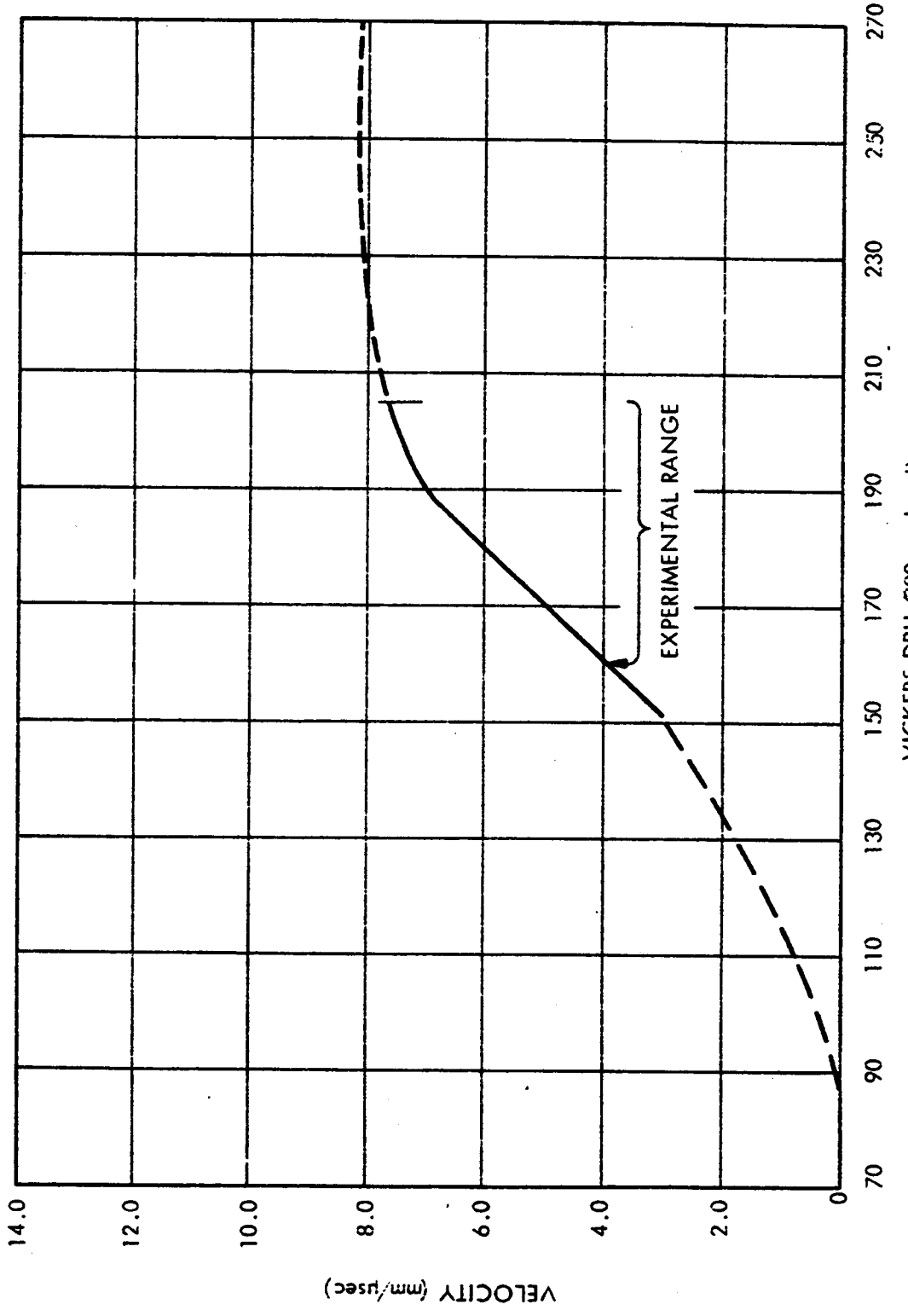

Figure 41. Plot of Extrapolated Velocity vs. Hardness for PETN in Armco Iron

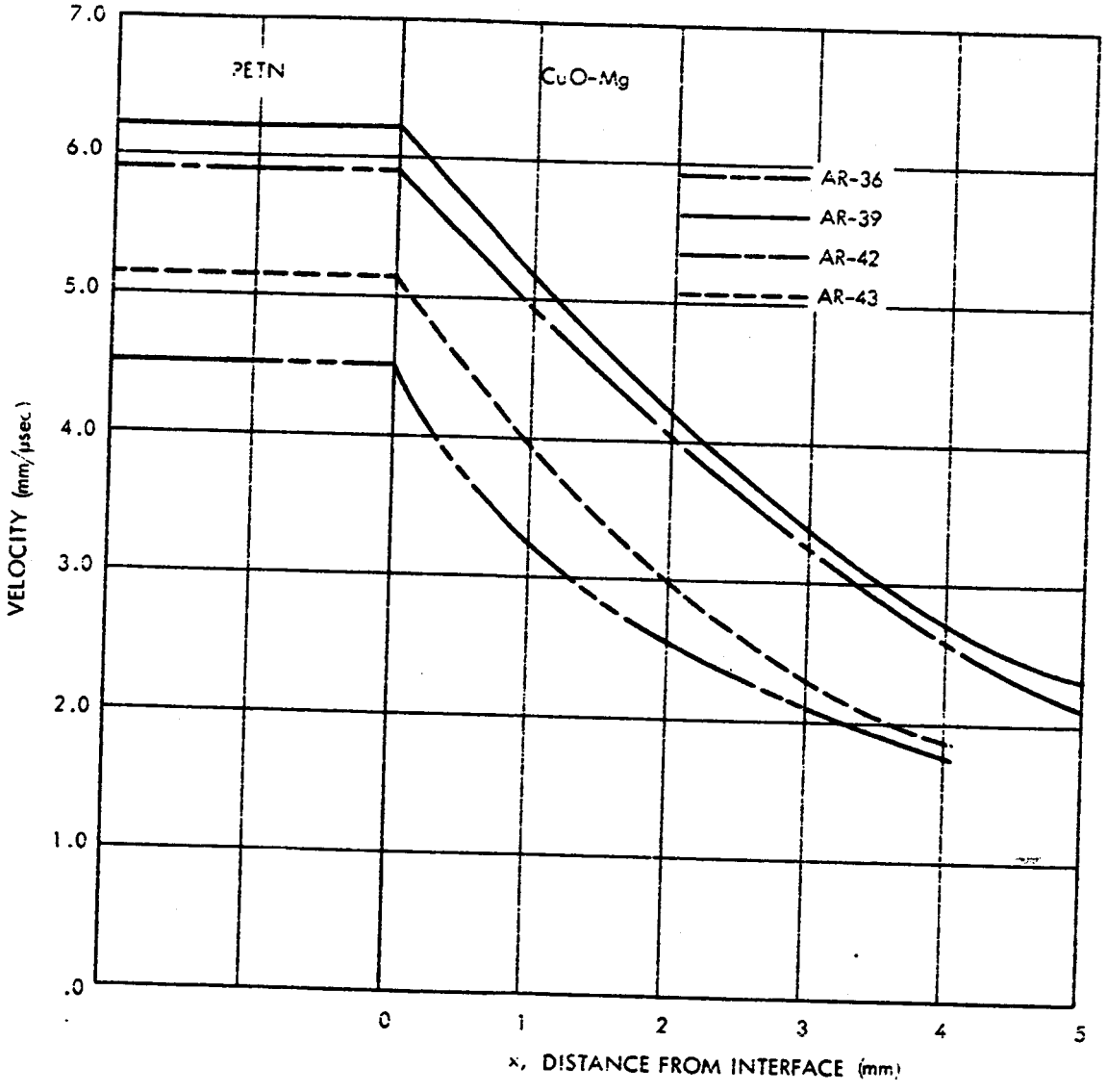

Figure 42. Velocity Decay Curves for CuO-Mg Acceptor (Metallurgical Data)

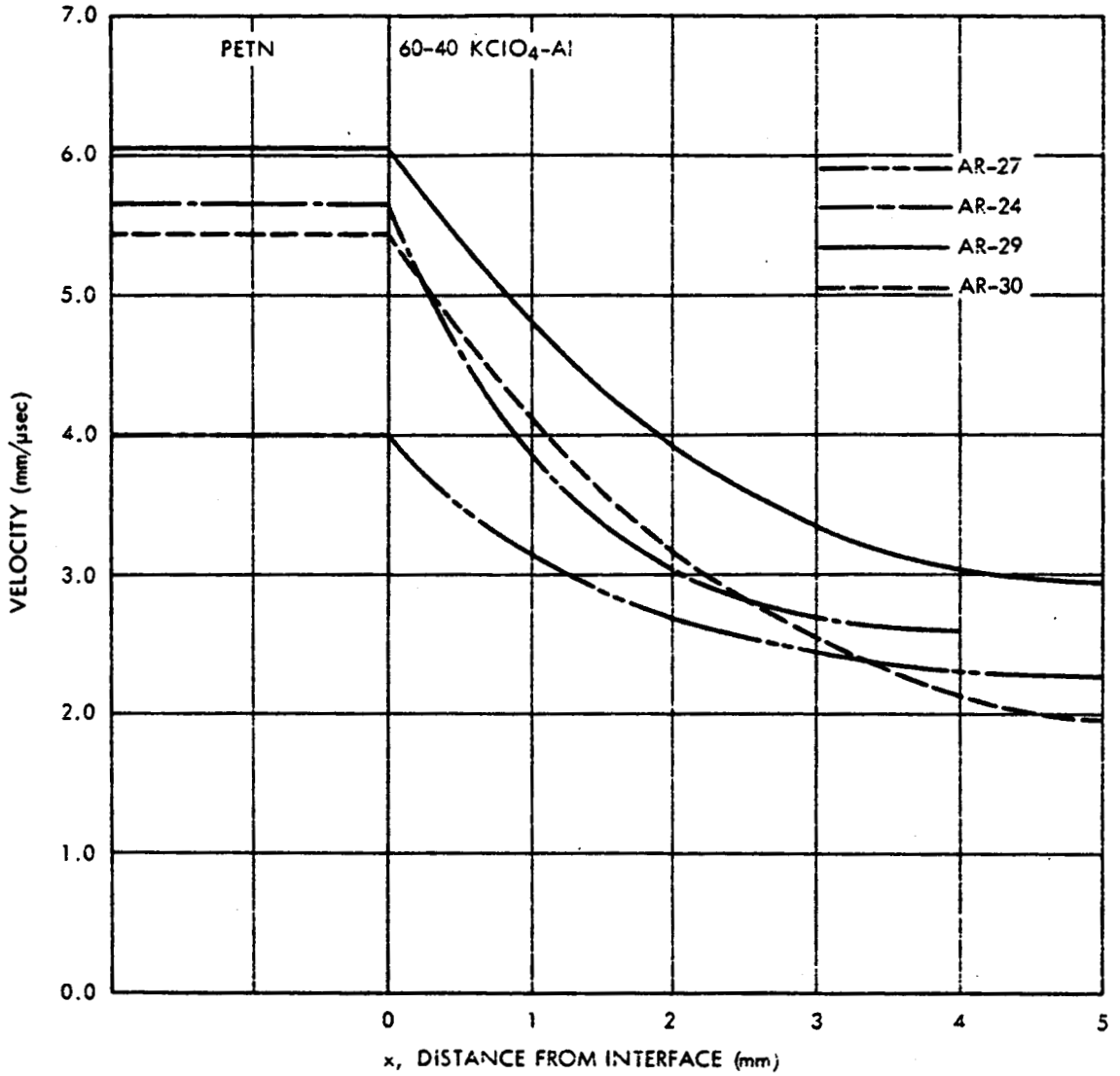

Figure 43. Velocity Decay Curves for 60-40 $KClO_4$-Al Acceptor (Metallurgical Data)

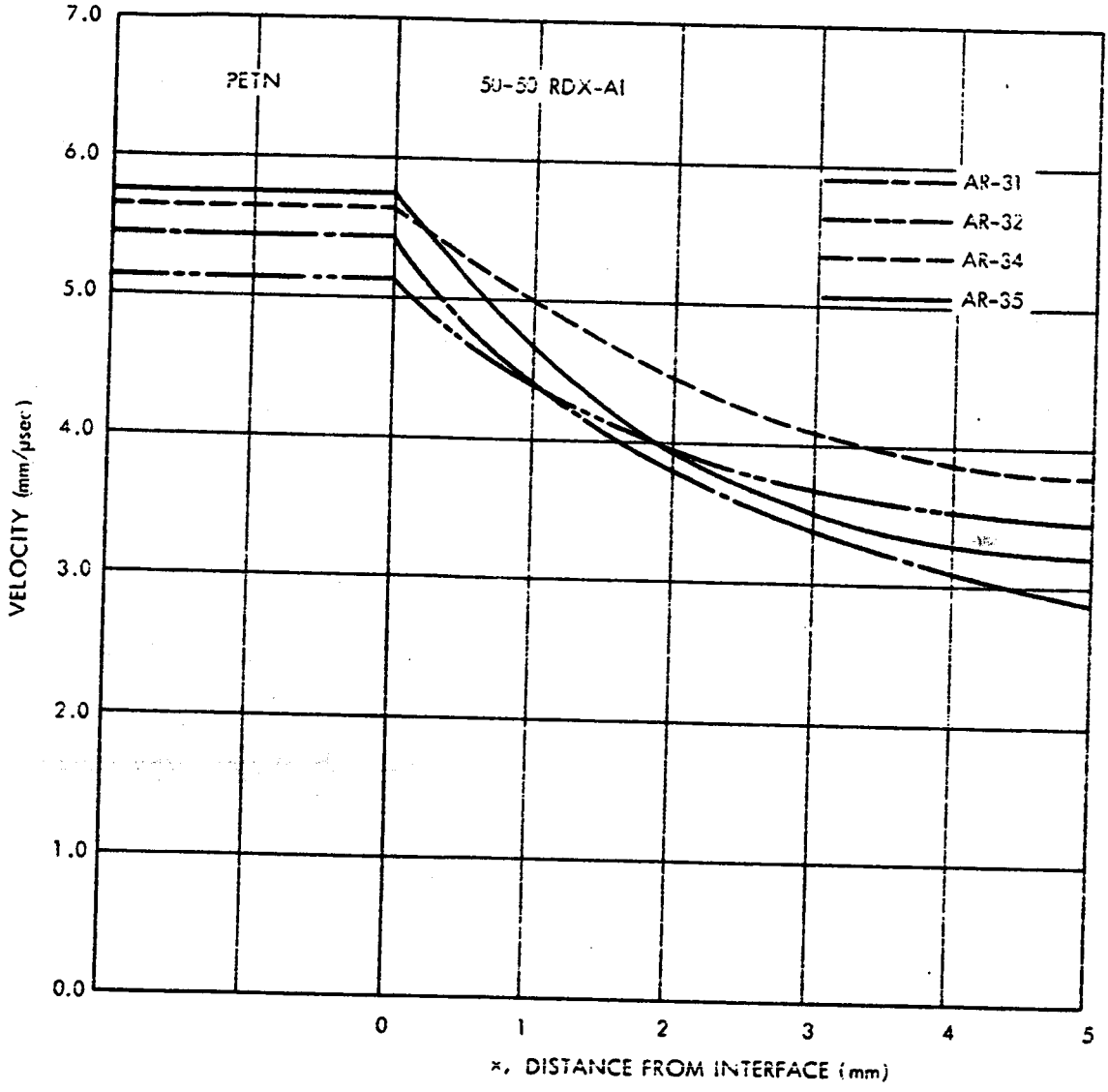

Figure 44. Velocity Decay Curves for 50-50 RDX-Al Acceptor (Metallurgical Data)

small intervals. Figure 45 shows a typical plot of these incremental velocities and the "best-fit" curve drawn through the data points. The smooth curves were then redrawn in families to indicate family relationships. Families for the pyrotechnic mixes are shown in the velocity vs. distance plots of Figures 46 through 54. These plots indicate that both CuO-Mg and CuO-Fe_2O_3-Mg have rapid velocity decays, dropping to very low values in 10 millimeters. Similar behavior was evidenced by the $KClO_4$-Al, but the 60-40 mix took somewhat longer to decay to a given value and appeared to approach a steady state velocity of approximately 1.0 mm/μsec; it was not clear whether this was a stable state. Between 5 and 10 millimeters after the interface the 50-50 RDX-Al had established a constant deflagration rate between 2.0 and 2.5 mm/μsec. The 25-75 RDX-Al decayed rapidly toward zero velocity.

Figures 55, 57, and 59 show the semilog plots of $D - D_o$ vs. distance for the pyrotechnic mixes, as determined from Figures 42, 43, and 44. The same figures supplied data for the log-log plots of D/D_1 vs. distance in Figures 56, 58, and 60. The values of "k" and "a" determined from the above graphs are presented in Table X.

Table X

VALUES OF "a" AND "k" FROM METALLURGICAL DATA

Test	Donor		Acceptor			
Serial No.	Type	ρ gm/cm^3	Type	ρ gm/cm^3	k	a (mm)
AR-36	PETN	1.025	CuO-Mg	1.70	0.51	1.4
AR-39	PETN	1.201	CuO-Mg	1.687	0.668	1.02
AR-42	PETN	1.205	CuO-Mg	1.685	0.558	1.0
AR-43	PETN	1.01	CuO-Mg	1.705	0.553	1.28
AR-31	PETN	1.036	RDX-Al	1.01	0.294	0.99
AR-32	PETN	1.000	RDX-Al	0.999	0.145	1.90
AR-34	PETN	1.143	RDX-Al	1.016	0.186	2.00
AR-35	PETN	1.219	RDX-Al	0.976	0.229	1.27
AR-24	PETN	1.227	$KClO_4$-Al	1.206	0.213	1.09
AR-27	PETN	1.019	$KClO_4$-Al	1.185	0.219	1.78
AR-29	PETN	1.221	$KClO_4$-Al	1.194	0.315	1.32
AR-30	PETN	0.995	$KClO_4$-Al	1.181	0.529	1.06

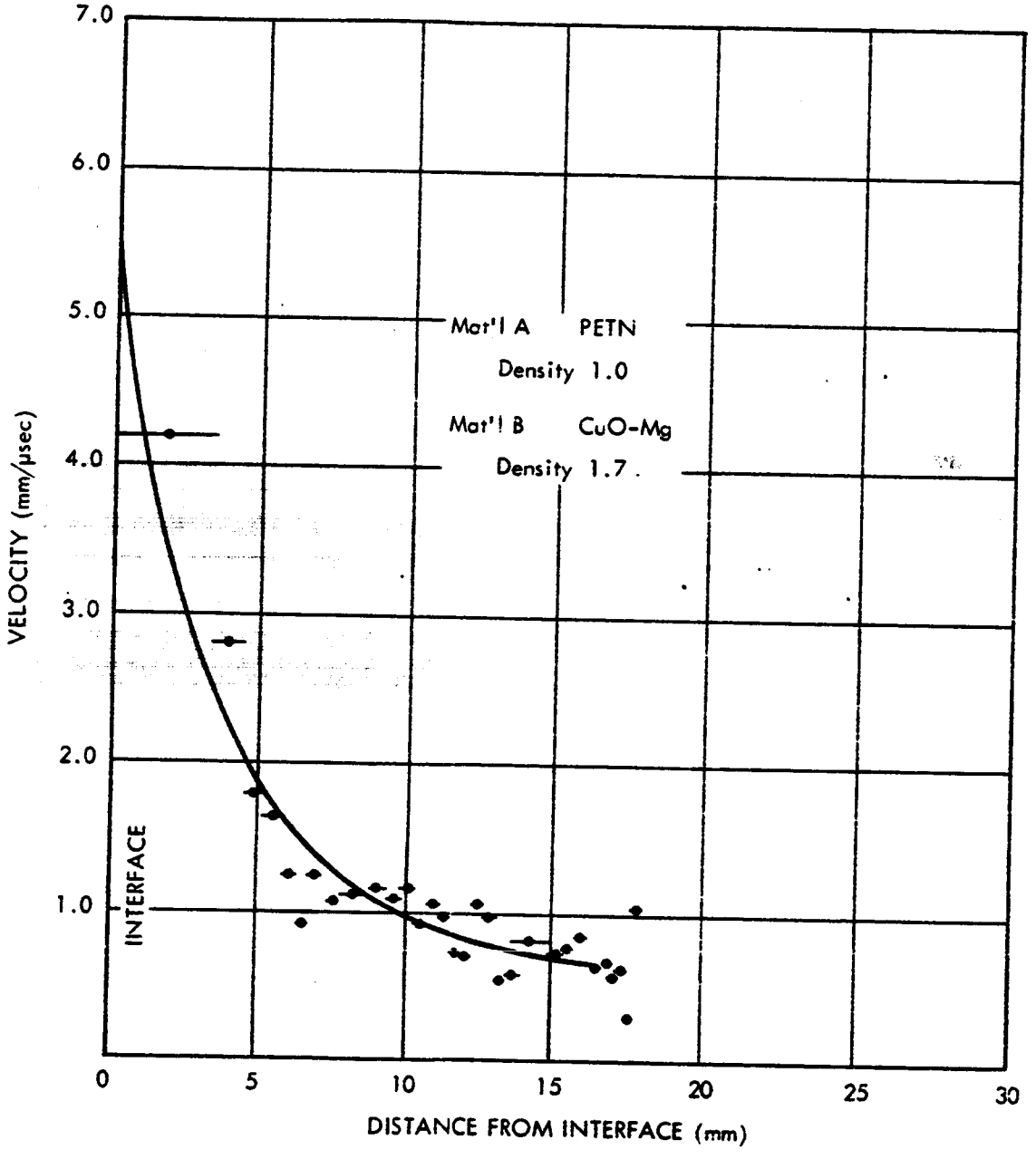

Figure 45. Plot of Typical Electrical Measurement and "Best-Fit" Curve

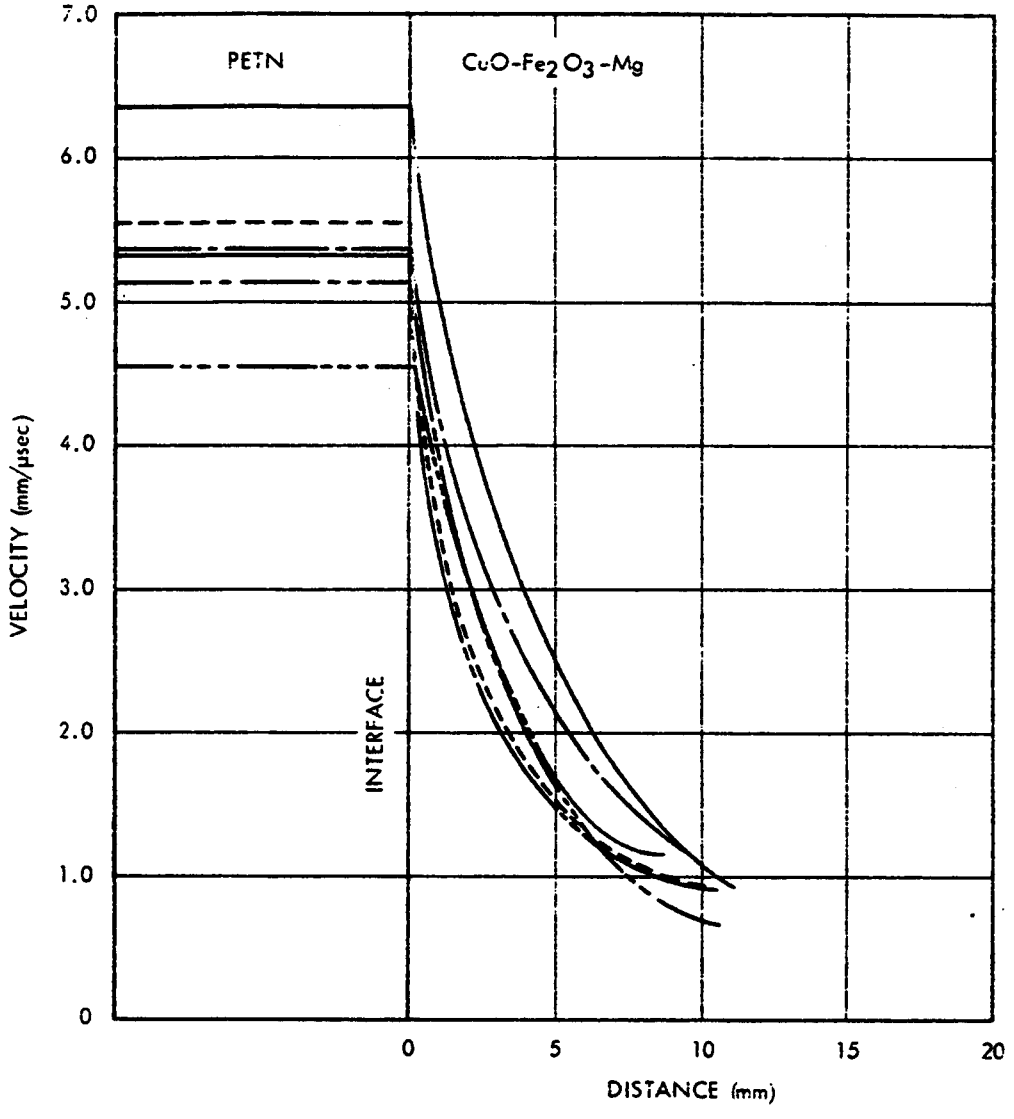

Figure 46. Velocity Decay Curves for $CuO-Fe_2O_3$-Mg Acceptor (ρ = 1.5 gm/cm^3) in Brass Test Bodies (Electrical Data)

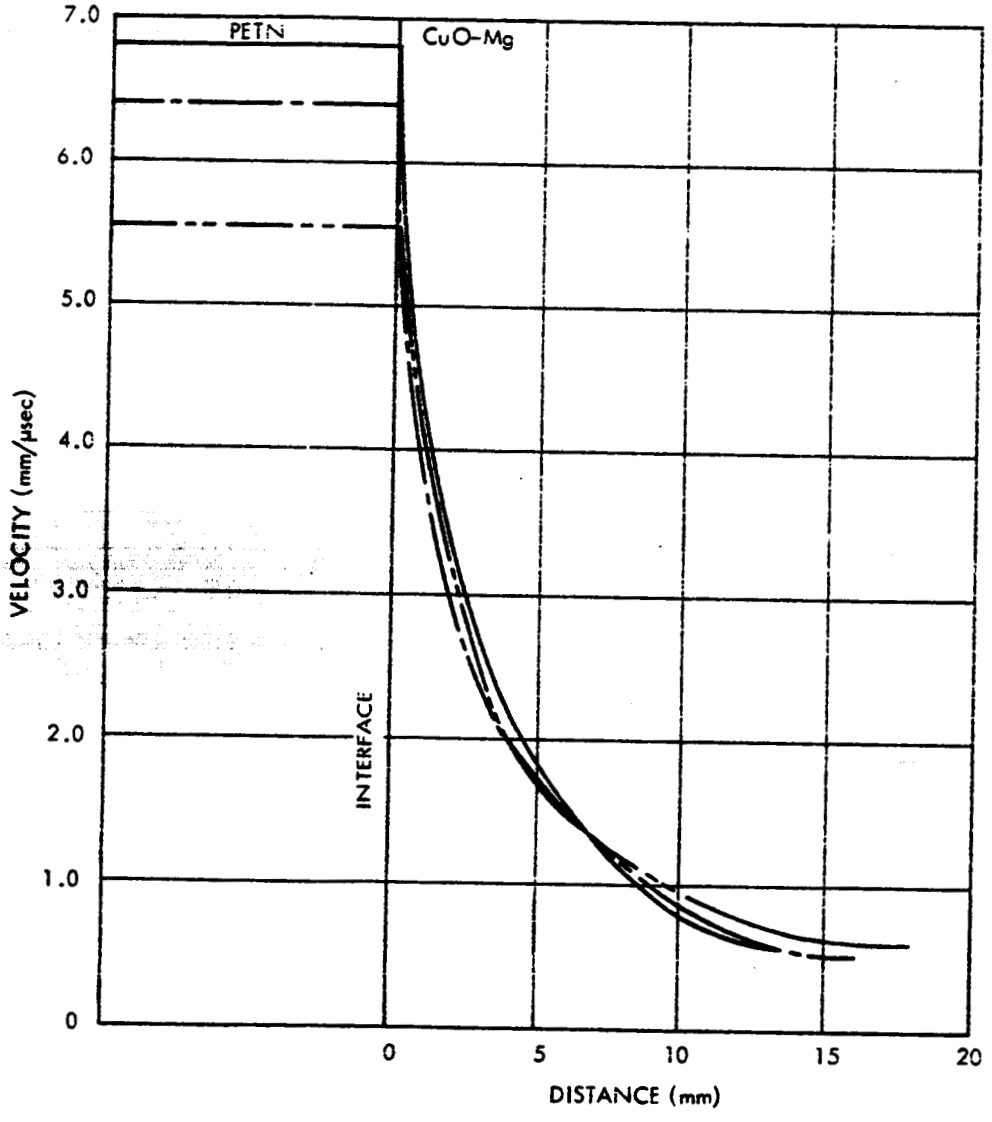

Figure 47. Velocity Decay Curves for CuO-Mg Acceptor (ρ = 1.7 gm/cm^3) in SS301 Test Bodies (Electrical Data)

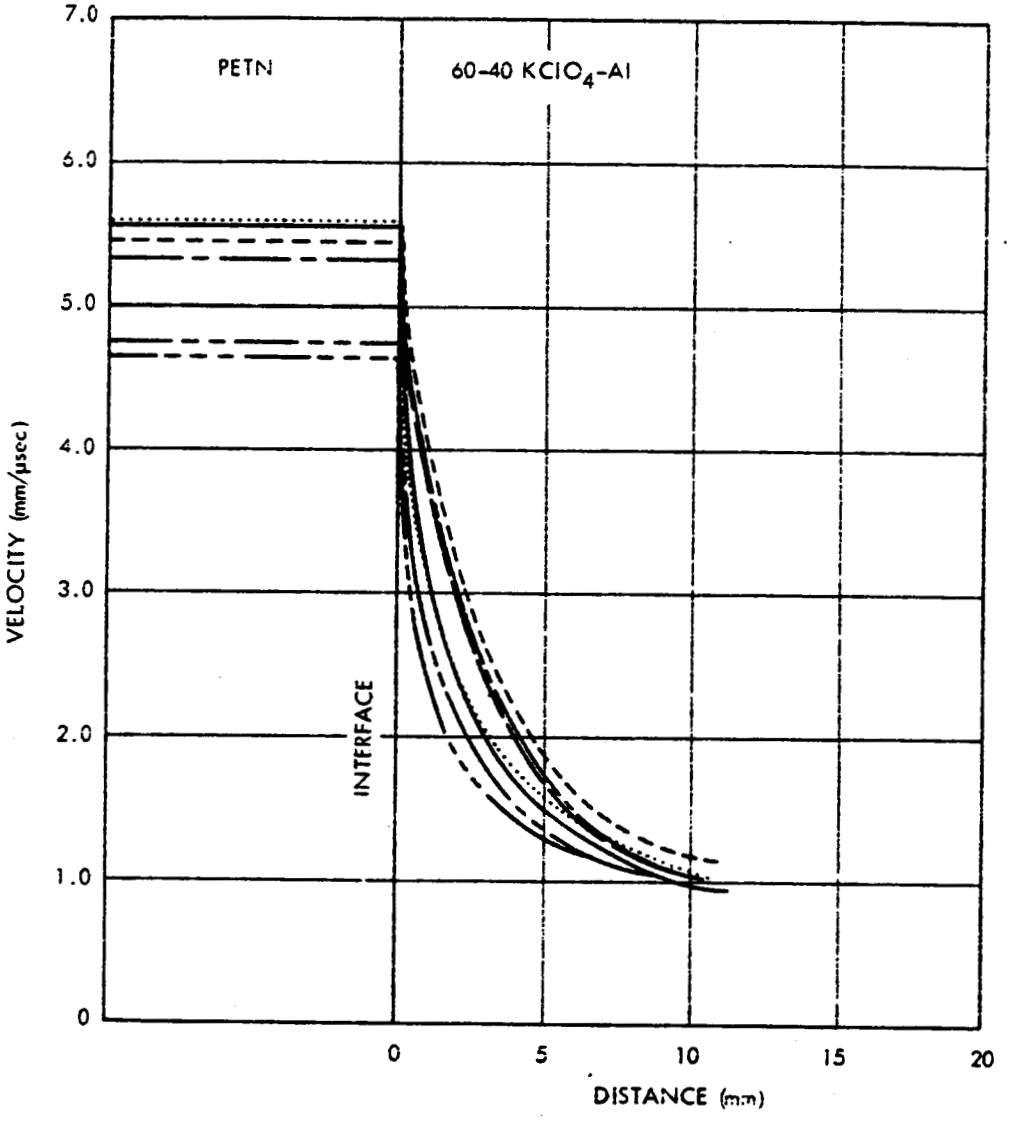

Figure 48. Velocity Decay Curves for 60-40 $KClO_4$-Al (ρ = 1.2 gm/cm^3) in Brass Test Bodies (Electrical Data)

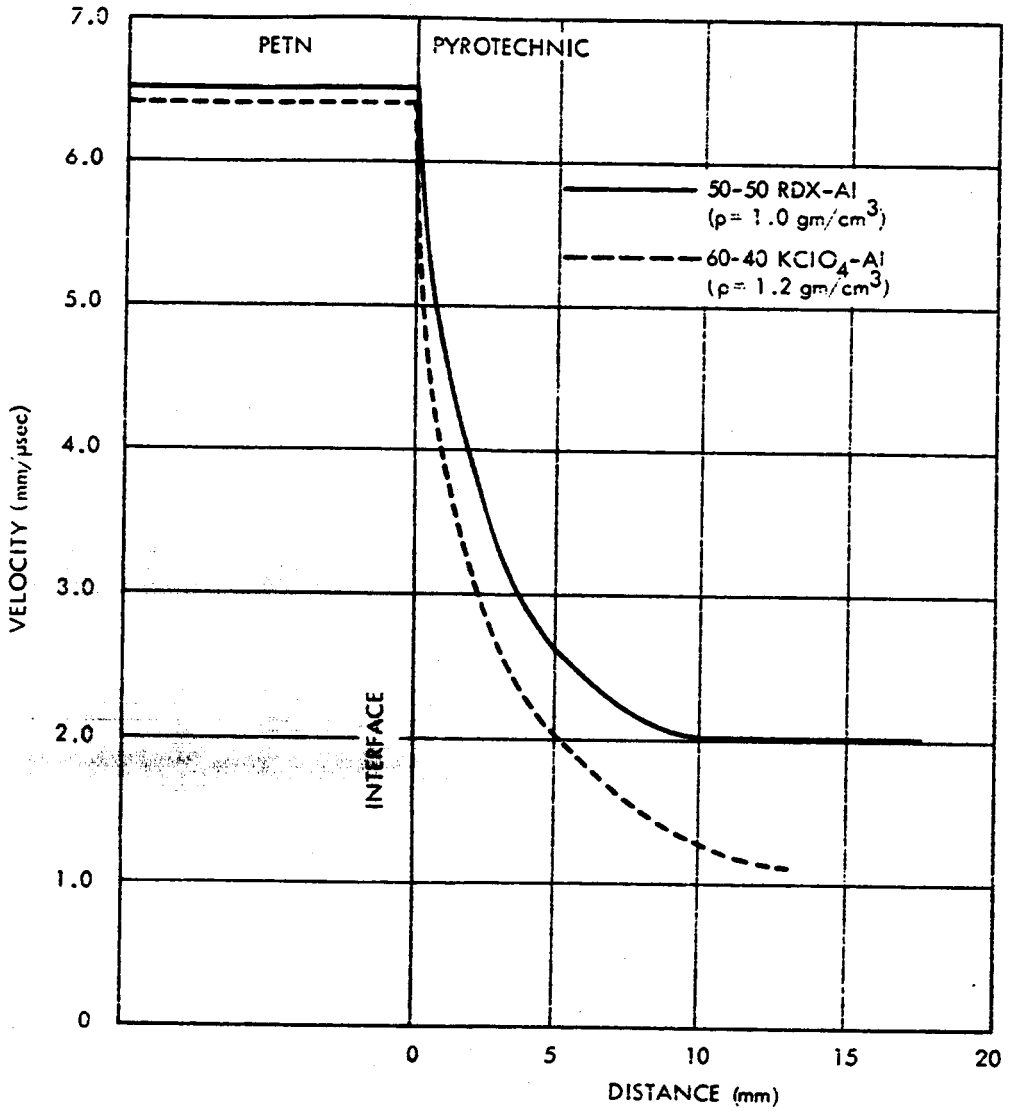

Figure 49. Velocity Decay Curves for 50-50 RDX-Al and 60-40 $KClO_4$-Al in Armco Iron Test Bodies (Electrical Data)

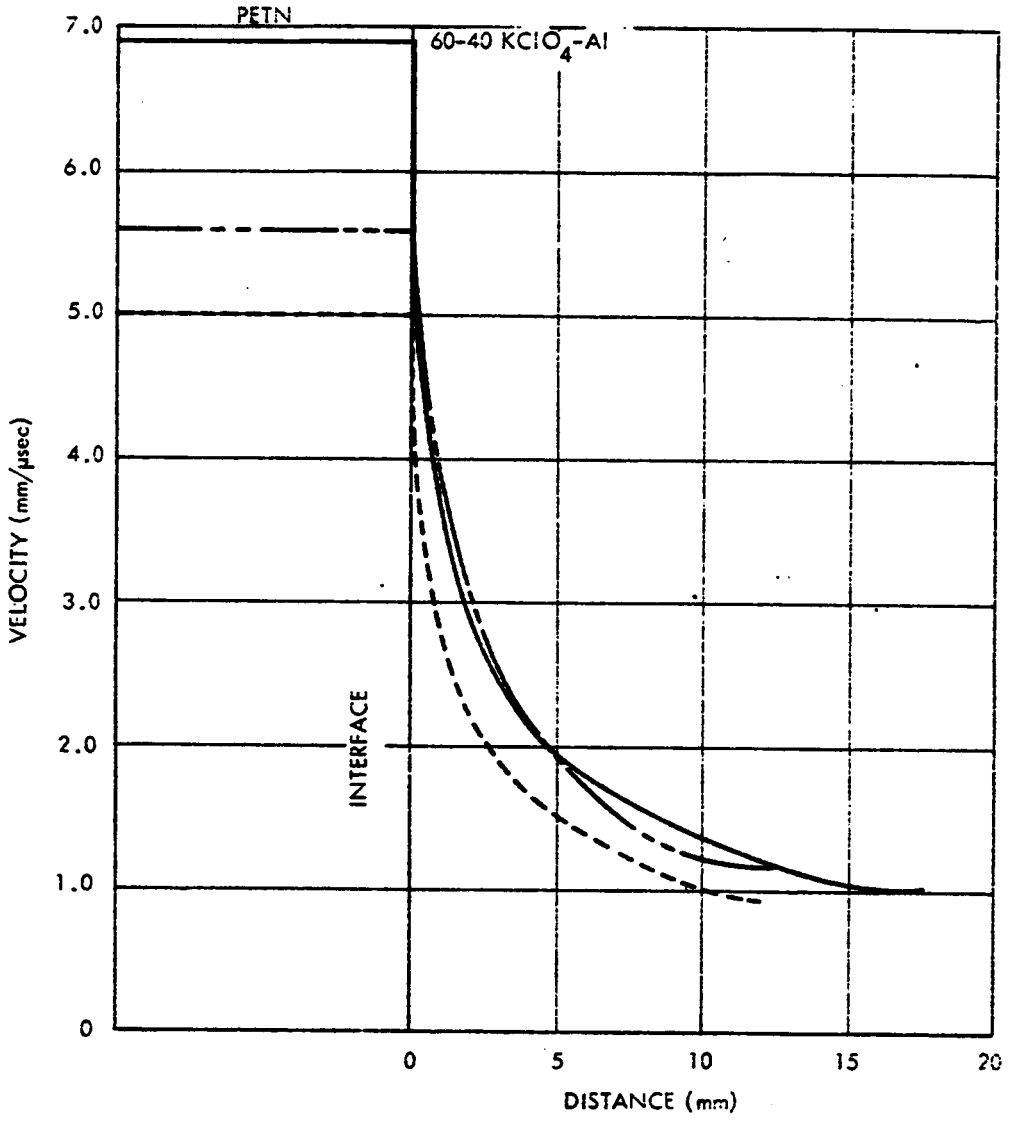

Figure 50. Velocity Decay Curves for 60-40 $KClO_4$-Al (ρ = 1.2 gm/cm^3) in SS301 Test Bodies (Electrical Data)

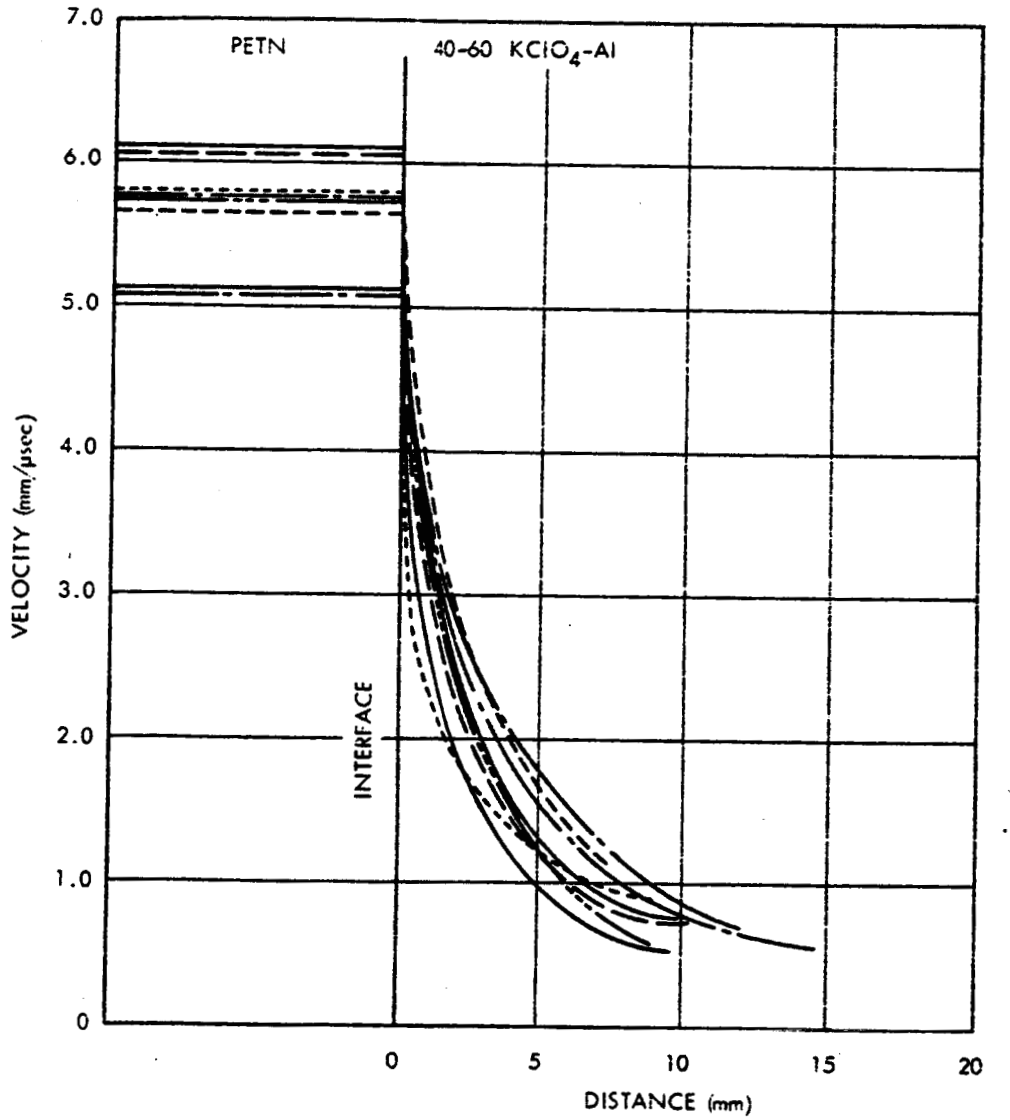

Figure 51. Velocity Decay Curves for 40-60 $KClO_4$-Al (ρ = 1.5 gm/cm^3) in Brass Test Bodies (Electrical Data)

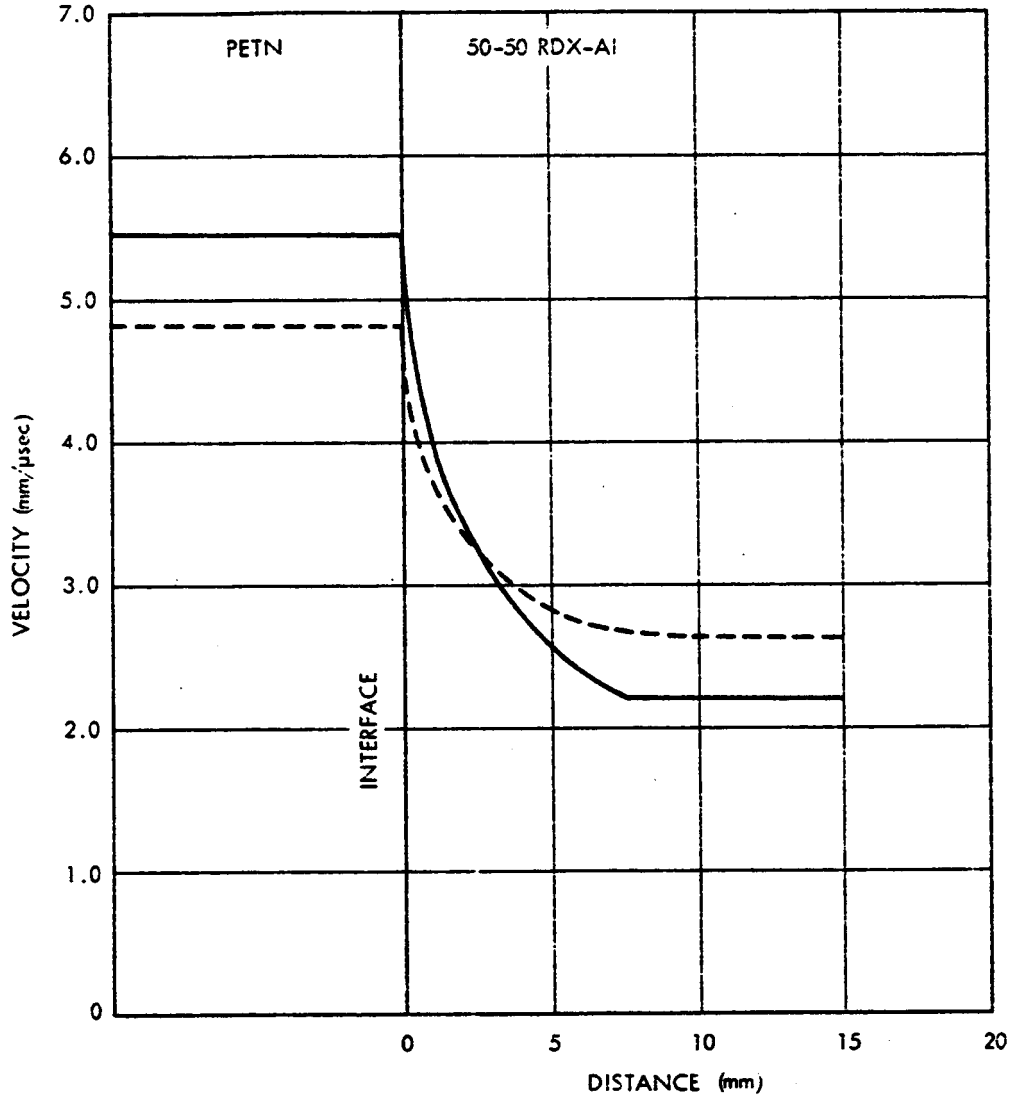

Figure 52. Velocity Decay Curves for 50-50 RDX-Al (ρ = 1.0 gm/cm^3) in Brass Test Bodies (Electrical Data)

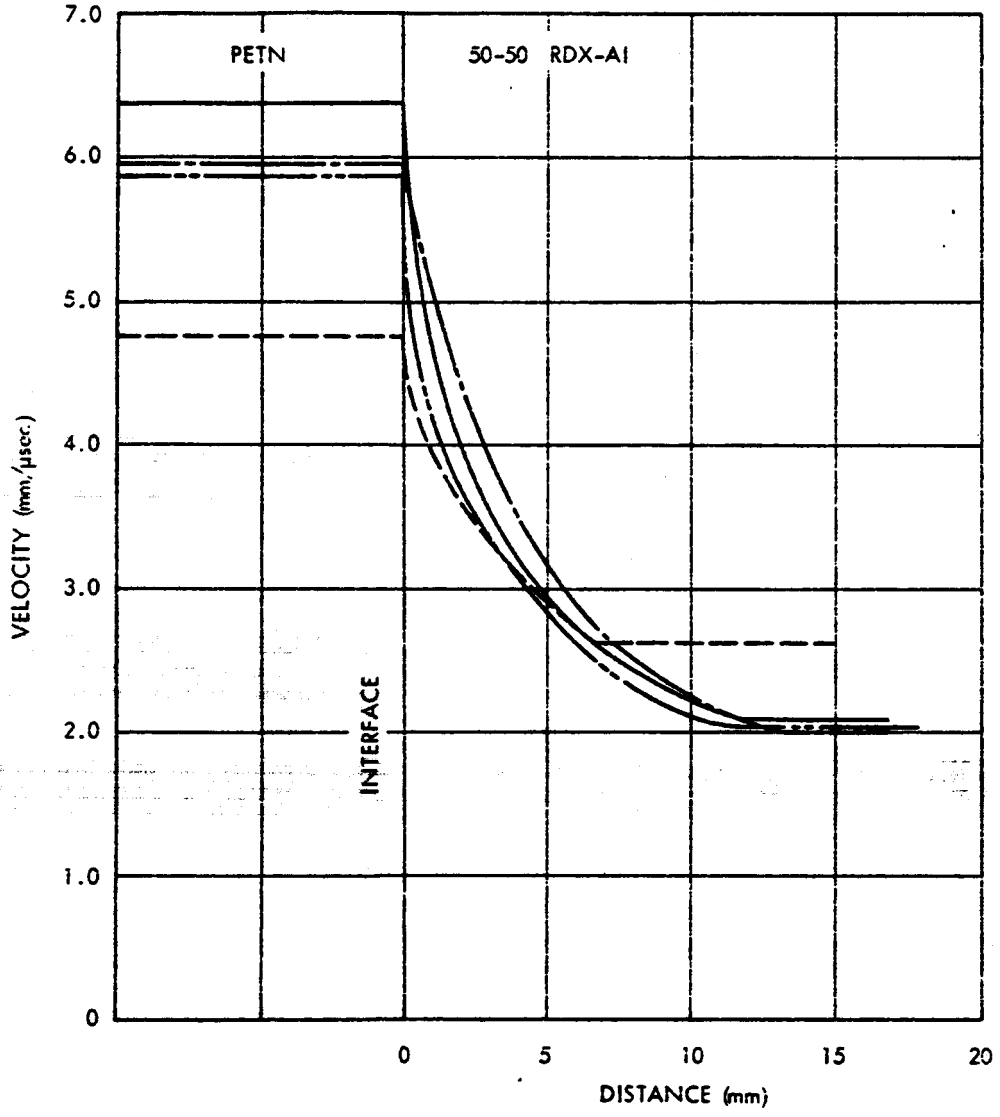

Figure 53. Velocity Decay Curves for 50-50 RDX-Al (ρ = 1.0 gm/cm^3) in SS301 Test Bodies (Electrical Data)

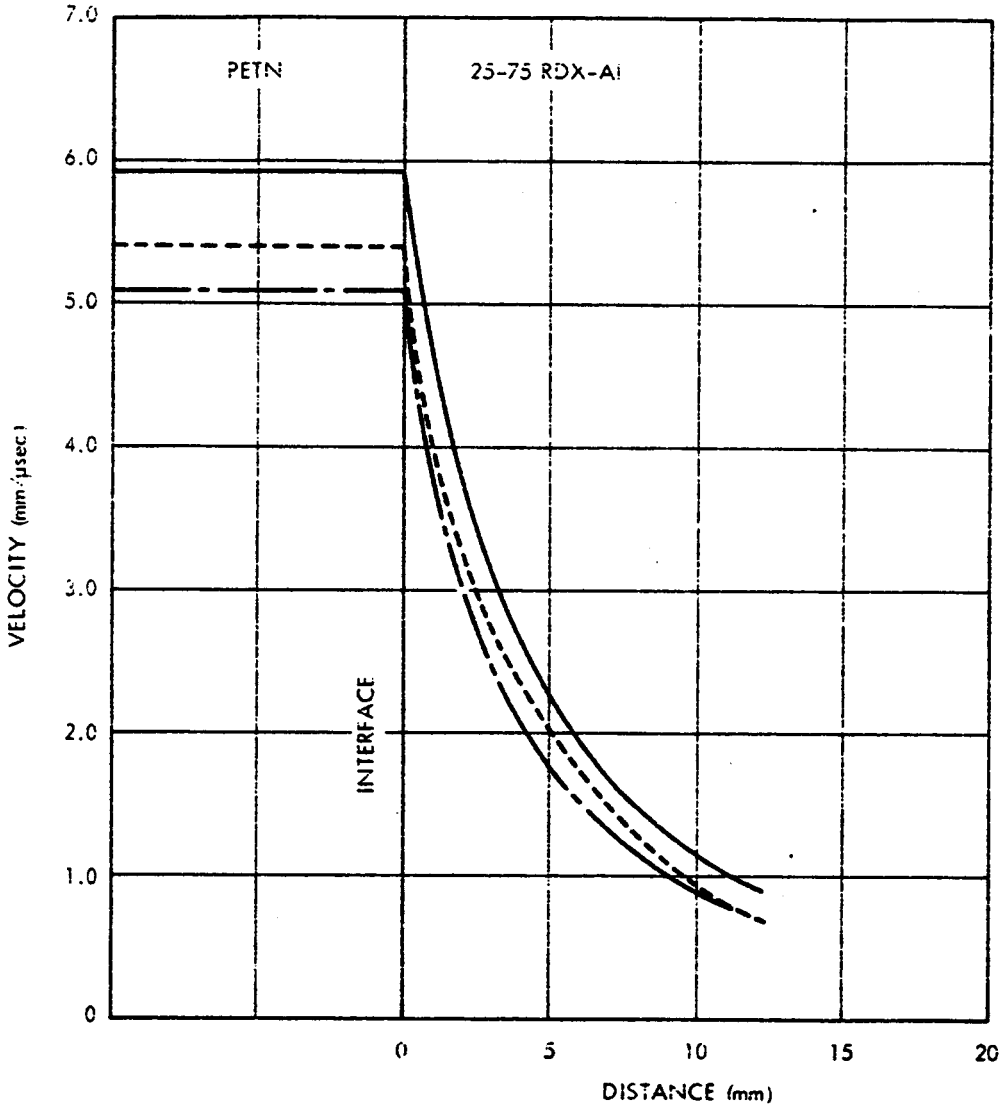

Figure 54. Velocity Decay Curves for 25-75 RDX-Al (ρ = 1.0 gm/cm^3) in Brass Test Bodies (Electrical Data)

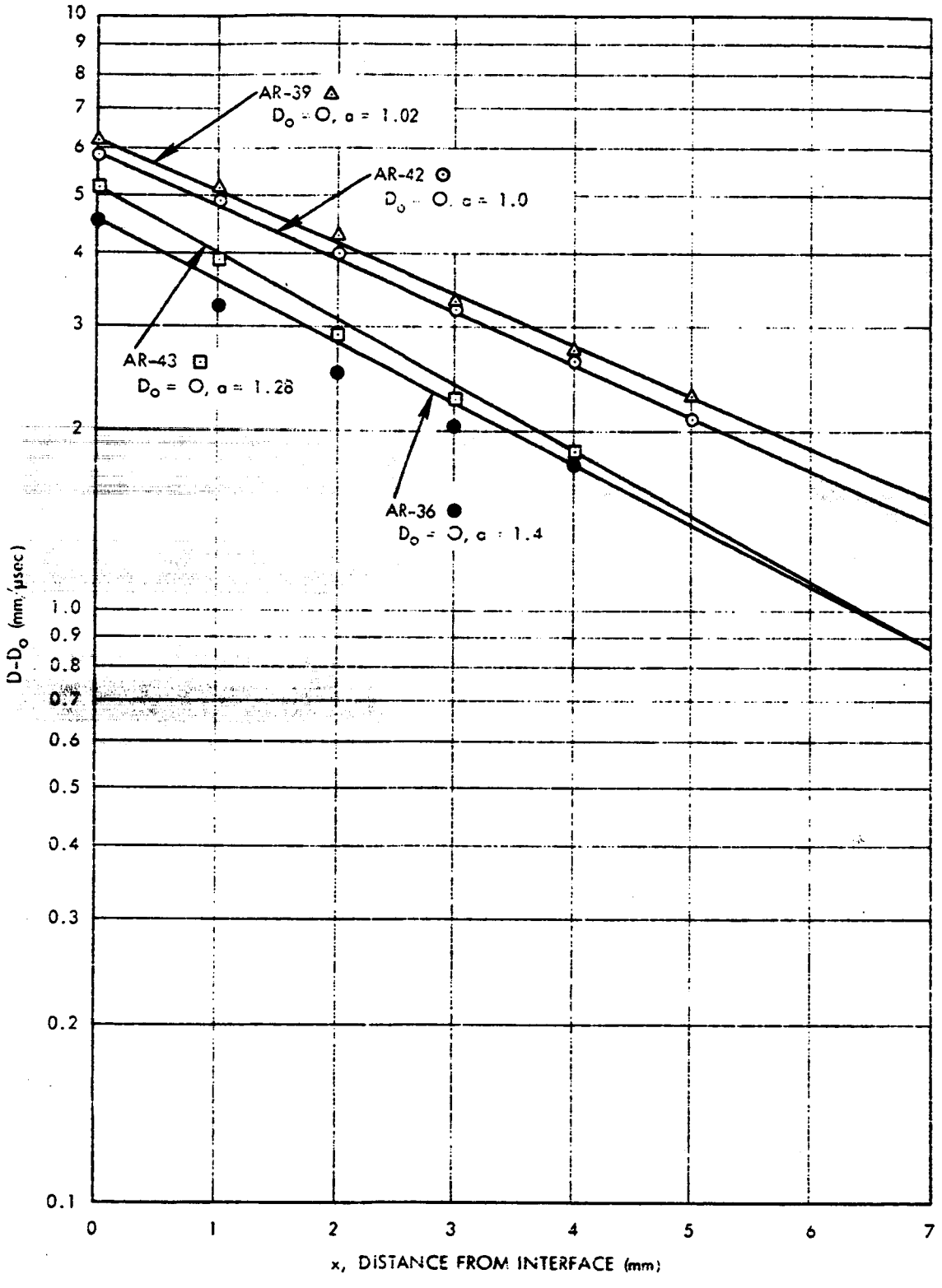

Figure 55. Plot of D - D_o vs. Distance from Interface for CuO-Mg Acceptor

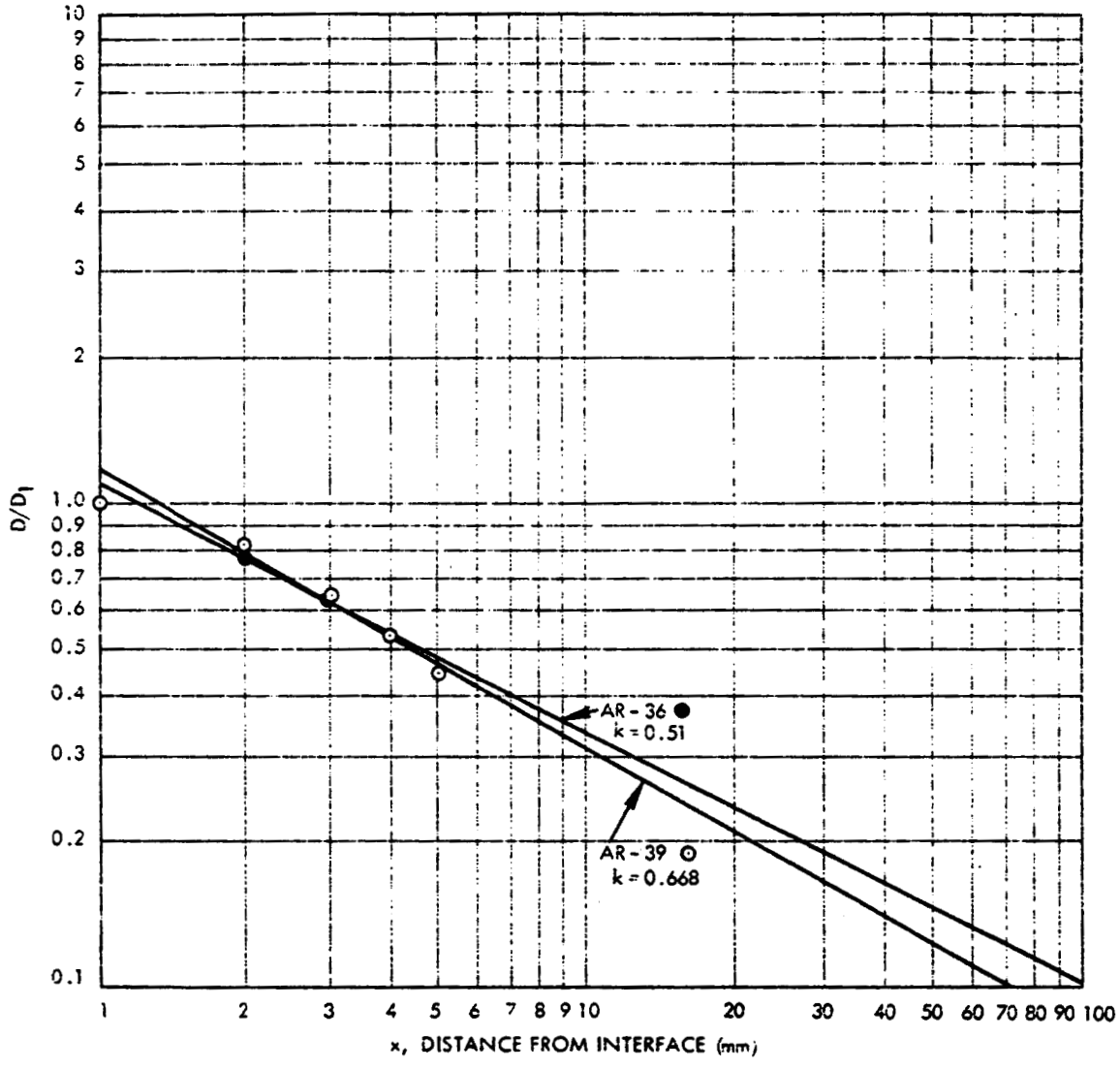

Figure 56. Plot of D/D_1 vs. Distance from Interface for CuO-Mg Acceptor (Sheet 1 of 2)

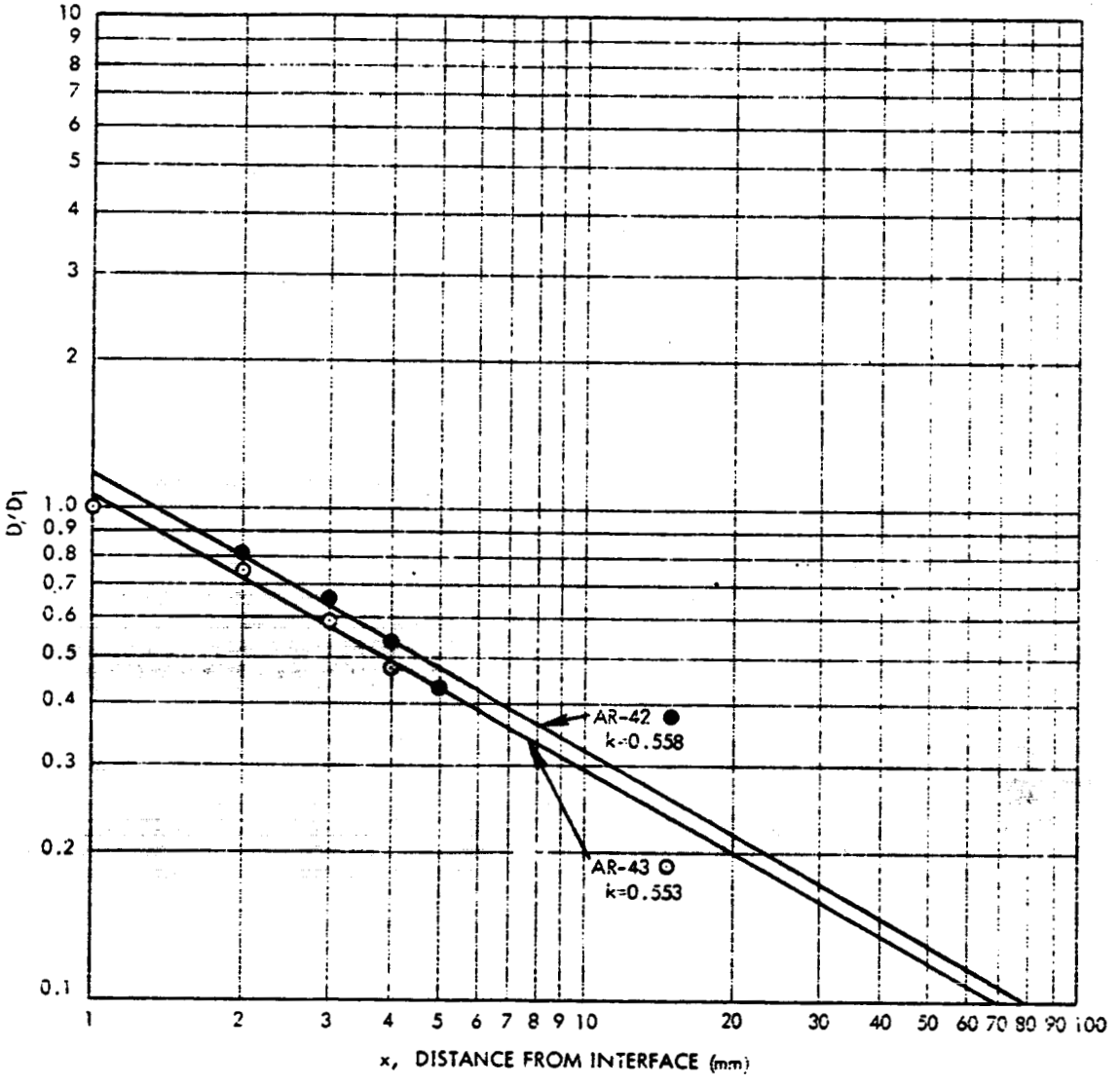

Figure 56. Plot of D/D_1 vs. Distance from Interface for CuO-Mg Acceptor (Sheet 2 of 2)

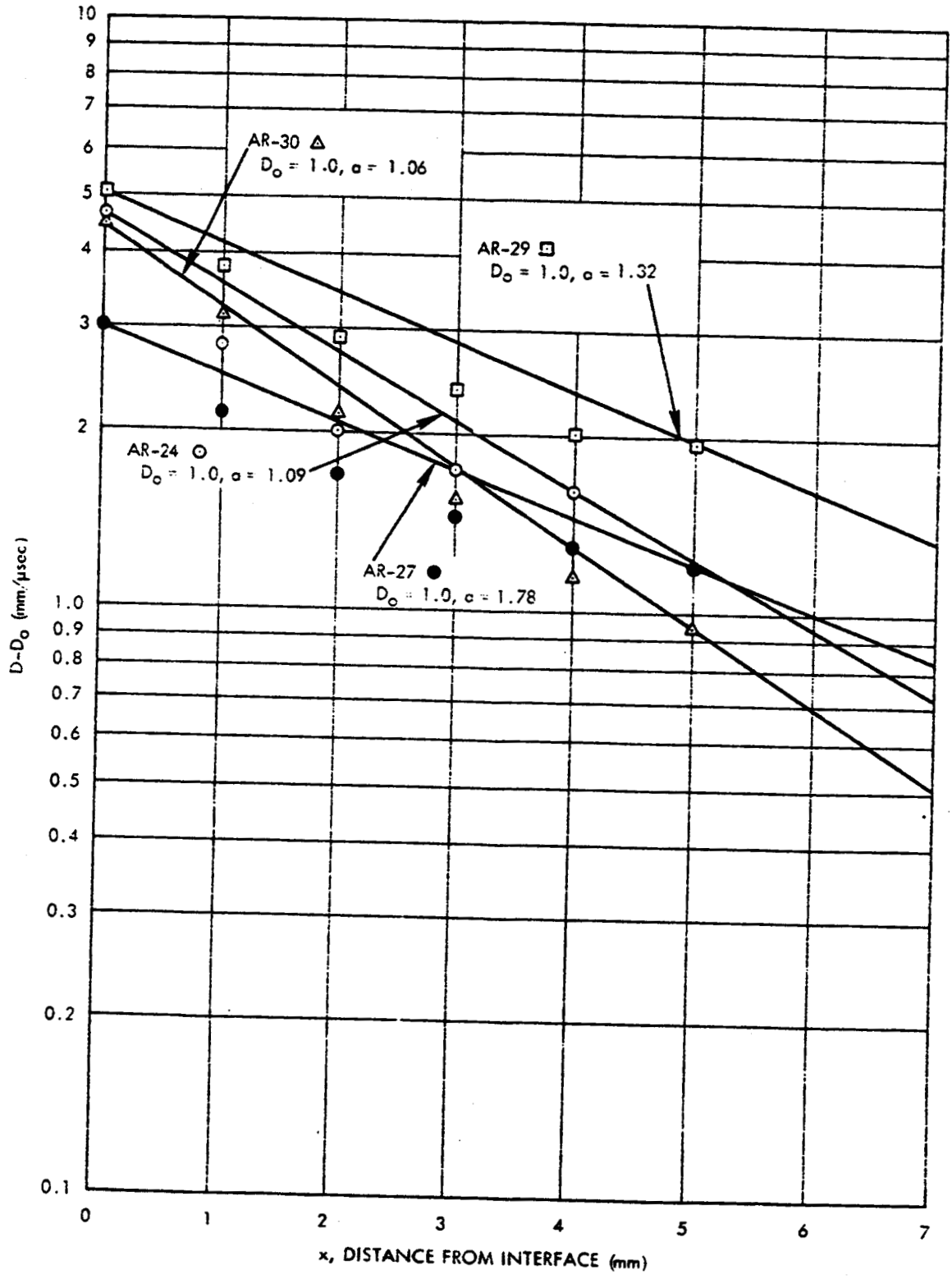

Figure 57. Plot of D - D_o vs. Distance from Interface for $KClO_4$-Al Acceptor

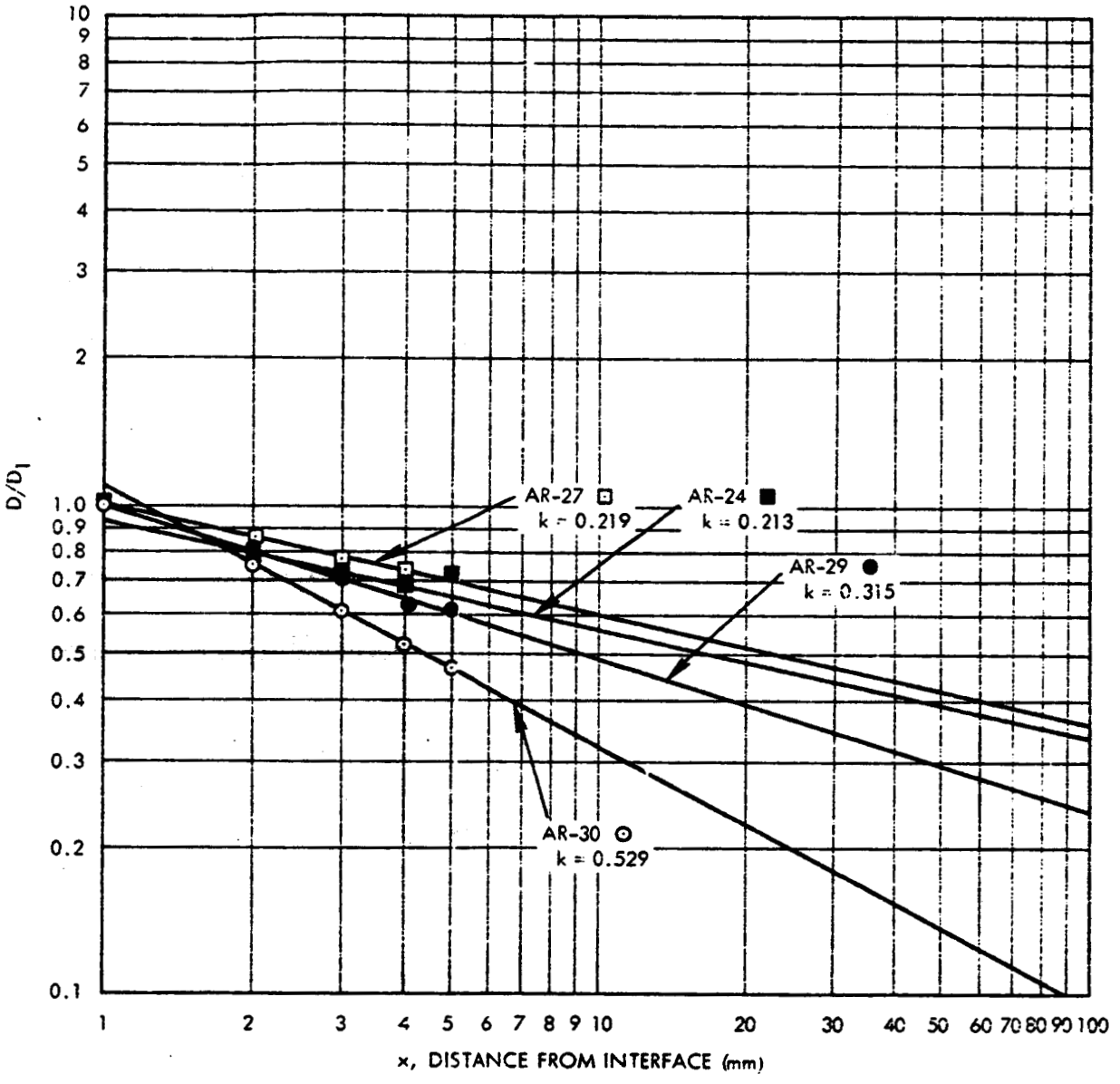

Figure 58. Plot of D/D_1 vs. Distance from Interface for $KClO_4$-Al Acceptor

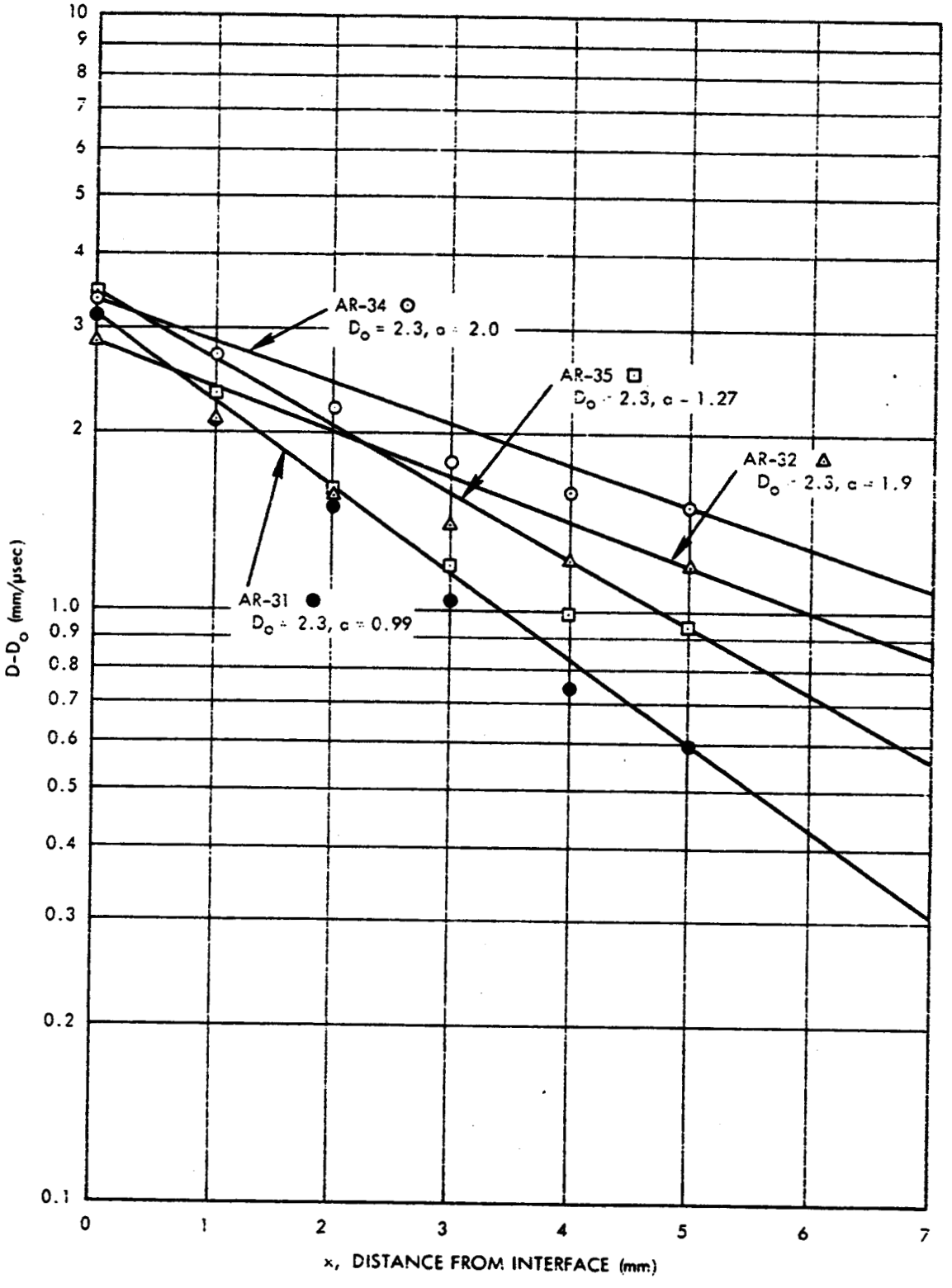

Figure 59. Plot of D - D_0 vs. Distance from Interface for 50-50 RDX-Al Acceptor

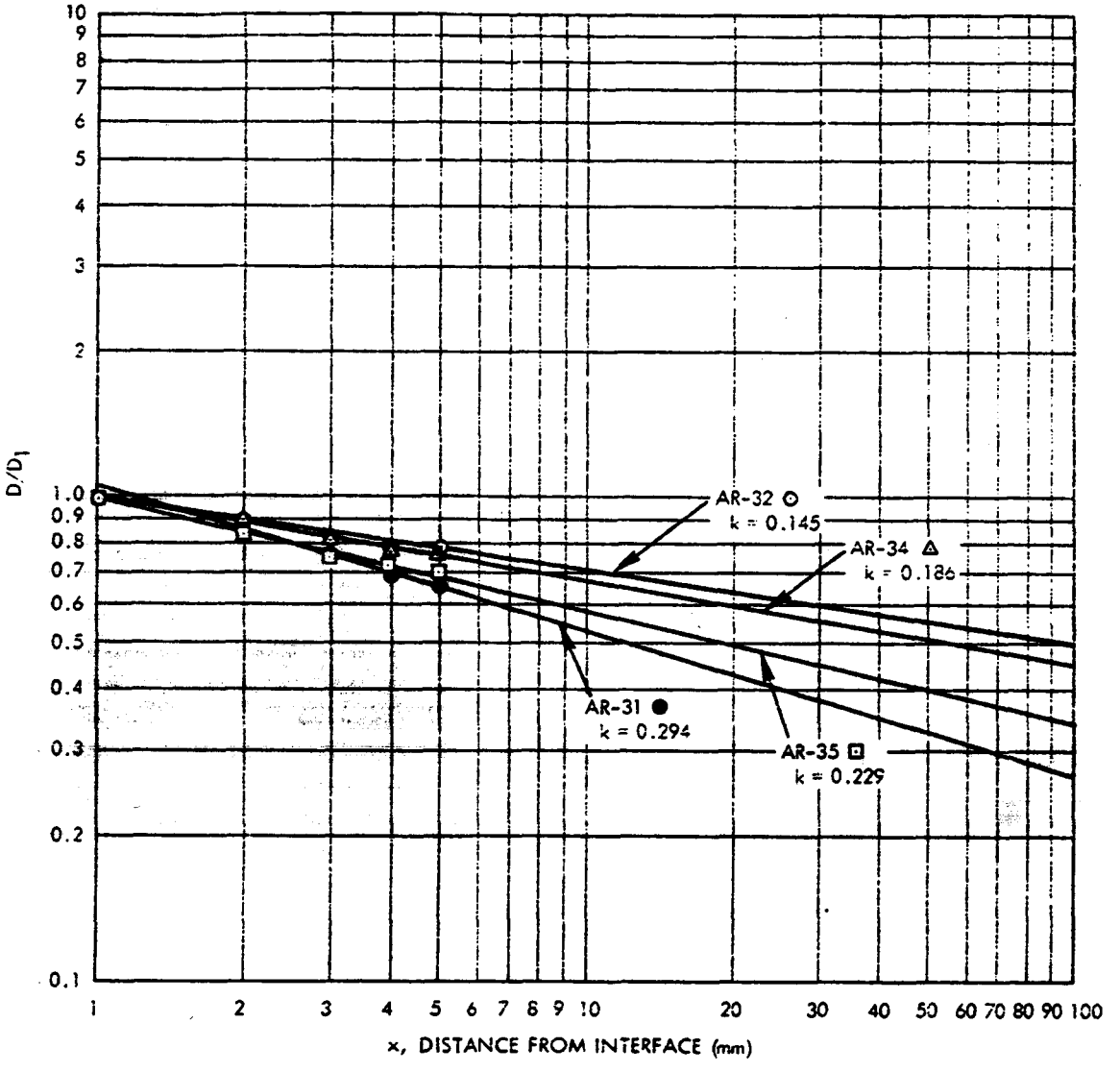

Figure 60. Plot of D/D_1 vs. Distance from Interface for RDX-Al Acceptor

Typical electrical probe curves from each family of curves for velocity vs. distance (Figures 46 through 54) were the source of values for the semilog plots in Figures 61, 63, and 65. Log-log plots obtained from the same electrical data are presented in Figures 62, 64, and 66; values of "k" and "a" found from these plots are presented in Table XI.

Table XI

VALUES OF "a" AND "k" FROM ELECTRICAL PROBE DATA

Acceptor mix		ρ gm/cm^3	k	a (mm)
50-50	RDX-Al	1.0	0.506	0.91
50-50	RDX-Al	1.0	0.361	0.81
50-50	RDX-Al	1.0	0.428	1.0
25-75	RDX-Al	1.0	0.936	1.9
60-40	$KClO_4$	1.2	0.637	2.4
60-40	$KClO_4$	1.2	0.576	2.6
60-40	$KClO_4$	1.2	0.757	2.5
40-60	$KClO_4$	1.5	0.770	1.5
76-24	CuO-Mg	1.7	0.78	1.9
$CuO-Fe_2O_3$-Mg		1.5	1.1	1.7

No direct correlation of the data between metallurgical and electrical techniques was possible for the pyrotechnic mix data because hardness measurements were not sufficiently sensitive to deflagration pressures. Poor electrical probe traces were obtained in the Armco iron shots and time did not permit reshooting this series with the sensitive 0.5-mil Moleculoy probe. In most cases electrical probe data yielded higher values of "k" than hardness measurements did, indicating generally a more rapid velocity decay from electrical measurements. Electrical probe data gave values of "a" of 1 or 2 millimeters, appreciably smaller than expected from similar materials presented by Eyring for larger diameter columns. When corrected for column diameter, however, they appear reasonable, even though somewhat short. The values of "a", in the range of 0.8 mm for 50-50 RDX-Al, appear to indicate that the aluminum is not immediately entering into the reaction, as these values are close to the 0.8 millimeter

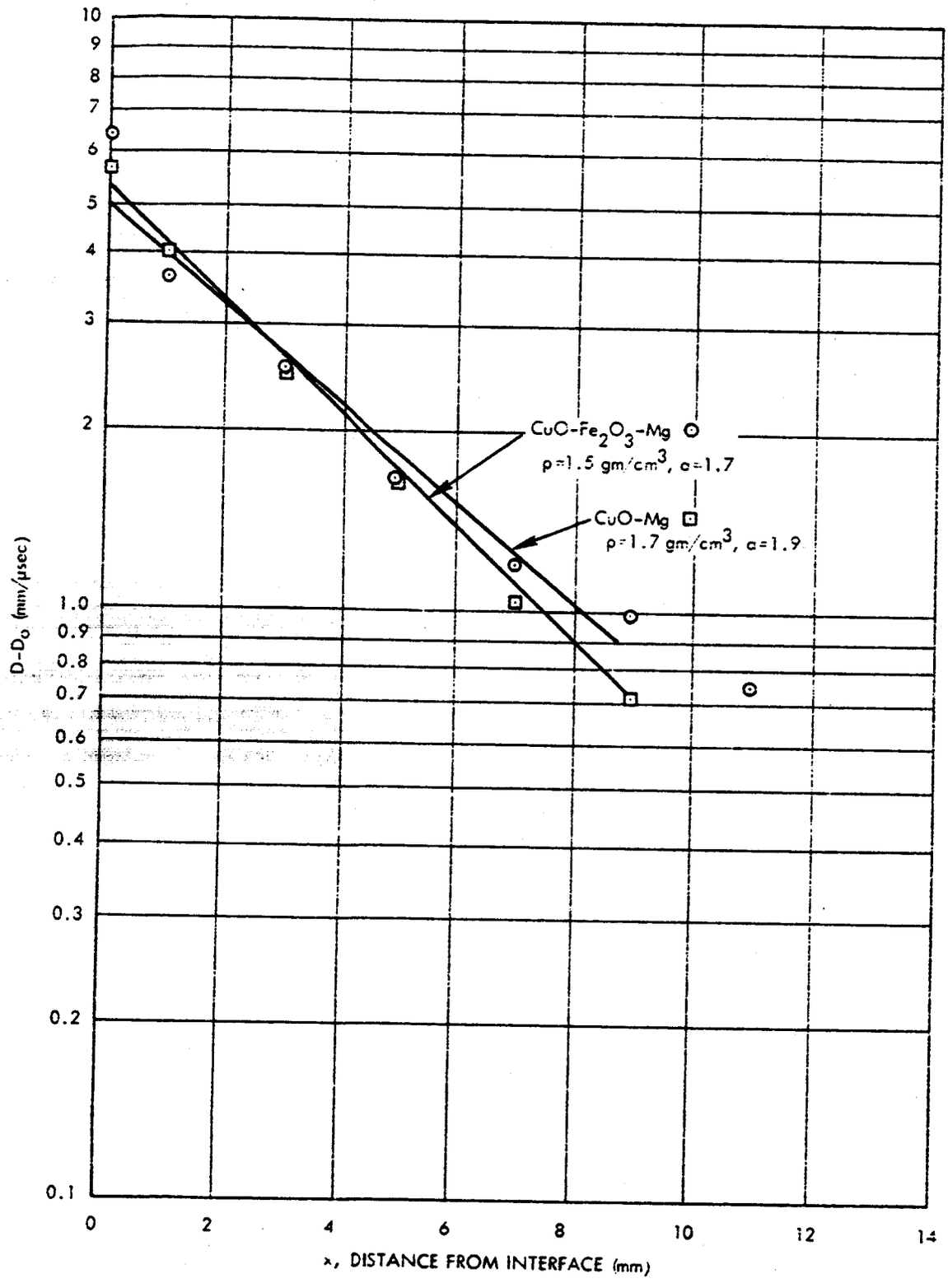

Figure 61. Plot of D - D_0 vs. Distance from Interface for CuO-Fe_2O_3-Mg and CuO-Mg Acceptors (Electrical Data)

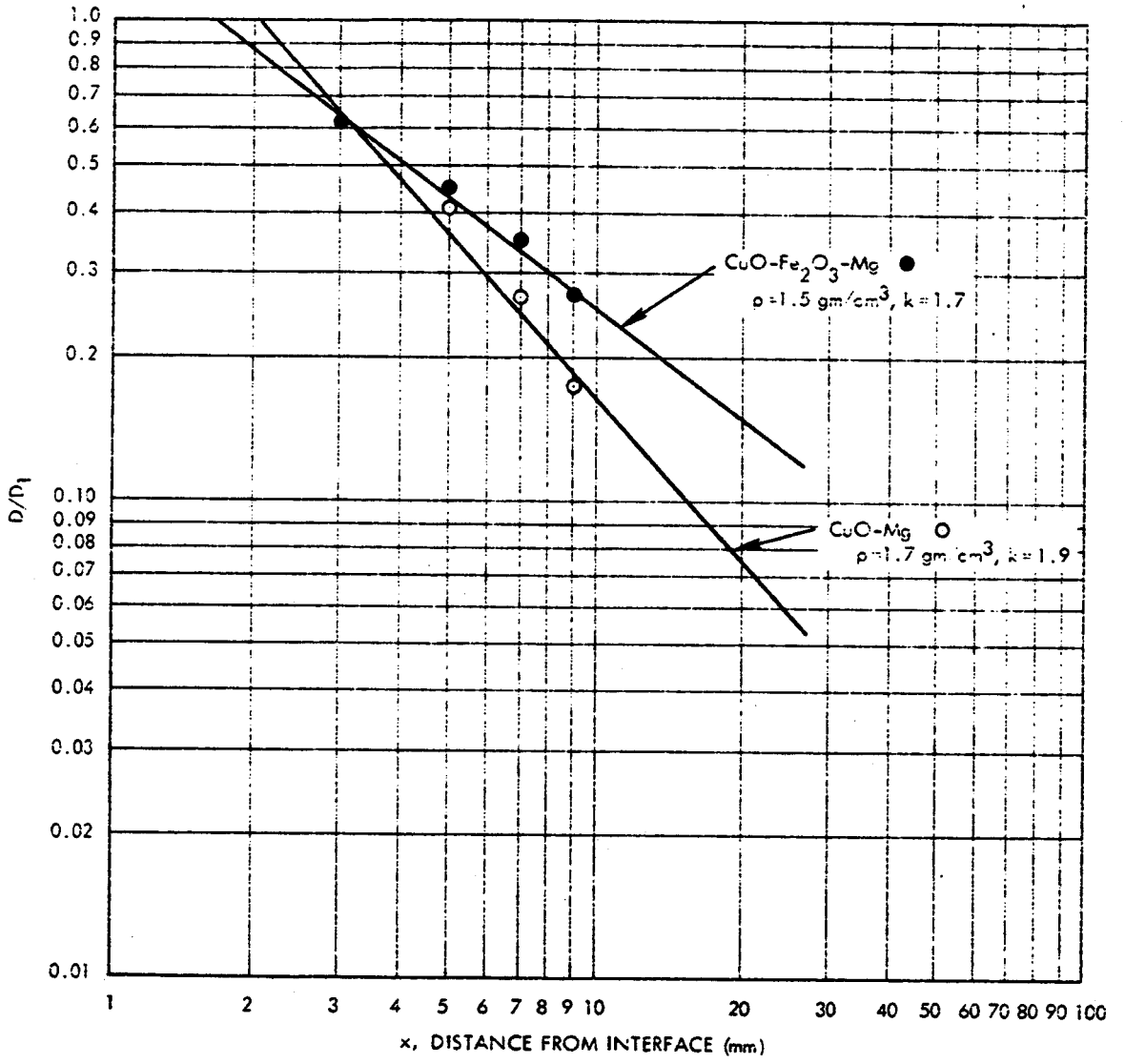

Figure 62. Plot of D/D_1 vs. Distance from Interface for $CuO-Fe_2O_3$-Mg and CuO-Mg Acceptors (Electrical Data)

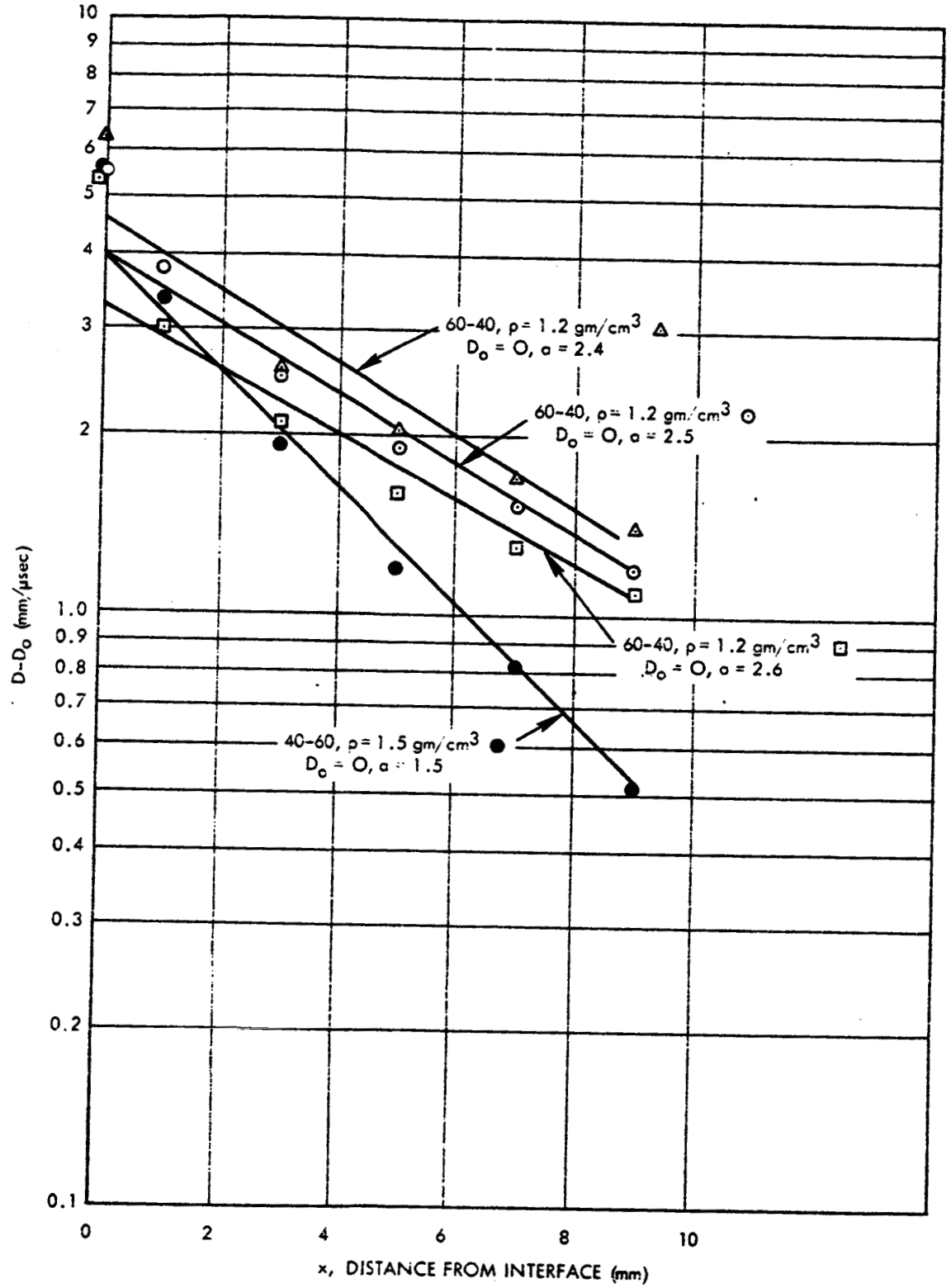

Figure 63. Plot of D - D_o vs. Distance from Interface for $KClO_4$-Al Acceptor (Electrical Data)

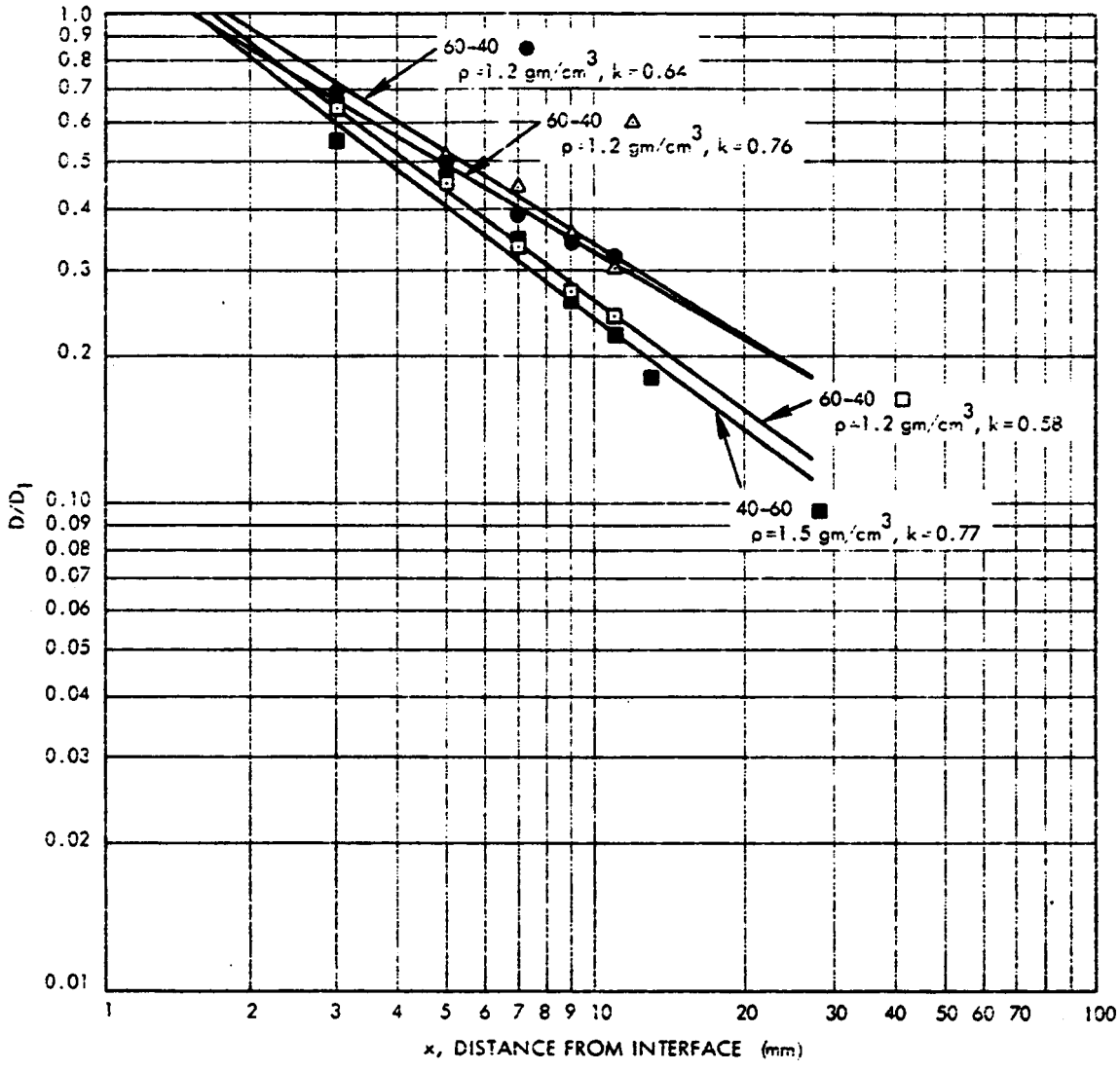

Figure 64. Plot of D/D_1 vs. Distance from Interface for $KClO_4$-Al Acceptor (Electrical Data)

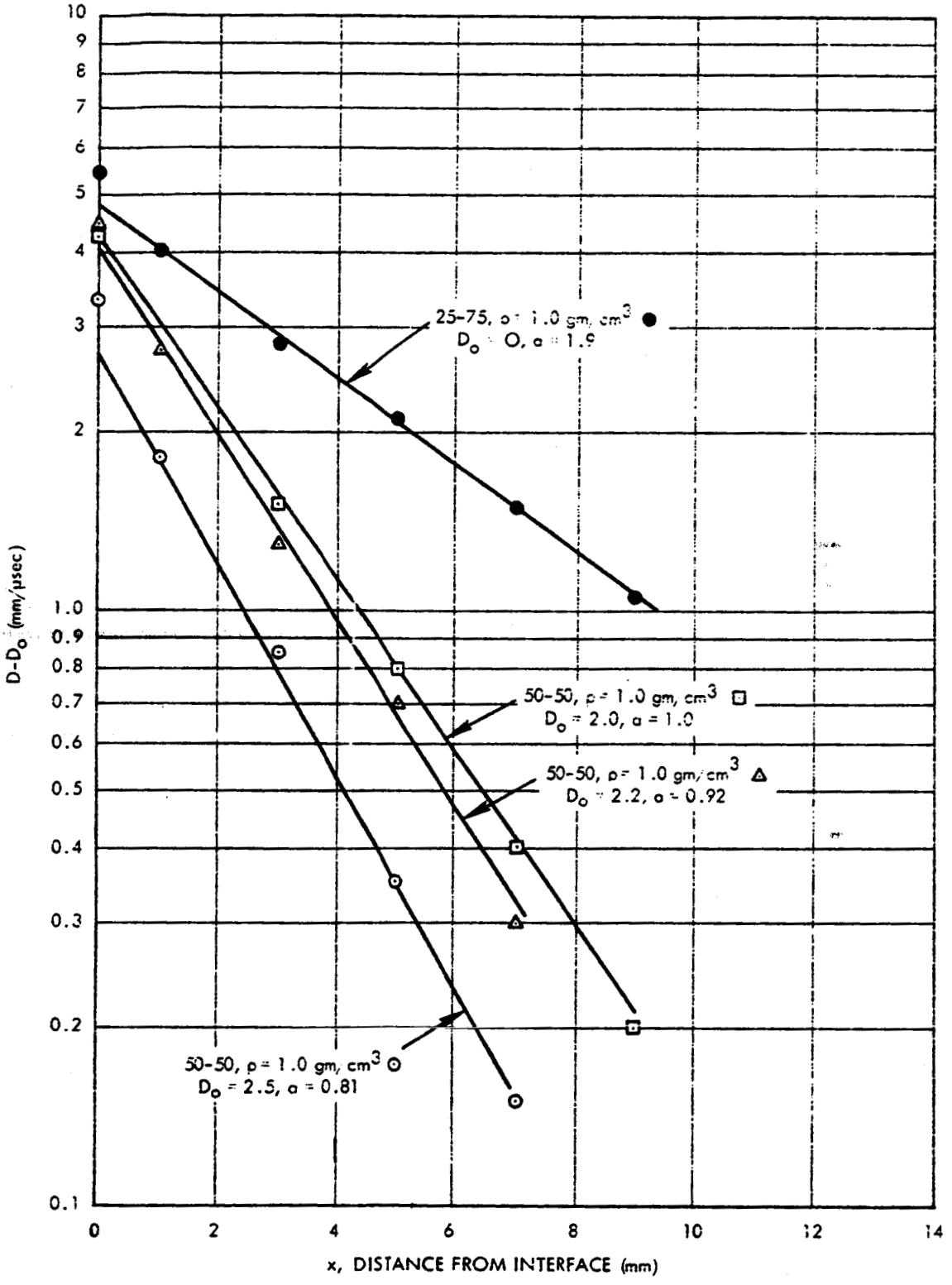

Figure 65. Plot of D - D_o vs. Distance from Interface for RDX-Al Acceptor (Electrical Data)

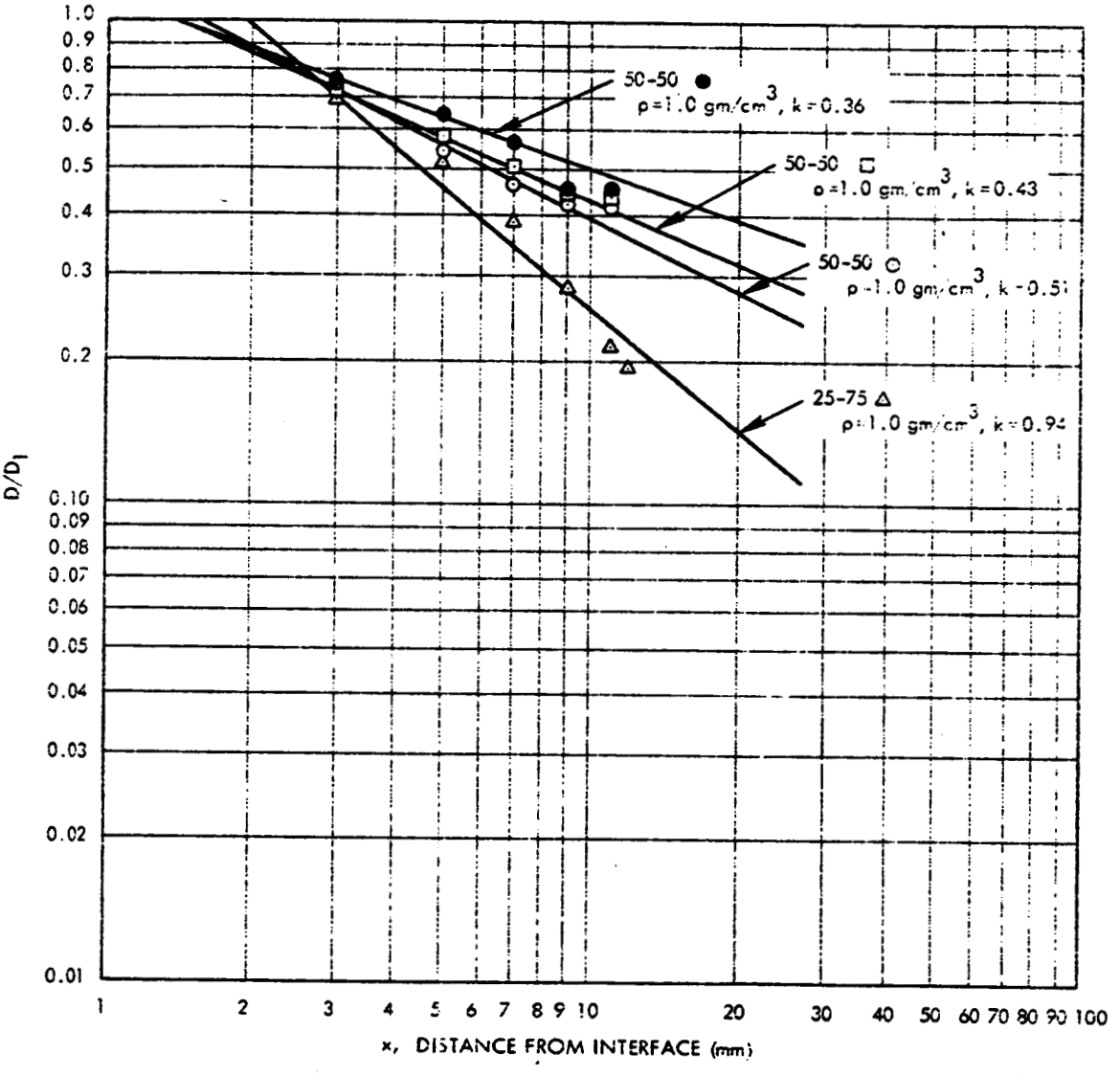

Figure 66. Plot of D/D_1 vs. Distance from Interface for RDX-Al Acceptor (Electrical Data)

value that Eyring predicts for pure RDX. However, Eyring's values are for the ideal detonation, while our measurements were made in a column only 0.1 inch diameter. In this case, even though we have massive confinement, the reaction zone thickness would be expected to be somewhat less than the ideal value. Thus, the extent to which the aluminum enters the immediate reaction remains unclear.

D. PETN/PETN THRU-BULKHEAD SYSTEM

Two series of shots were fired in a simulated TBI configuration consisting of a mild steel donor and bulkhead and a brass acceptor pressed against the bulkhead by a positioning fixture. In both series the donor was loaded with PETN at a constant density of 1.65 gm/cm^3. The first series utilized acceptors loaded with PETN at 1.0 gm/cm^3, and the second series PETN at 1.25 gm/cm^3. Bulkhead thicknesses of 75, 90, and 105 mils were used in each series. The 1-mil sandwich probe was inserted in the acceptors in both series.

Table XII shows the results of the first series of TBI shots. Average velocity is presented since there was a low level of low-frequency ringing in the probe traces for this series, which rendered any small interval measurements questionable.

Velocity vs. distance from TBI bulkhead for the second TBI series is plotted in Figures 67 and 68. Significant data from these graphs is compiled in Table XIII.

Acceptor density in the first series should have yielded steady state velocities of 5.6 mm/μsec. It may be noted that the average velocities are below the steady state value in all but one case, and that with increasing bulkhead thickness the average velocities tend to fall, indicating a slower buildup to a steady state. The same behavior can be noted in detail for the second series in Figures 67 and 68.

The data on delay in Tables XII and XIII (time from detonation entering the acceptor to initial probe reading) also indicate that the period before pressure rise to the level to cause probe closure is longer on the average for thicker

bulkheads. This conclusion is supported by data in the TBI tables and graphs on distance monitored by the probe.

Figures 67 and 68 show that steady state detonation velocities can be achieved in a TBI system in 5 to 10 millimeters from the bulkhead, if bulkhead thicknesses of 90 mils or less are employed. The data on the 105-mil bulkhead case indicates that this is a marginal bulkhead thickness, where some danger of failure to transfer exists. This data is especially interesting in light of the knowledge that the 120-mil bulkhead generally produces failure to transfer (failure to re-establish detonation in the acceptor).

Table XII

RESULTS OF FIRST TBI SERIES
(TBI Acceptors Loaded with PETN at 1.0 gm/cm^3)

TBI	Approximate Bulkhead Thickness (mils)	Delay (μsec)	Average Velocity (mm/μsec)	Distance Monitored (mm)
3	75	0.2	5.33	10.4
4	75	0.2	5.05	10.6
5	75	0.7	5.38	9.42
6	75	0.9	5.66	9.62
7	75	0.7	5.00	9.00
11	90	0.4	5.47	10.4
12	90	0.5	5.42	12.5
13	90	0.7	5.28	10.2
14	90	0.6	5.19	8.56
24	90	0.5	4.80	8.15
15	105	0.9	5.23	9.41
16	105	1.0	5.14	7.71
17	105	0.6	5.00	9.50
18	105	0.7	5.05	10.1
19	105	0.9	5.14	8.99

Table XIII

RESULTS OF SECOND TBI SERIES
(TBI Acceptors Loaded with PETN at 1.25 gm/cm^3)

TBI	Approximate Bulkhead Thickness (mils)	Delay (μsec)	Final Velocity (mm/μsec)	Distance Monitored (mm)
20	75	0.25	6.32	10.8
21	91	0.8	6.40	10.4
22	90	0.5	6.73	10.0
23	90	0.7	6.36	9.4
26	91	0.5	6.32	9.0
27B-45S	106	1.2	6.35	6.0
31	102	0.7	5.95	7.6
32	103	0.7	4.88	5.6
34	106	0.8	6.32	7.5
35	104	0.8	6.42	6.5

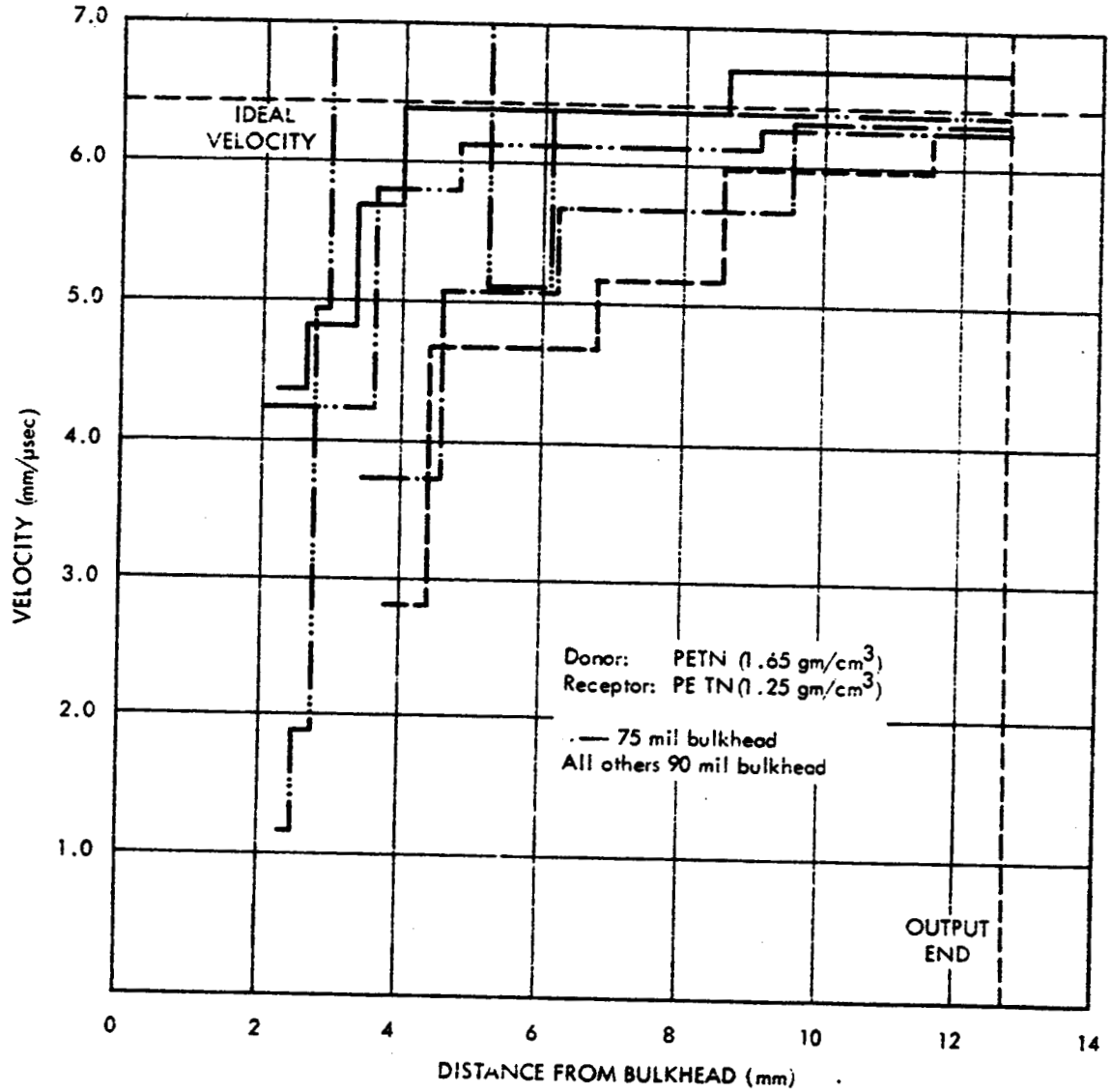

Figure 67. Plots of Velocity vs. Distance in Thru-Bulkhead Geometry (75- and 90-mil Bulkheads)

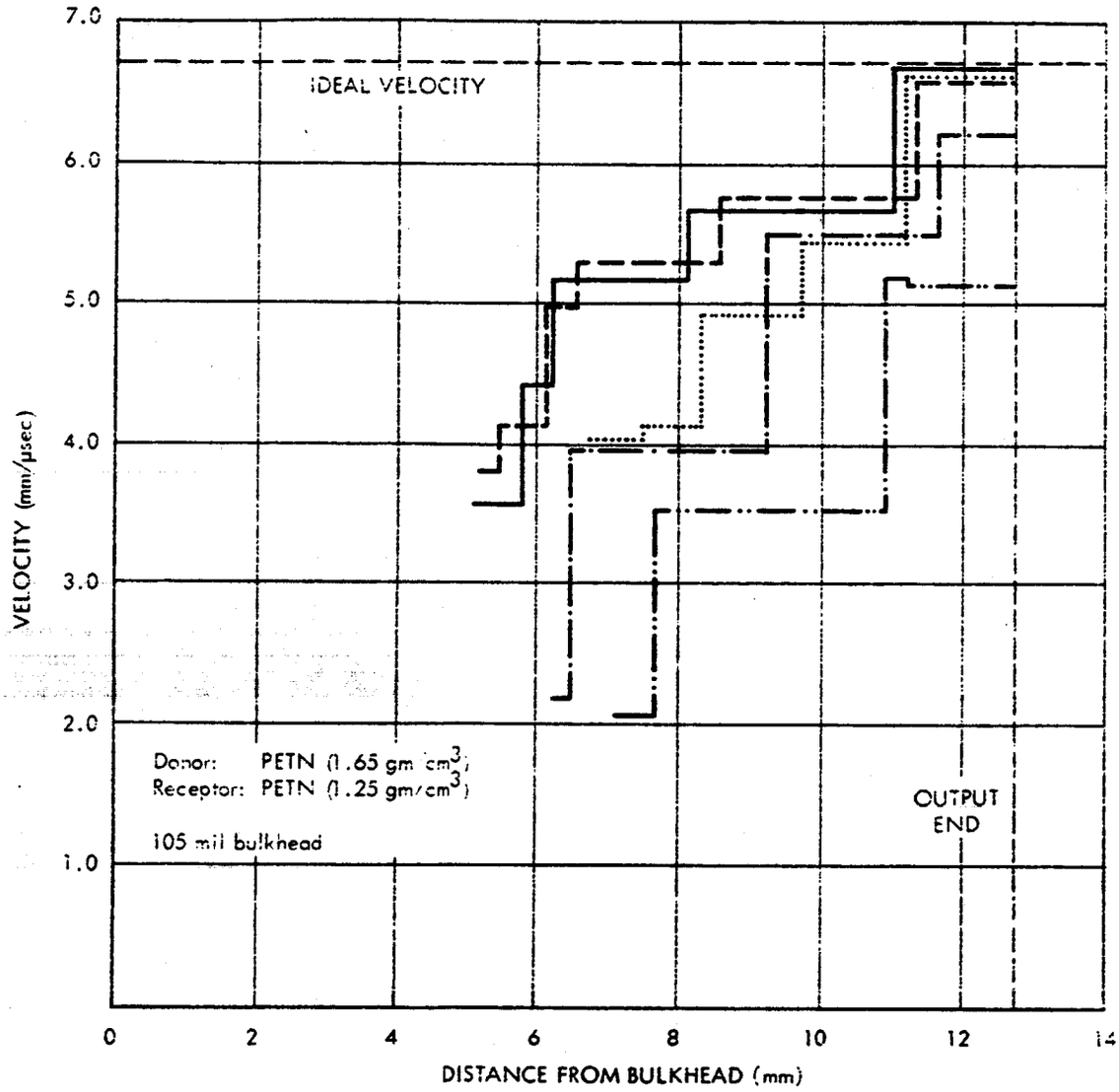

Figure 68. Plots of Velocity vs. Distance in Thru-Bulkhead Geometry (105-mil Bulkhead)

IV CONCLUSIONS

The experiments which have been carried out indicate the following conclusions may be drawn relative to the primary goals of the research:

A. CHEMICAL TRANSITIONS

(1) Detonation-to-deflagration transitions may be obtained in distances well under 1 inch with a wide variety of types of deflagration mixes.

(2) When the direct coupling technique is used as was the case in the majority of the experiments in this work, the transition is made more reliably and in a shorter distance if the detonation velocity and resulting shock pressure is low and the density of the deflagrating mix is of the order of 50-75% of crystal density.

(3) The shape of the transition curve may be fairly well approximated by the theory of Eyring assuming a reaction zone width that is suprisingly low, being only a few times the length of the column radius.

(4) The detonation velocity may be degraded in steps if the primary detonation velocity is too high for a reliable transition to deflagration directly. In this case the length of the transition zone from one detonation velocity to another may be estimated from Eyring's theory using conventional values of the reaction zone width (corrected for column diameter) for the second explosive. After steady state is achieved a second step may be made from the lower detonation velocity to deflagration. Proper choice of the intermediate may still make it possible to make the total transition in less than an inch.

(5) Additives such as aluminum when blended with conventional high explosives such as RDX seem to provide effective transition mixes although their effectiveness as ignition mixes was not evaluated.

B. MECHANICAL TRANSITIONS

(1) Ignition of PETN through a metal barrier can provide transition coupling for an ignition mix by providing a 5 to 10 mm zone in which the detonation velocity in the PETN is building up to high order detonation. This low velocity region provides a low-shock flame output which is desirable for ignition of deflagrating mixes. The length of the transition zone does not appear as reproducible as would be desired to assure reproducibility of the ignition, although no igniter outputs were measured to test the effect of the variability of the zone length on ignition.

(2) PETN does not appear to be the best explosive to use with the metal barrier technique since the range of thicknesses of barrier to provide a desirably long buildup zone is relatively small. In the present work it was found that barrier thicknesses of 90 mils were a bit too short, 105 mils was quite good (giving 5 to 10 mm low velocity region) and 120 mils was too thick to give reliable ignition. A more desirable explosive would have a wider barrier thickness range to make this feature less critical and give slightly longer build up distances. RDX is a possible choice since it is known to have longer build up distances than PETN.

(3) An air barrier was developed in a related program. (The development of the TBI for Saturn Applications referred to in the Introduction, P.O. M3J3XS-941503 with S&ID Division of NAA.) This proved to be a very effective coupling device between a detonating explosive and the deflagrating material. The air barrier was not studied further in this program, but is mentioned here for completeness.

C. TECHNIQUES

1. Metallurgical Techniques

In general the use of hardness measurements to determine reaction front velocities seems quite practicable. Results of most shots in the Armco iron were definitely usable and meaningful.

The metallurgical results could certainly have been improved by a greater quantity of hardness measurements, especially in transition regions. This could best be accomplished with an automated hardness tester such as recently placed on the market.* Results could very likely be improved if measurements were made on both sides of the explosive channel and averaged out before plotting.

The vacuum melted stainless steel 301 should be re-evaluated for future studies since it is felt that it should have more shock sensitivity than it indicated in our experiments. In addition, future effort should include measurements in the ranges of PETN velocities above 8.0 and below 4.0 mm/μsec, thus eliminating the need for extrapolation.

*Branson Instruments, Inc., Series C Research Sonodur Microhardness Tester

The unique advantage of the metallurgical technique is that it is a permanent source of data for an explosive event. If the original set of hardness results seems questionable, new hardness traverses along several sections can be run for re-examination, thus avoiding local anomalies in the structure.

2. Electrical Techniques

The electrical probe techniques developed in this study were generally very successful. They produced considerable substantive data simply, reliably, accurately, and reproducibly.

Further work on the probe might be directed toward use of thinner and weaker insulating materials than those used, and experiments with 0.5-mil insulated wire with a linear resistivity in the order of 300 to 600 ohms/ft. This lower resistance would shorten the response time below the 1 μsec observed with the 0.5-mil insulated Moleculoy probe (3600 Ω/ft). It would also be interesting to investigate interface problems with different diameter explosive channels, and observe transition velocities at an even faster sweep rate than was used.

Considerable velocity data is available in each photograph and the two traces provide two independent readouts of probe performance. It would be desirable to have the velocity slopes read automatically in order to make full use of the data present in each picture.

The electrical probe proved to be a very useful research tool for velocity measurements in explosives and pyrotechnics. It is a very flexible technique which can be modified to fit many different geometries and conditions. It could also be quite useful in the development and proving out of a pyrogen initiator, particularly of the Thru-Bulkhead configuration.

BIBLIOGRAPHY

1. Amster, A. B., Review of Scientific Instruments, Vol. 31, No. 2, (Letter to the Editor), February 1960.

2. Amster, A. B., Kendall, P. A., Veillette, L. J. and Harrell, B., The Review of Scientific Instruments, Vol. 31, No. 2, February 1960.

3. Anderson, R., Brown, R. S. and Shannon, L. J., "Ignition Theory of Solid Propellants," AIAA Solid Propellant Rocket Conference, Palo Alto, California, January 29-31, 1964.

4. Anderson, R., Brown, R. S., Thompson, G. T. and Ebeling, R. W., "Theory of Hypergolic Ignition of Solid Propellants," AIAA Heterogeneous Combustion Conference, Palm Beach, Florida, December 11-13, 1963.

5. Andreev, K. K., Proc. Roy. Soc., (London) A246, 257 (1958).

6. Baer, A. D., Ryan, N. W. and Salt, D. L., "Propellant Ignition by High Convective Heat Fluxes," Solid Propellant Rocket Research, Vol. 1, 1960.

7. Bean, C. M., Cachia, G. P. and Kirkham, J., "A Colliding Ball High Explosive Impact Sensitivity Testing Machine," Third Symposium on Detonation, Naval Ordnance Laboratory, White Oak and Office of Naval Research, September 26-28, 1960.

8. Bergsman, E. Borje, "Some Recent Observations in Micro-Hardness Testing," ASTM Bulletin, September 1951, pages 37-43.

9. Bowden, F. P. and Yoffe, A. D., Fast Reactions in Solids, Butterworths, 1958.

10. Bowden, F. P. and Yoffe, A. D., Initiation and Growth of Explosion in Liquids and Solids, Cambridge Univ. Press, 1952.

11. Bray, K. N. C., "Comment on Thermal Ionization Behind Strong Shock Waves," AIAA Journal, Vol. 2, No. 6, June 1964.

12. Brown, R. S., Wirrick, T. K. and Anderson, R., "Theory of Ignition and Ignition Propagation of Solid Propellants in a Flow Environment," AIAA Solid Propellant Rocket Conference, Palo Alto, California, January 29-31, 1964.

13. Cachia, G. P. and Whitbread, E. G., Proc. Roy. Soc., (London) A246, 268 (1958).

14. Campbell, A. W., Davis, W. C. and Travis, J. R., Phys. Fluids, 4, 498 (1961).

15. Campbell, A. W., Davis, W. C. and Travis, J. R., "Third Symposium on Detonation," Princeton Univ., 1960.

16. Cantrell, R. H., Hart, R. W. and McClure, F. T., "Linear Acoustic Gains and Losses in Solid Propellant Rocket Motors," AIAA Journal, Vol. 2, No. 6, June 1964.

17. Cawsley, G. F., Farrands, J. L. and Thomas, S., "Observations of Detonation in Solid Explosives by Microwave Interferometry," Proc. Roy. Soc., 248A, 499-521 (1958).

18. Cook, Melvin A., Faraday Society Discussions, No. 22, 1956.

19. Cook, Melvin A., The Science of High Explosives, Reinhold Publishing Corporation, New York.

20. Cook, Melvin A., Doran, Ray L. and Morris, Glen J., "Measurement of Detonation Velocity by Doppler Effect at Three-Centimeter Wavelength," Journal of Applied Physics, Vol. 26, No. 4, April 1955.

21. Cook, Melvin A., Keyes, Robert T. and Udy, Lex L., "Propagation Characteristics of Detonation-Generated Plasmas," Vol. 30, No. 12, December 1959.

22. Cook, Melvin A., Pack, D. H., Cosner, L. N. and Gey, W. A., J. Appl. Phys., 30, 1579 (1959).

23. Curran, D., Katz, S., Kelly, J. and Nicholson, M., "Pressure Required for Transformation Twinning in Explosively Loaded Low-Carbon Steel," Trans. AIME, 215, 151-3 (1959).

24. DeCarli, P. and Kelly, J., "Explosive Hardening of Stainless Steels," Stanford Research Institute Report PG-3357.

25. Dieter, G. E., "Metallurgical Effects of High Intensity Shock Waves in Metals," Response of Metals to High-Velocity Deformation, Interscience, N. Y.

26. Emond, Lloyd, "Vickers-Knoop Hardness Conversion," Metal Progress Data Sheet, September 1958, page 96-B.

27. Erkman, John O., "Explosively Induced Nonuniform Oblique Shocks," Stanford Research Institute Technical Report 010-58, June 3, 1958.

28. Evans, Marjorie W. and Ablo, C. M., "Theories of Detonation," Journal of Chemical Review, 129 (1951).

29. Evans, Marjorie W., Beyer, R. B. and McCulley, L., The Journal of Chemical Physics, Vol. 40, No. 9, 1 May 1964, pages 2431-2438.

30. Friedman, Morton, "A Correlation of Impact Sensitivities by Means of the Hot Spot Model," Ninth Symposium (International) on Combustion at Cornell University, Ithaca, N. Y., August 27 to September 1, 1962, Academic Press, 1963.

31. Gibson, Frank C., Bowser, Merle L. and Mason, Chas. M., "Method for the Study of Deflagration to Detonation Transition," The Review of Scientific Instruments, Vol. 30, No. 10, American Institute of Physics, October 1959.

32. Giesler, Maj. B. E., Irwin, O. R., Roark, G. L. and Salzman, P. K., "Detonation Hazards of Large Solid Rocket Motors," Paper presented at 21st Interagency Solid Propulsion Meeting, San Francisco, California, June 9-11, 1965.

33. Hart, R. W. and Cantrell, R. H., "Amplification and Attenuation of Sound by Burning Propellants," AIAA Journal, Vol. 1, No. 2, February 1963.

34. Hershkowitz, Joseph, "The Combination of Granular Mixture of Potassium Perchlorate and Aluminum Considered as Either a Deflagration or a Detonation," Picatinny Arsenal Technical Report No. 3063, January 1963.

35. Heusinkveld, M. and Holzer, F., "Method of Continuous Shock Front Position Measurement," The Review of Scientific Instruments, Vol. 35, No. 9, September 1964.

36. Hirano, Ken-chi, Cohen, M., Averbach, B. L. and Ujiive, N., "Self Diffusion in Alpha Iron During Compressive Plastic Flow," Transactions of the Metallurgical Society of AIME, Vol. 227, August 1963.

37. Hussein, Sabri, "High-Frequency Zener Limiters," IEEE, May 1965.

38. Jacobs, P. W. M. and Tompkins, F. C., Chemistry of the Solid State, (Garner, W. E., ed.), Chapter 7, Butterworths, 1955.

39. Jaffe, I., Beauregard, R. and Amster, A., ARS Journal, 32, 22 (1962).

40. Jameson, R. L., Lukasik, S. J. and Pernick, B. J., "Electrical Resistivity Measurements in Detonating Composition B and Pentolite," Journal of Applied Physics, Vol. 35, No. 3, March 1964.

41. Jones, O. E. and Holland, J. R., "Bauschinger Effect in Explosively Loaded Mild Steel," Journal of Applied Physics, Vol. 33, No. 6, June 1964.

42. Macek, A., Chem. Revs., 62, 41 (1962).

43. Majowicz, J. M. and Jacobs, S. J., Classified Naval Ordnance Laboratory Report, March 1958, also Bull. Am. Phys. Soc., Ser. II, 3, 293 (1958).

44. Majowicz, J. M. and Jacobs, S. J., "Initiation to Detonation of High Explosives by Shocks," Fluid Dynamics Division, American Physical Society, 10th Anniversary Meeting, Lehigh University, Bethlehem, Pa., November 25-27, 1957.

45. McAlevy, III, R. F., Cowan, P. L. and Summerfield, M., "The Mechanism of Ignition of Composite Solid Propellants by Hot Gases," Solid Propellant Rocket Research, Vol. 1, 1960.

46. Pakulak, Jr., Jack M. and Taylor, C. A., The Thermal Decomposition Classification of Propellants, U.S. Naval Ordnance Test Station, China Lake, California.

47. Price, Donna and Jaffee, Irving, "Safety Information from Propellant Sensitivity Studies," AIAA Journal, Vol. 1, No. 2, February 1963.

48. Seay, G. E. and Seely, L. B., Jr.: Appl. Phys. 32, 1092 (1961).

49. Smith, Cyril Stanlen, "Metallographic Studies of Metals After Explosive Shock," Transactions of The Metallurgical Society of AIME, October, 1958.

50. Strehlow, Roger A. and Dyner, Harry B., "One-Dimensional Detonation Initiation," AIAA Journal, Vol. 1, No. 3, March 1963.

51. Sultanoff, M. and Boyle, V. M., ONR Symposium Report ACR-52, September 26-28, 1960, page 520.

52. Whitbread's paper on effect of duration on initiation, "Les Ondes de Detonation," September 1961, Paris, Editions du Centre National de la Recherche Scientifique, 15 Quai Anatole, France, 1962.

53. Zukas, E. G. and Fowler, C. M., "The Behavior of Iron and Steel Under Impulsive Loading," Response of Metals to High-Velocity Deformation, Interscience (1960).

54. International Conference on Sensitivity and Hazards of Explosives, London, October 1-3, 1963. Preprints - ER&D Establishment, Ministry of Aviation.

55. Link Ordnance Division, Interoffice Correspondence, Contact Report, D. E. Davenport, Karl Ockert, Rohm and Haas, Huntsville, Alabama (at AOA Meeting at Wright-Patterson Air Force Base), Subject: Detonation to Deflagration.

56. NOL Technical Report 64-66, "Behavior of Plexiglas Under Shock Loading by a Tetryl Donor."

57. Technical Documentary Report No. ASD-TDR-62-535, "Investigate the Effect of High Dynamic Pressures Upon the Metallurgical Properties of Iron and Titanium Base Alloys," prepared for Wright-Patterson Air Force Base, Ohio, by the Aerojet-General Corp., Downey, California, February 1963.

58. Eyring, Henry; Powell, R. E.; Duffey, G. H.; and Parlin, R. B.; "The Stability of Detonation", Chem. Revs., 45, 69 (1949).